공학박사 학위논문

Regulation of human mesenchymal stem cell differentiation by controlling collagen hydrogel contraction

콜라겐 하이드로겔 수축의 조절을 통한 인간 중간엽 줄기세포의 분화 결정

2022 년 8 월

서울대학교 대학원

공과대학 화학생물공학부

김 슬 하

Regulation of human mesenchymal stem cell differentiation

by controlling collagen hydrogel contraction

지도 교수 박 태 현

이 논문을 공학박사 학위논문으로 제출함

2022 년 8 월

서울대학교 대학원

화학생물공학부

김 슬 하

김슬하의 공학박사 학위논문을 인준함

2022 년 7 월

위 원 장 김 병 수 (인)

부 위 원 장 박 태 현 (인)

위 원 황 석 연 (인)

위 원 김 정 아 (인)

위 원 박 희 호 (인)

Abstract

Regulation of human mesenchymal stem cell differentiation by controlling collagen hydrogel contraction

Seulha Kim

School of Chemical and Biological Engineering

The Graduate School

Seoul National University

Collagen is the most abundant protein in the extracellular matrix of mammals and has a great effect on various cell behaviors including adhesion, differentiation, and migration. However, it is difficult to utilize collagen gel as a physical scaffold *in vitro* because of its severe contraction. A decrease in the overall hydrogel volume induces changes in cell distribution and mass transfer within the gel. Uncontrolled mechanical and physiological factors in the fibrous matrix result in uncontrolled cell behaviors in the surrounding cells. From this point of view, the effects of regulating collagen contraction on stem cell differentiation was investigated.

First, a method preventing the contraction of collagen hydrogel was developed. Two strategies were used to minimize the contraction of collagen gel. A disk-shaped frame made of polydopamine-coated polydimethylsiloxane (PDMS) prevented horizontal contraction at the edge

of the hydrogel. The sequentially cross-linked collagen gel with alginate outer shell structure inhibited vertical gel contraction. The physical properties of the hydrogel fabricated in this study were similar to those of pure collagen hydrogel. The combined method synergistically prevented the hydrogel from shrinkage in long-term 3D cell culture.

In freely contracting collagen hydrogel, stem cell lineage could not be regulated as intended even if the appropriate chemical inducers were used. Only adipogenic induction was preferred in cells. It was investigated how cells perceived the external environment in collagen hydrogels through analysis of Yes-associated protein (YAP) nuclear localization from a mechanotransduction perspective. Using a polydopamine-coated frame and alginate outer shell, I figured out whether the prevention of collagen contraction and the consequent high cell contractile force within the gel matrix contribute to the differentiation fate of ADSCs, thereby leading to osteogenesis.

With a focus on the adipogenic tendency in ADSCs cultured in contracting collagen hydrogel, the effect of contraction rate on adipogenesis was analyzed. When the contraction was delayed using the polydopamine-coated frame, a higher proportion of cells formed lipid droplets in the cytosol than in the freely contracting collagen hydrogel. These mature adipocytes actively responded to the fatty acid stimulus. In conclusion, it was able to induce rapid and uniform adipogenesis of human mesenchymal stem cells by temporal regulation of contraction.

Furthermore, an *in vitro* model that reproduced the inflammatory response in morbidly obese adipose tissue was developed. Obesity-induced chronic inflammation is the major cause of insulin resistance underlying metabolic syndrome. However, inflammation-induced phenomena in *in vivo* adipose tissue are not sufficiently reproduced in two-dimensional studies using adipocyte cell lines, *in vitro*. It was hypothesized that this gap between *in vitro* and *in vivo* was due to the exclusion of cell-ECM interaction. When the pro-inflammatory factors and excess fatty acid were treated to

ADSCs induced adipogenesis in collagen hydrogel, fat concentrated in the cells was distributed to the surrounding cells as cell division was promoted. The phenomenon that adipose tissue expansion is caused by inflammation in *in vivo* adipose tissue was reproduced in this model.

In summary, I developed a method to control collagen contraction and investigated its effect on ADSCs. In addition, it was shown that only regulation of the collagen contraction was enough to control the stem cell lineage of mesenchymal stem cells and enabled recapitulation of cell behaviors *in vivo*. The development of this contraction inhibition platform made it possible to investigate the influence of regulation of cellular microenvironments. The platform can be used to broaden our understanding of the fundamental mechanism underlying cell-matrix interactions and reproduce extracellular matrix *in vivo.*

Keywords: mesenchymal stem cells (MSC), collagen hydrogel, mechanotransduction, adipogenesis, inflammation, pro-inflammatory cytokine

Student Number: 2018-35705

Contents

List of figures

List of tables

List of abbreviations

ADSCs: adipose tissue-derived mesenchymal stem cells

AM: adipogenic medium

αMEM: alpha minimum essential medium

AMM: adipogenic maintenance medium

bFGF: basic fibroblast growth factor

BGLAP: bone γ-carboxyglutamate protein

Bleb: blebbistatin

BMSCs: bone-marrow derived mesenchymal stem cells

BSA: bovine serum albumin

C: collagen only hydrogel

CA-IPN: homogeneous hydrogel composed of collagen and alginate interpenetrating network

CA-shell: collagen and alginate hydrogel having cross-linked alginate outer shell, manufactured by sequential gelation steps

CA: unless noted otherwise, indicating CA-shell

CAF: CA-shell hydrogel fabricated within polydopamine coated frame (window frame)

CDK1: cyclin dependent kinase 1

CEBPA: CCAAT/enhancer-binding protein α

CEBPB: CCAAT/enhancer-binding protein β

CF: C hydrogel fabricated within polydopamine coated frame (window frame)

Cps: count per second

DAPI: 4',6-diamidino-2-phenylindole

DDW: double distilled water

DMEM: Dulbesco’s minimum essential medium

DPBS: Dulbecco's phosphate-buffered saline

dsDNA: double strand DNA

ECM: extracellular matrix

EDC: 1-ethyl-3-(3-dimethyl aminopropyl) carbodiimide hydrochloride

EDS: energy dispersive X-ray spectroscopy

EDTA: 2,2',2",2"'-(ethane-1,2-diyldinitrilo) tetraacetic acid

FBS: fetal bovine serum

FF-BSA: fatty acid free-bovine serum albumin

GAPDH: glyceraldehyde 3-phosphate dehydrogenase

GLUT4: insulin-responsive glucose transporter 4

HBSS: Hank’s balanced salt solution

IBMX: 3-isobutyl-1-methylxanthine

ICC: immunocytochemistry

IL-1β: interleukin-1β

IL-6: interleukin-6

INF: inflammatory condition (addition of pro-inflammatory cytokines)

IPN: interpenetrating networks

ISO: isoproterenol

MFI: mean fluorescence intensity

MMP: matrix metalloproteinase

MSCs: mesenchymal stem cells

MYC: MYC proto-oncogene

OA: oleic acid

OM: osteogenic medium

PA: polyacrylamide

PBS: phosphate buffered saline

PBST: phosphate buffered saline with Tween 20

PDA: polydopamine

PDMS: polydimethylsiloxane

PPARG: peroxisome proliferator-activated receptor gamma

PS: penicillin streptomycin

qRT-PCR: quantitative reverse transcription-polymerase chain reaction

ROCKi; rho-associated coiled-coil containing protein kinase inhibitor

RUNX2: runt-related transcription factor 2

SDS: sodium dodecyl sulfate

SEM: scanning electron microscope

SOX2: SRY-box transcription factor 2

Sph: spheroid

SPP1: secreted phosphoprotein 1

TAZ: transcriptional coactivator with PDZ-binding motif

TE: trypsin-EDTA

TNFα: tumor necrosis factor α

YAP: yes-associated protein

Chapter 1.

Research background and objectives

Chapter 1. Research background and objectives

Extracellular matrix (ECM) constituting the cell microenvironment not only provides structural support, but also determines the cell fate including migration, differentiation, proliferation and survival [1]. In mammals, collagen is the most abundant ECM protein of the connective tissue. Collagen constitutes almost 25% of the total body protein in humans: 75% of the dry weight of skin, 80% of the organic component in bone, and over 90% of tendon and cornea. Especially, collagen type I is well known as a major structural protein accounting for more than 90% of all collagen types [2]. Collagen is used in the form of coating, hydrogel, or scaffold to recapitulate the *in vivo* microenvironment. Therefore, it is essential to understand the dynamics of collagen-cell interaction.

Despite its importance, it is difficult to manipulate collagen *in vitro* due to its flexible fibril networks formed by self-assembly [3]. Unlike the *in vivo* environment in which connective tissues hold each other in all directions, the cell-collagen matrix interaction induces collagen gel contraction *in vitro*. The structure collapses easily into a small mass within a few days [4, 5]. Gel shrinking induces changes in mass transfer efficiency, cell distribution, and adhesive ligand density of surrounding matrix. Therefore, the mechanical and morphological factors should be controlled to provide a uniform cellular microenvironment during the culture period and to design reproducible experiments [6].

Therefore, this research focused on controlling the three-dimensional microenvironment *in vitro* by regulating the spontaneous contraction of collagen. Through the method of controlling the contraction of collagen hydrogel, dynamic stimuli can be applied to the cells

that cultured in three-dimensional (3D) environment and improve our understanding of complex physiological events in the body.

Chapter 2.

Literature review

Chapter 2. Literature review

2.1 Human mesenchymal stem cells

Stem cells are undifferentiated cells that are capable of self-renewal and having differentiation potential. Mesenchymal stem cells (MSCs) are classified as adult stem cells, because they can be extracted from adults while maintaining the characteristics of stem cells [7]. Although the differentiation potential of MSCs is lower than that of embryonic stem cells, it has the advantage of being able to be used for tissue engineering without ethical problems and immune rejection (when extracted from the patient). MSCs can be extracted from various sources such as bone marrow, fat, umbilical cord, and molars, and can differentiate into various cells including bone, adipose, muscle, and cartilage.

Two widely studied MSCs are bone-marrow derived mesenchymal stem cells (BMSCs) and adipose tissue-derived mesenchymal stem cells (ADSCs) [8, 9]. Both cells can be induced to differentiate into mesenchymal lineage: osteoblast, adipocyte, and chondrocyte. Compared to BMSCs, ADSCs have the disadvantage of being relatively difficult to induce osteogenesis and chondrogenesis [7]. However, ADSCs are attracting attention as a cell source for tissue engineering because ADSCs have the advantage of being easily harvested by a non-invasive method [10].

2.2 Extracellular matrix

Extracellular matrix (ECM) is assembly of secreted molecules that constitute the cell microenvironment [1]. It is composed of collagens, glycosaminoglycans, proteoglycans, and growth factors *etc* [11]. Role of ECM is much more than just structural support. ECM composition and mechanical properties differ according to location and health state *in vivo* [12]. Cells respond to the physical factors of ECM by interaction between integrin binding and cytoskeleton. Integrins are heterodimer receptors having 18 α subunits and 8 β subunits that assembled into 24 combinations. Different combinations of integrin dimer are used to bind different ECM molecules and enable transmission of different signaling in cell [13]. By active interaction between cell and ECM alter the cell behaviors like migration, differentiation, proliferation *etc.* Therefore, in order to understand the microenvironment of cells, it is essential to focus on ECM.

2.3 Collagen

"Collagen" is a generic term for extracellular proteins that 3 strands of α-chain are assembled to form triple-helix structure [14]. Twenty-eight types of collagen have been found, and they usaully have a repeating structure of Gly-X-Y (X and Y represent any amino acids, but usually proline and hydroxyproline) [15]. Among them, collagen type I is the main component of the connective tissue of organs such as skin, bones, tendon, ligaments, and eyes. The biggest difference between collagen type I and other components of the ECM is that collagen type I has a long fiber structure. Multiple strands of fiber can be bundled to produce a strong force like a ligament or tendon, and multiple cells can attach to same strand and transmit the pulling force to each other. Because of this, vertebrates can construct tissues

with higher stiffness in their body than invertebrates [2].

2.4 Alginate

Alginate is carbohydrate chain derived from seaweed that is one of the most widely used biomaterials because of its simple gelation method, hydrophilicity, and bioinert properties. Alginate is block copolymer containing blocks of (1,4)-linked β-D-mannuronate (M) and α-L-guluronate (G) residues. Hydrogel can be easily fabricated with addition of divalent cations to form intramolecular cross-linking between G-blocks [16, 17].

Exposure to $CaCl_2$ aqueous solution is a simple method, but it is mainly used for cell encapsulation to form beads because gelation occurs too quickly and forms a heterogeneous gradient shell [18]. $CaSO_4$ and $CaCO_3$ can be used as Ca^{2+} sources to slow the gelation rate with their low solubilities. Although these methods have the advantage of making a homogeneous gel, they can decrease cell viability because the cell culture medium cannot be added for a long reaction time [19-21]. In this study, $CaCl_2$ solution was used to form the alginate shell structure only on the outside.

2.5 Polydopamine

Polydopamine (PDA) coating is inspired by a mussel adhesive protein that promotes attachment to virtually any type of organic or inorganic material [22]. Repeating structure of dopamine and lysine residues in the Mytilus edulis foot protein-5 enables strong adhesion even in underwater environments. Dopamine polymerizes at an alkaline condition and form

a thin PDA layer. Amine and thiol groups can form covalent bond to the PDA. This reaction allows the biological material to be immobilized on the PDA-coated surface with a high degree of freedom. Therefore, it has been utilized in surface coating of microfluidics or biomaterials [23-25]

2.6 Mechanotransduction

Cells constantly interact with chemical and physical stimuli from surrounding microenvironment. Mechanotransduction is the process that cells respond to physical stimuli of microenvironment by changing their behaviors [26]. In particular, many studies have been conducted on whether specific physical stimuli can determine stem cell lineage in MSCs. In general, physical properties similar to the physical conditions of actual bone and adipose tissue induce the differentiation of cells into individual lineages.

Several key factors, cell spreading, stiffness, viscoelasticity, cell volume, cell-ECM interaction, etc. are proved to contribute to promoting osteogenesis above adipogenesis. In the opposite case, adipogenesis is promoted [27-29].

The main way for cells to sense these stimuli is the change in cell tension. When the cells firmly bind the adhesive ligand of the surrounding ECM, the force is transmitted to the nucleus through the cytoskeleton, leading to nuclear distortion. Through the expanded nuclear pore, the mechanosensitive Yes-associated protein (YAP) translocate from the cytoplasm into the nucleus [27, 30]. With observing YAP localization, it can be indirectly estimated how MSCs perceive their surrounding physical environment.

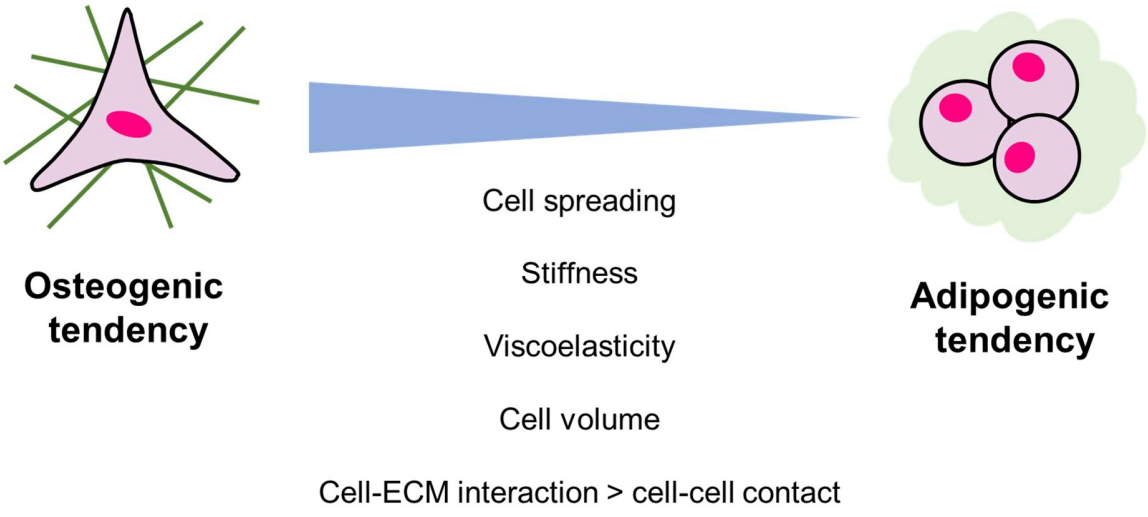

Figure 2.1 Physical factors discovered to induce mechanotransduction of mesenchymal stem cell

Chapter 3.

Experimental procedures

Chapter 3. Experimental procedures

3.1 Fabrication of window frame

Polydimethylsiloxane (PDMS; Dow Corning, Sylgard184) sheet measuring 1 mm in thickness was polymerized at 70 °C overnight. Holes measuring 3 mm in diameter were punched on the sheet (Figure 3.1A). Frame was coated with 2 mg/mL dopamine hydrochloride (Sigma, H8502) in pH 8.6 Tris (Sigma, T5941) solution overnight (Figure 3.1B). The manufactured frames were sterilized by UV and stored at room temperature until use.

3.2 Fabrication of hydrogel

Polyacrylamide (PA; Biosesang, AC4004-050-00) sheet measuring 1 mm in thickness was polymerized with ammonium persulfate (Sigma, 09913) and N,N,N′,N′-tetramethylethylenediamine (Sigma, T9281). PA sheet was incubated with cell culture medium and placed under the window frame. A mixture of 2 mg/mL collagen type I (Corning, Collagen I high concentration rat tail, 354249), 5 mg/mL sodium alginate (Sigma, A2033) and 500 cells/μL was neutralized with NaOH and 10× Hank's balanced salt solution (HBSS; Welgene, LB 203-03) at 4 °C (Figure 3.1C). Collagen-alginate mixture was poured in the frame 10 μL/hole and incubated at 37 °C for 30 min (Figure 3.1D). Hydrogels were incubated in amounts exceeding 10 mM $CaCl_2$ solution for 5 min and transferred to a cell culture medium (Figure 3.1E).

The polydopamine coating support hydrogel structure at the surface and PA sheet protect hydrogel from drying during 37 °C incubation. The PA sheet prevents PDMS frame from sticking to the cell cultureware (Figure 3.1F). In the absence of the PA sheet, hydrogel torsion occurs when lifting the frame with a tweezer and $CaCl_2$ solution is applied to only one side of the hydrogel (Figure 3.1G).

The preparation of collagen only hydrogel (C) was identical to CA-shell fabrication except for the addition of alginate and $CaCl_2$ solution. To prepare the CA-interpenetrating network (IPN) group, 1 M $CaCl_2$ was added to the gel solution by 1% (v/v) and mixed rapidly. The mixture was cross-linked simultaneously at 37°C for 30 min.

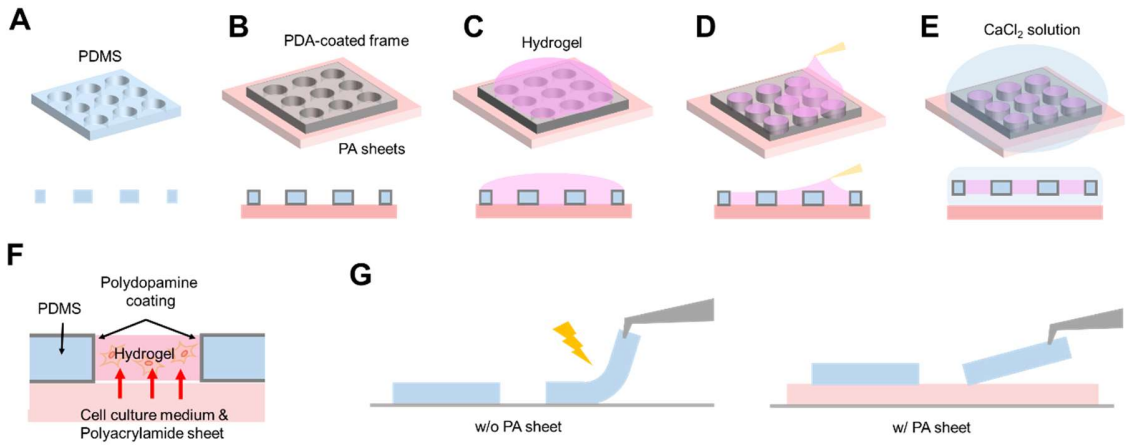

Figure 3.1 Schematic illustration describing the fabrication step of window frame and CA-shell hydrogel

3.3 Analysis of mechanical properties and morphology of hydrogel

3.3.1 Scanning electron microscopy and energy dispersive X-ray spectroscopy (SEM-EDS) analysis

Four groups of hydrogels were prepared without cells: C, CA-IPN, CA-shell-outside, and CA-shell-inside. Only one side of CA-shell hydrogel was exposed to $CaCl_2$ solution in the alginate cross-linking step, and the exposed side was defined as outside and the unexposed side was defined as inside. Hydrogels were fixed in cold 2.5% (v/v) glutaraldehyde in Dulbecco's phosphate-buffered saline (DPBS) for 24 h and washed for 30 min three times. Gels were serially dehydrated in diluted ethanol solution (30, 50, 70, 90, and 100% ethanol in DPBS for 30 min each, and then left in 100% ethanol overnight at 4°C. Hydrogels were completely dried in a vacuum chamber overnight. After drying, gels were coated with platinum and analyzed with a field emission scanning electron microscope (SEM; Jeol, JSM-7800F Prime). The Ca, C, and O content levels were analyzed via EDS analysis.

3.3.2 Young's modulus measurement

Young's modulus was measured in wet conditions using hydrogel disks measuring 10 mm in diameter and 2 mm in height. Hydrogel disks were incubated in DPBS overnight and placed on a spatula. The excess water was eliminated by absorbing the water with lens paper before measurement. The compressive force according to the change in height of the

hydrogel was measured with a tensile tester (Shimadzu, EZ-SX). Young's modulus was calculated from the slope at the initial linear region of the graph.

3.3.3 Rheological characterization

Viscoelastic properties of hydrogels were measured with a stress-controlled rheometer (TA Instrument, AR-G2) using a 10 mm steel plate. The rheometer gap was 850-1000 μm. A cylindrical hydrogel measuring 10 mm in diameter and 5 mm in height was fabricated using a PDMS mold (without coating, reagent volume 200 μl) and held at 37°C in 1× HBSS for 3 days before measurement. The hydrogel was loaded onto the plate with a stainless steel spatula and excess buffer was eliminated by a paper towel. Strain sweep was performed to confirm the linear elastic regime. Storage modulus (G') and loss modulus (G") of hydrogels were measured by oscillatory frequency sweep. An oscillatory frequency sweep was conducted at 0.5% strain in the frequency range from 0.62 to 10 Hz.

3.3.4 Diffusivity test

Hydrogels were incubated in transwell (Corning, 3413) for diffusivity test. During the fabrication step, 12 μg of fluorescein-conjugated bovine serum albumin (FITC-BSA) was added to the 200 μl hydrogel. In the CA-shell group, $CaCl_2$ solution was added only to the transwell bottom in contact with the surface of DPBS solution. The DPBS solution containing the released FITC-BSA from the hydrogel was collected for measurement and exchanged with new DPBS every hour. The quantification of FITC-BSA was performed at

495 nm excitation-525 nm emission wavelength using a TECAN plate reader (TECAN, SPARKTM 10M).

3.4 Cell culture

3.4.1 Maintain of ADSCs

ADSCs were purchased from Lonza (PT 5006) and used in the experiment from passages 4 to 6. Cells were cultured in Alpha Minimum Essential Medium (αMEM; Gibco, 32571036) supplemented with 10% fetal bovine serum (FBS; Biowest, S1520), 50 units/mL penicillin, 50 μg/mL streptomycin (PS; Gibco, 15140-122), 50 μg/mL primocin (Invivogen, ant-pm-1) and 5 ng/mL recombinant human basic fibroblast growth factor (bFGF; Peprotech, 100-18C). Cells were transferred to a new flask using 0.25% trypsin-EDTA (TE; Gibco, 25200-056) when cells reached 90% confluence. All cells were cultured in a humidified incubator at 37°C with 5% CO_2.

3.4.2 Induction of adipogenesis

Formulation of adipogenic medium (AM) used in chapter 4 and 5 was composed of αMEM supplemented with 10% FBS, 1% PS, 50 μg/mL primocin, 100 nM dexamethasone (Sigma, D4902) 200 μM 3-isobutyl-1-methylxanthine (IBMX; Sigma, I7018), 100 μM indomethacin (Sigma, I7378), and 1 μg/mL recombinant human insulin (Peprotech, 10-365). AM used in chapter 6 and 7 was slightly modified: αMEM supplemented with 10% FBS, 1% PS, 50 μg/mL primocin, rosiglitazone (TCI, R0106) 2 μM, 250 nM dexamethasone, 200 μM IBMX, 100 μM indomethacin, and 1 μg/mL recombinant human insulin. AM was replaced by adipogenic maintenance medium (AMM) after treatment of AM for 3 days. AMM was composed of αMEM supplemented with 10% FBS, 1% PS, 50 μg/mL primocin, and 1 μg/mL

recombinant human insulin. Cell culture in AM refers to induction of adipogenesis with AM for 3 days and change in culture medium to AMM.

3.4.3 Induction of osteogenesis

Osteogenic medium (OM) was prepared as αMEM supplemented with 10% FBS, 50 units/mL penicillin, 1% PS, 50 μg/mL primocin, 100 nM dexamethasone, 50 μg/mL ascorbic acid-2-phosphate, and 10 mM β-glycerophosphate (Sigma, G9422). The medium was refreshed every three days.

3.4.4 Fatty acid stimulus

Oleic acids (OA; Sigma, O1008) were conjugated with fatty acid free bovine serum albumin (FF-BSA; Biovision, 7921) before treated to cells. OA medium was prepared as 500 μM OA was conjugated with 1% (v/v) FBS and 2% (w/v) FF-BSA in Dulbesco's minimum essential medium (DMEM) for 10 min at 55°C. Cells were cultured in the OA medium for 7 days. To induce lipolysis, isoproterenol (TCI, I0260) is used to stimulate the cells with β-adrenergic agonist. 10 μM isoproterenol hydrochloride was treated to the cell for 24 h after OA treatment.

3.4.5 Pro-inflammatory cytokine treatment

Tumor necrosis factor α (TNFα; Peprotech, 300-01A) and interleukin-1β (IL-1β; Peprotech, 200-01B) were treated to mimic chronic inflammation observed in obese adipose

tissue. AMM or OA medium supplemented with 10 ng/ml TNFα and10 ng/ml IL-1β were indicated as inflammatory (INF) condition.

3.5 Characterization of cell behavior and differentiation

3.5.1 Quantitative reverse transcription-polymerase chain reaction (qRT-PCR)

Ten hydrogels were collected and pooled to extract RNA in 1 sample. Alginate was removed from the hydrogels including alginate by incubation at 37°C for 20 min in 0.02 M sodium citrate and 0.02 M EDTA solution. RNA was extracted using TRIzol (Invitrogen, 15596026). The cDNA was synthesized using a SuperiorScript III cDNA synthesis kit (Enzynomics, EZ405). qRT-PCR was performed using a SensiFAST SYBR (Bioline, BIO-92020) and StepOnePlus real-time PCR system (Applied Biosystems, 4376600). Primer sequences used in this study are listed in Table 3.1. The relative fold induction was calculated by $_{\Delta\Delta}$CT method. Human glyceraldehyde 3-phosphate dehydrogenase (*GAPDH*) gene was selected as housekeeping gene. Primers used in experiments were described in the table (Table 3.1).

Gene			Sequence (5' →3')	T_m (℃)	Product size (bp)
Housekeeping Gene	*GAPDH*	F	TTCACCACCATGGAGAAGGC	59.96	256
		R	TCTTCTGGGTGGCAGTGATG	59.67	
Osteogenic marker gene	*RUNX2*	F	GCGCATTCCTCATCCCAGTA	59.89	176
		R	GGCTCAGGTAGGAGGGGTAA	60.03	
	SPP1	F	GCCGAGGTGATAGTGTGGTT	59.75	261
		R	ATCTGGACTGCTTGTGGCTG	60.32	
	BGLAP	F	ATGAGAGCCCTCACACTCCT	59.96	254
		R	TCAGCCAACTCGTCACAGTC	59.97	
Adipogenic marker gene	*PPARG*	F	CGACCAGCTGAATCCAGAGT	59.47	85
		R	GGTCAGCGGGAAGGACTTTA	59.39	
	CEBPA	F	TATAGGCTGGGCTTCCCCTT	60.03	94
		R	AGCTTTCTGGTGTGACTCGG	59.97	
	CEBPB	F	TACTACGAGGCGGACTGCT	60.08	148
		R	GGTACGGGCTGAAGTCGATG	60.53	
Pluripotency and proliferation marker gene	*SOX2*	F	ACCAGCGCATGGACAGTTAC	60.67	187
		R	TAGGTCTGCGAGCTGGTCAT	60.68	
	MYC	F	TACAACACCCGAGCAAGGAC	59.97	189
		R	AGCTAACGTTGAGGGGCATC	60.11	
	CDK1	F	CTGGGGTCAGCTCGTTACTC	59.83	170
		R	TCCACTTCTGGCCACACTTC	59.89	
Lipid deposition-related marker gene	*CD36*	F	AGTTCTCAGCTGCTATGCCG	60.18	158
		R	CTCAGCGTCCTGGGTTACAT	59.46	
	GLUT4	F	CGTCTCCATTGTGGCCATCT	60.11	140
		R	TCCAGTTGGAGAAACCAGCC	59.89	

Table 3.1 Sequence of primers used in qRT-PCR.

3.5.2 Immunocytochemical analysis (ICC)

Hydrogels were fixed with 4% paraformaldehyde in PBS (phosphate buffered saline) for 30 min. Cells were permeabilized with 0.25% Triton-X 100 diluted in 0.1% (v/v) Tween 20 in PBS (PBST) solution for 1 h at room temperature. Samples were blocked with 3% (w/v) bovine serum albumin (BSA) in PBST for 1 h. PPARγ (Merch, ABN1445), RUNX2 (Santacruz, sc-390351), and YAP (Santacruz, sc-101199) primary antibodies were diluted 1:1000 to 1% (w/v) BSA in PBST solution. Samples were incubated in primary antibody solution at 4°C overnight. After 1 hour washing at room temperature, the samples were treated with the secondary antibodies diluted in 1% BSA in PBST for 1 h at room temperature. Cells were stained with 3 ng/mL 4',6-diamidino-2-phenylindole (DAPI) and diluted in 1:1000 Alexa 594-conjugated phalloidin or Alexa488-conjugated phalloidin (Invitrogen, A12381, A12379) in PBST for 30 min. 4,4-Difluoro-1,3,5,7,8-Pentamethyl-4-Bora-3a,4a-Diaza-s-Indacene (BODIPY; Invitrogen, D3922) was used as a lipid probe diluted in 2 μg/mL DPBS to stain the samples for 30 min. Between every step, samples were washed at least 3 times with PBST. Hydrogels were observed using a confocal laser scanning microscope (Carl Zeiss, LSM710) installed at the National Center for Inter-university Research Facilities (NCIRF) at Seoul National University.

3.5.3 Calculation of protein intranuclear localization ratio

Staining procedures were same with the immunostaining methods. For the quantification of YAP and RUNX2 intranuclear localization, the fluorescence of the stained YAP in nuclear and cytoplasmic locations was determined with DAPI and phalloidin. The

image with the largest cross-section of the nucleus in the Z-stack image was selected for analysis. Subregions were selected in the nuclear and cytoplasmic locations. Fluorescence intensity was measured by ImageJ software. The nuclear/cytoplasmic ratio was calculated by dividing the average intensity of protein in the nuclear subarea by the average intensity of cytoplasmic subarea [29].

3.5.4 Cell contraction inhibition

ADSCs were cultured in OM. Cells were treated with 10 μM Y27632 (ROCKi; STEMCELL Technologies, 129830-38-2) and 20 μM blebbistatin (Bleb; Peprotech, 8567182). The inhibitor concentrations were determined based on the preceding studies [31-33]. The normal group includes cells cultured for 27 h in OM. Day 0+ group represents cells treated with the inhibitor for 27 h since the hydrogel fabrication. Day 1+ group contains cells cultured for 24 h in OM first and treated with inhibitor for an additional 3 h.

3.5.5 Quantification of double strand DNA (Picogreen assay)

Samples were digested with 40 μl of digestion buffer (0.1 mg/ml proteinase K (Invitrogen, AM2542), 100 mM NaCl, 1 mM EDTA, 10 mM Tris-HCl, pH 7.4, and 0.5% (w/v) sodium-dodecyl sulfate (SDS) in double distilled water (DDW)) for 24 hr at 50°C. The concentration of double strand DNA (dsDNA) was measured using a PicoGreen™ dsDNA Assay Kit (Invitrogen, P11496) according to the manufacturer's instructions.

3.5.6 Quantification of triglyceride

Triglyceride colorimetric assay kit (Cayman, 10010303) was purchased and assay procedure was modified. Triglyceride in hydrogel samples was dissolved out by NP40 substitute assay reagent included in assay kit. The sample was placed in the NP40 solution, and the heat cycle of 80℃ 5 min and 4℃ 5 min was repeated three times. Enzymatic hydrolysis of triglyceride was performed according to manufacturer's instructions.

3.5.7 Oil red O staining and quantification of stained fat

Oil red O staining was performed according to the established protocol [34]. The hydrogel samples were fixed with 4% paraformaldehyde in PBS for 30 min and washed with DPBS. Hydrogel samples were incubated in 60% (v/v) isopropanol in DDW for 30 min. The 3.5 mg/mL Oil red O in 100% isopropanol was mixed with DDW in a ratio of 6:4 and filtered. The samples were stained with Oil red O working solution for 30 min and washed with DDW at least 3 times. For quantification, 30 hydrogel samples were collected and pooled as a single sample. Samples were dried first to exclude the factors based on the volume difference between groups, and dissolved in 300 μl of 100% isopropanol for 1 h. The absorbance of Oil red O was measured at 520 nm with TECAN plate reader. As a blank, the same amount of hydrogel without cells was stained similarly and dissolved.

3.6 Statistical analysis

All quantitative analyses were expressed as mean ± standard deviation or mean value with box plot. Gray squares marked in the box plot indicate the mean value. The statistical significance was determined by analysis of variance (ANOVA) and unpaired t-test using SPSS software. Post-hoc tests were performed; Tukey test for groups with equal variance and Tamehane T2 test for groups with unequal variance. Statistical significance is indicated in the graph with with *, **, and *** representing $p < 0.05$, $p < 0.01$, and $p < 0.005$, respectively. Word ‘ns’ indicates ‘non significant’

Chapter 4.

Prevention of collagen contraction

without losing its physical properties

Chapter 4. Prevention of collagen contraction without losing its physical properties

4.1 Introduction

Collagen is the most abundant protein in the extracellular matrix of mammals and has a great effect on various cell behaviors including adhesion, differentiation, and migration. However, it is difficult to utilize collagen gel as a physical scaffold *in vitro* because of its severe contraction. Decrease in the overall hydrogel volume induces changes in cell distribution, and mass transfer within the gel. Uncontrolled mechanical and physiological factors in the fibrous matrix result in uncontrolled cell behaviors in the surrounding cells.

To improve the mechanical strength and stability of collagen as a cell culture platform, additional covalent bond formation of gel has been attempted using glutaraldehyde, 1-ethyl-3-(3-dimethyl aminopropyl) carbodiimide hydrochloride (EDC) and genipin [35-39]. However, the excessively cross-linked collagen differs structurally from natural collagen and alters the gel degradation rate or mechanical properties, in addition to increasing the risk of cytotoxicity [40].

Further attempts have been made to control the mechanical properties by forming IPN with other materials. One of the most frequently used hydrogels is alginate that is obtained from seaweed, which undergoes rapid gelation via cation addition. The IPN hydrogel was manufactured by mixing the collagen, alginate, and Ca^{2+} ion sources such as $CaCl_2$, $CaSO_4$,

or $CaCO_3$ [20, 21, 41, 42]. IPN hydrogel also has a limitation in that it brings a difference from the properties of the pure collagen hydrogel.

In this study, two strategies were used to minimize the contraction of collagen gel. A disk-shaped frame made of PDA-coated PDMS frame prevented horizontal contraction at the edge of the hydrogel (Figure 4.1A). The sequentially cross-linked collagen gel with alginate outer shell (CA-shell) structure inhibited the vertical gel contraction (Figure 4.1B). The combined method synergistically prevented the hydrogel from shrinkage in long-term 3D cell culture. The physical properties of the hydrogel fabricated in this study were similar to that of pure collagen gel but completely changed the cell behavior within the gel by inhibition of gel contraction. The platform can be used to broaden our understanding of the fundamental mechanism underlying cell-matrix interactions and reproduce extracellular matrix *in vivo*.

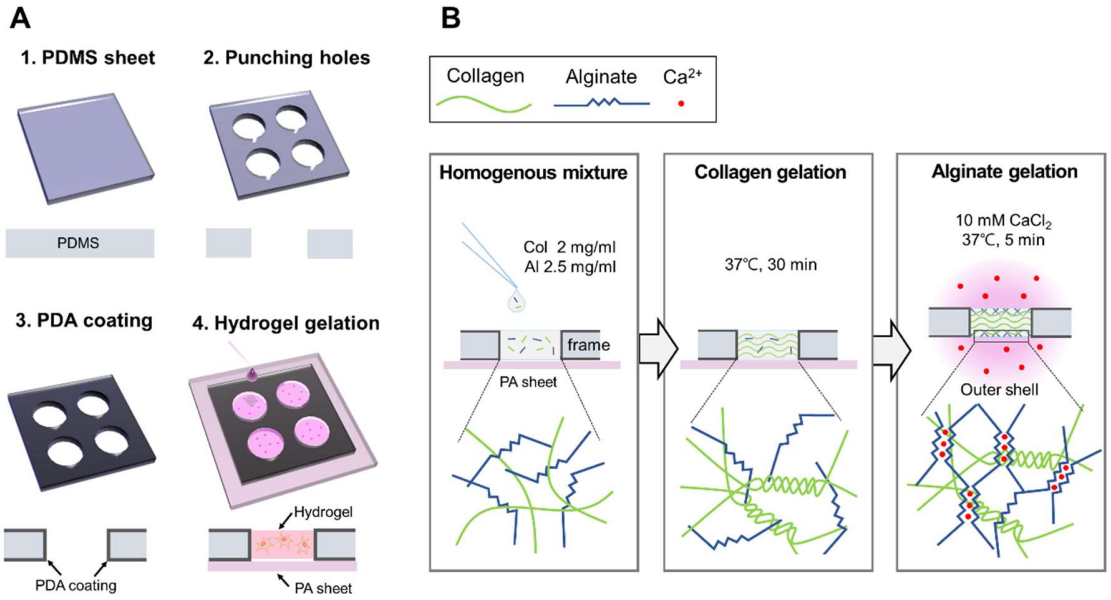

Figure 4.1 Fabrication of a window frame for preventing horizontal collagen contraction and hydrogel with alginate outer shell (CA-shell) to prevent vertical collagen contraction

(A) Fabrication of window frame. The polydimethylsiloxane (PDMS) sheet with circular holes is coated with polydopamine (PDA). The coating on the wall of the cylindrical hole prevents radial shrinkage of the hydrogel. The frame is placed on the polyacrylamide (PA) sheet absorbing HBSS buffer to prevent hydrogel drying and torsion during the preparation step.
(B) Sequential gelation for fabrication of CA-shell hydrogel. A mixture of collagen, alginate, and cell was incubated initially to induce collagen fiber self-assembly. Next, hydrogel was exposed to $CaCl_2$ solution resulting in the formation of cross-linked alginate outer shell.

4.2 Effect of polydopamine and alginate on collagen contraction

It was investigated whether the contraction of the collagen hydrogel could be prevented using the alginate outer shell and the window frame. In preliminary test, the contraction level of collagen hydrogel was higher when ADSCs were cultured in OM than in AM (Figure 4.2A). Therefore, the subsequent experiments were performed in OM unless otherwise stated. Polymerization of C or CA-shell hydrogel in a non-coated frame leads to contraction and detachment of hydrogels from the frame within a day. By day 7, the shrunk C group hydrogels lost transparency and appeared as black aggregates under a bright-field microscope (Figure 4.2B). Addition of the alginate outer shell decreased the degree of shrinkage or even prevented it partly. The average size of hydrogel was reduced to 7% in the C group and 28% in the CA group on day 7 (Figure 4.2C). Subsequently, the size was no longer reduced and remained constant (data not shown).

The use of frames prevented the CA group from gel contraction (Figure 4.2D). When the edge of the CA group was observed, cell densities differed between the edge and the inner region of hydrogel even on day 1. By day 7, the edge of the hydrogel was condensed into a dense cell wall (indicated by white arrow) and the cell density was substantially different from the cell density of the initial hydrogel. However, there was no difference in the cell distribution at the center and the edge of CAF group, even on day 30.

The physical appearance of CF and CAF groups were compared to investigate whether the contraction of collagen hydrogel could be prevented with the frame alone. In the CF group, most of the hydrogels were detached off the frame and the contraction occurred in a day (data not shown). The undetached hydrogel samples were selected and analyzed. Cell distributions

both at the hydrogel center (C side) and at the hydrogel the edge connected to the frame (E side) were visualized by DAPI staining (Figure 4.2E). Z-stack images of the hydrogels were observed in the side view. In the CF group, the vertical thicknesses of the gel on the C side and the E side were considerably non-uniform, indicating that vertical contraction occurred at the C side like a concave lens. On day 14, the thickness of C side was approximately 3-fold less than that of the E side in the CF group. In contrast, the CAF group showed a relatively homogeneous cell distribution even on day 14. It was confirmed that the alginate outer shell combined with the window frame prevent collagen contraction.

This result of blocking the contraction of the collagen hydrogel only by physical force (by frame only) was similar to the results of the previous studies that prevented the contraction of the collagen hydrogel using a micropillar system [33, 43]. By penetrating the hydrogel with the micropillar, the contraction in the direction opposite to the axis of the pillar could not be prevented, and the cells were aligned in the direction of contraction. However, by using alginate and frame together in this thesis, omnidirectional contraction was prevented and cells were maintained in a not aligned state in the hydrogel.

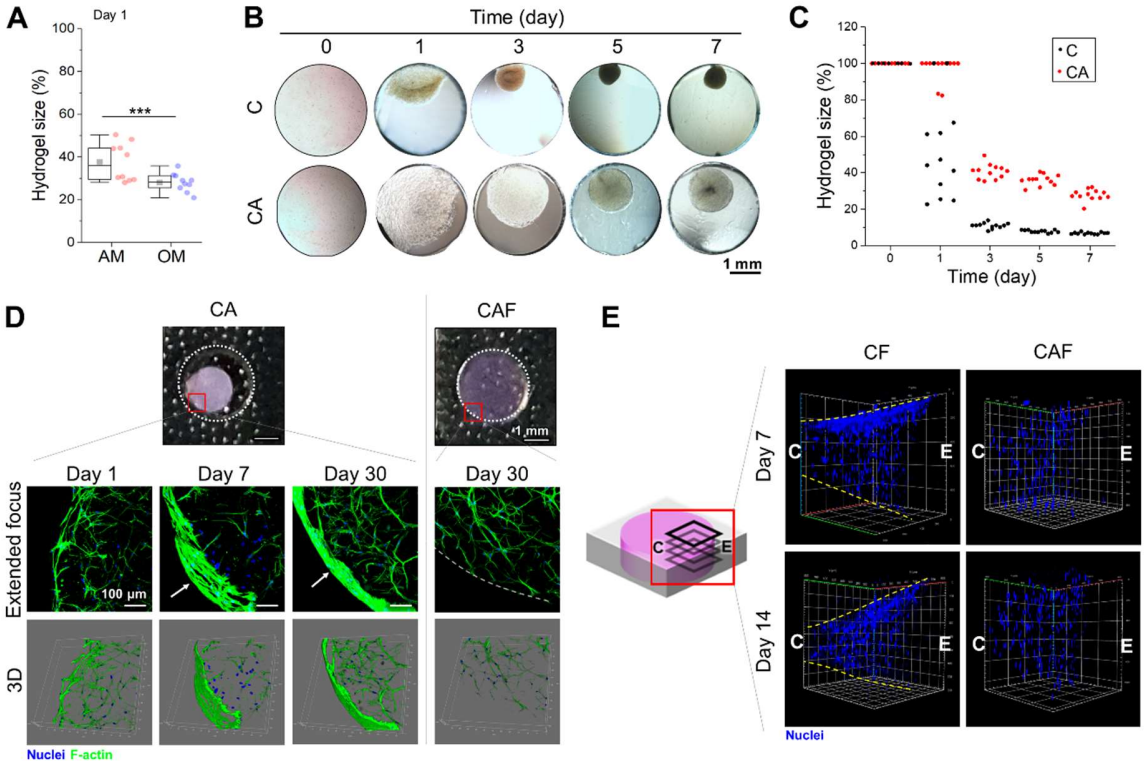

Figure 4.2 Synergistic effect of alginate outer shell and window frame on prevention of collagen contraction.

(A) Difference in contraction between the ADSCs cultured in AM and OM for 24 h. ADSCs had a stronger tendency to contract the gel in the OM than AM. The contraction levels were normalized with an initial hydrogel size of 100% (n = 10).

(B, C) Effect of alginate on gel contraction (without the frame). Hydrogels were prepared in a non-coated frame. (**B)** Representative images of hydrogel contracting over time. (**C)** Quantification of C and CA hydrogel size decreasing over time (n = 12).

(D) Change in cell distribution within CA hydrogel depending on the existence of window frame. Cells were condensed at the edge of hydrogels in the CA group. White arrows indicate cell aggregate formation at the hydrogel edge. White dashed line in CAF image indicates the border line between hydrogel and frame.

(E) Vertical contraction of the hydrogel under confocal microscopy. Nuclei were stained (DAPI, blue). C and E marked in the image indicate the center of hydrogel and the edge of hydrogel, respectively. Yellow dashed lines indicate the outline of hydrogel

4.3 Effect of cell culture conditions on hydrogels

It was investigated whether the crosslinking of alginate in the hydrogel could be gradually induced only with Ca^{2+} included in the cell culture media. When $CaCl_2$ solution was not added separately, alginate was not sufficiently crosslinked with cations in the medium. and could not inhibit the contraction of CA. The degree of contraction was almost similar to that of the C group, and it seems that existence of alginate only did not contribute to inhibit the contraction (Figure 4.3A).

It was investigated whether the window frame fixed the gel even when physical force was used. The CF hydrogels without cell were observed after 24 h in a rocker and shaking incubator (Figure 4.3B and C). None of the hydrogels was detached in a rocker. In a shaking incubator at 100 rpm, which is the speed of organoid cultivation, all hydrogels were attached to the frame for 24 h [44]. The window frame appears to support hydrogel appropriately even under practical conditions upon application of shear stress or agitation.

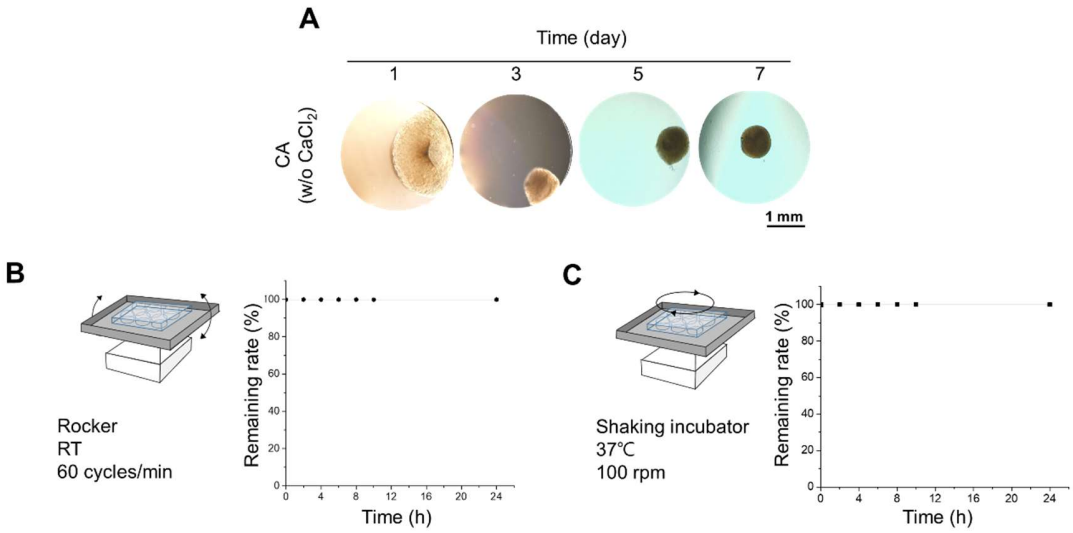

Figure 4.3 Effect of Ca^{2+} and physical shocks applied during the cell culture environment on the hydrogel.

(A) Effect of cations included in cell culture media to CA hydrogel contraction. In order to analyze the effect of divalent ions present on the medium on alginate crosslinking, CA gel was fabricated without the addition of $CaCl_2$ solution. CA w/o $CaCl_2$ group showed a similar contraction profile with C group in Figure 4.2B.

(B, C) Hydrogel detachment test using physical forces such as rocking and shaking. CF hydrogels without cells were used in the tests (n = 25).

4.4 Characterization of hydrogel composition

The internal composition and physical properties of the CA-shell hydrogel were investigated. Pure collagen hydrogel (C group) and a collagen-alginate interpenetrating polymer network hydrogel (CA-IPN) fabricated via homogeneous collagen-alginate cross-linking were compared as a control group. The hydrogel surface morphology was observed by SEM. In the C group fibers, stripes in a direction perpendicular to the axis of the fiber were observed at 50000× (Figure 4.4A, bottom), representing collagen fibril formation and a homogeneous gelation of collagen via self-assembly [45, 46]. The stripe pattern of the collagen fiber was also observed at the CA-IPN group and inside of the CA-shell group. In some regions of CA-IPN and outside of CA-shell, ribbon-like structures were observed (50000×, white dashed line), which look like crystals formed by the reaction of Ca^{2+} and phosphate ion in media [47]. These results suggest that Ca^{2+} ions are concentrated on the outside of CA-shell hydrogel, with composition inside similar to the collagen only hydrogel, forming a double-layered structure.

Energy dispersive spectroscopy (EDS) was conducted to corroborate this hypothesis. The CA hydrogels fabricated were separated from the frame after incubation overnight in DPBS w/o Ca^{2+} and Mg^{2+}, and the middle layer was cut out in the direction of the vertical axis of the disk-shaped gel and dried (Figure 4.4B). The weight percentage of Ca in the CA-IPN gel of the entire line scan of the hydrogel was almost four-fold higher than that of CA-shell (Figure 4.4C). Besides, the vertical distribution of Ca in CA-shell showed that Ca cps (count per second) was high on the outside surface of hydrogel. However, Ca cps decreased with a steep gradient toward the inside of the gel. (Figure 4.4D) Based on these results, alginate

cross-linking was initiated outside the CA-shell and the formed shell inhibited the penetration of Ca^{2+} ions into the gel. These results are consistent with the surface morphology data presented in Figure 4.4A. Accordingly, the intra-sectional Ca distribution of the CA-shell group is predicted as the multi-layered form.

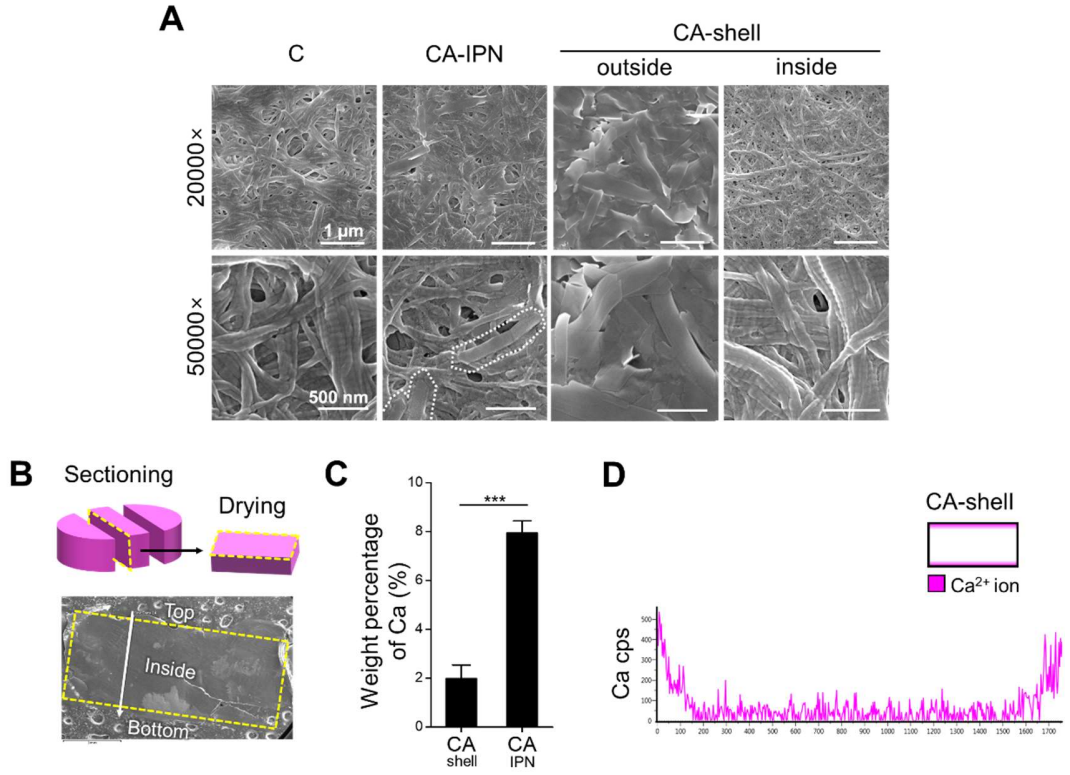

Figure 4.4 Concentrated Ca^{2+} ions on outer shell of CA-shell hydrogel.

CA-IPN groups were fabricated with simultaneous Ca^{2+} ion addition by mixing collagen and alginate. CA-shell groups were fabricated with subsequent Ca^{2+} ion addition after collagen gelation was completed.

(A) Scanning electron microscopic images of different types of hydrogel surface. In the CA-shell group, only one side of hydrogel was exposed to $CaCl_2$ solution in alginate cross-linking step, and the exposed side was defined as outside and the unexposed side was defined as inside. White dashed line indicates crystal-forming gelation in the presence of Ca^{2+}.

(B-D) Vertical distribution of calcium across the hydrogel from top to bottom. The Ca element distribution was analyzed by EDS. **(B)** Yellow outline indicates vertical cross-section of hydrogel and white arrow indicates line scan direction of EDS. **(C)** The graph shows the average weight percentage of Ca across the hydrogel line scan (n = 4). **(D)** Graph shows the amount of Ca existing across the line scan. Ca cps (count per second) decreased from the outside to the inside. The hydrogel structure based on the results is displayed on the right as a scheme.

4.5 Mechanical properties of hydrogels

To compare the mechanical properties of the gels between the groups, their Young's moduli and rheology were investigated (Figure 4.5A and B). Considering the similar gel composition, it is assumed that the inner region of CA-shell was similar to CA-w/o Ca^{2+} and the outer region of CA-shell was similar to CA-IPN. As a result, Young's modulus of CA-IPN was about 5-fold higher than that of the C group. CA-w/o Ca^{2+} showed no statistically significant difference with C group. The CA-shell group showed slightly higher modulus than the CA-w/o Ca^{2+} apparently due to the inhomogeneous composition of the CA-shell. The C, CA-w/o Ca^{2+}, and CA-IPN groups showed similar rheology.

Diffusivities of hydrogels were analyzed to confirm whether the cross-linked-alginate outer shell reduced the mass transfer as a physical obstruction during cell culture (Figure 4.5C and D). The amount of FITC-BSA diffused out was measured every hour. Details of the diffusivity experiment are described. Until the first 3 h, the cumulative amount of FITC-BSA of the C group was slightly higher, but it was reversed subsequently. After 8 h, the values reached saturation and the results were similar between groups. Consequently, the outer alginate shell did not interfere with mass transfer. CA-IPN hydrogel showed lower mass transfer efficiency than C or CA-shell hydrogels. These results indicate that a thin cross-linked alginate shell was formed as intended, and physical properties of inside were similar to pure collagen.

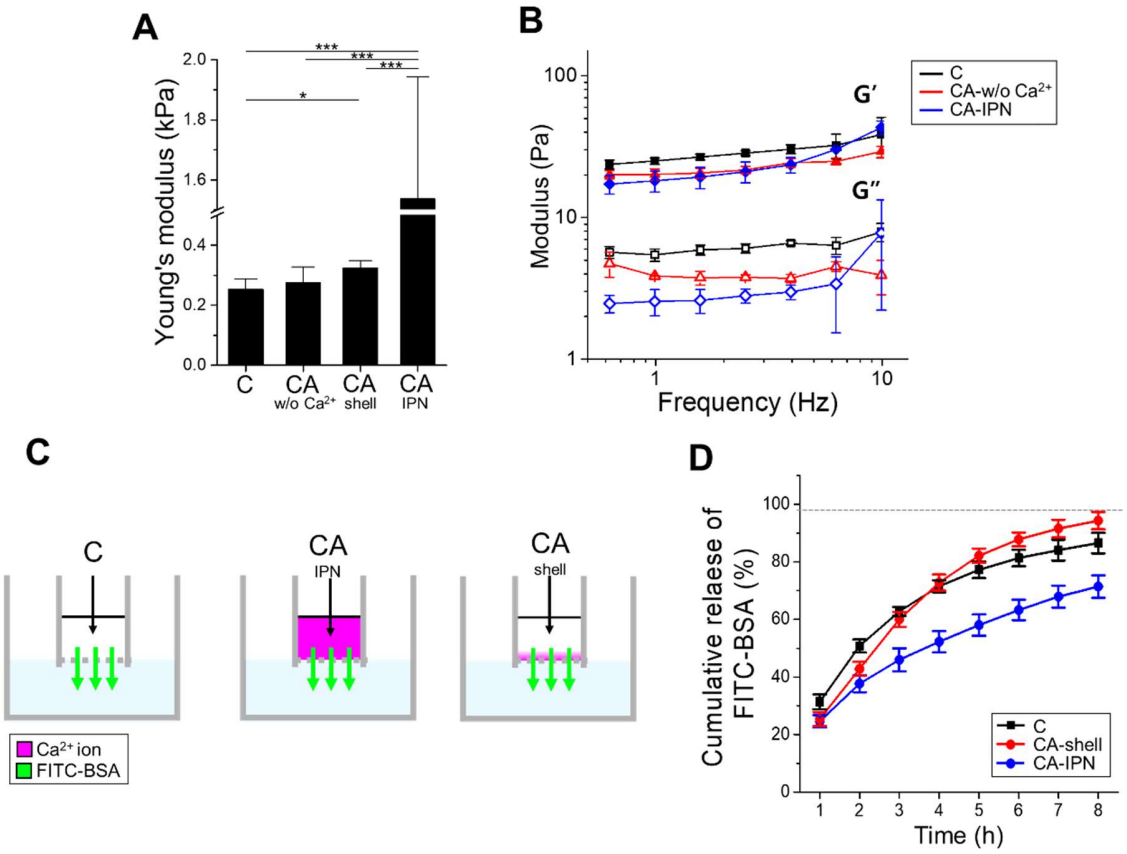

Figure 4.5 Mechanical properties of different types of collagen-alginate hydrogel.

(A) Young's modulus of the hydrogel. CA-shell group value was not significantly different from that of CA-w/o Ca^{2+} group (n = 3).

(B) Viscoelastic property of hydrogel. G' indicates storage modulus and G'' represents loss modulus. The CA-shell group was excluded from the rheology test due to its inhomogeneous structure leading to inconsistent measurements (n = 4).

(C) A schematic drawing showing the experimental design of the diffusivity assay.

(D) Diffusivity of hydrogel according to composition. FITC-BSA was homogeneously added in the hydrogel fabrication step. The DPBS in contact with the gel was exchanged every 1 h to measure the amount of diffused out FITC-BSA. The values were normalized with the total amount of FITC-BSA added initially to the hydrogel as 100% (n = 3).

4.6. Conclusions

The prevention of collagen hydrogel contraction is a challenging issue to be addressed. Hydrogel properties like adhesive ligand density, diffusivity, and stiffness, which are directly linked to cell functions, are altered by gel contraction. In this study, structural support for the collagen was developed using a PDA-coated frame and alginate outer shell that can prevent collagen contraction without significant changes in the gel's mechanical and structural properties. The collagen fabricated by sequential cross-linking with alginate generates a thin cross-linked alginate shell on the collagen externally, while the gel internal morphology and physical properties are similar to that of pure collagen.

Chapter 5.

Control of

human adipose tissue-derived mesenchymal stem cell lineage

by regulation of collagen contraction

Chapter 5. Control of human adipose tissue-derived mesenchymal stem cell lineage by regulation of collagen contraction

5.1 Introduction

As mentioned in this previous chapter, collagen hydrogels undergo rapid contraction by contraction force of ADSCs. The physical environment of the hydrogel is completely modified from the initial state during the contraction process. In this study, the effect of these changes on stem cell lineage determination was figured out in terms of mechanotransduction, using the platform developed in chapter 4. Human adipose tissue-derived mesenchymal stem cells (ADSCs) were induced adipogenesis and osteogenesis by chemicals included in induction media. In the freely contracting collagen hydrogel, stem cell lineage could not be controlled by chemical inducers and adipogenesis was promoted. On the other hand, the use of window frame and alginate outer shell allowed ADSCs differentiation towards the desired lineage by chemical induction. I hypothesized that this determination of cell fate is associated with mechanotransduction based on Yes-associated protein (YAP) localization. It was investigated whether the YAP nuclear localization was related to collagen contraction and can be controlled by the alginate outer shell and window frame.

5.2 Comparison of adipogenic and osteogenic gene expression profiles depending on the contraction

Adipogenesis and osteogenesis were induced in ADSCs embedded in the hydrogel to analyze the effect of contraction on cell behavior. The gene expression profile was obtained by qRT-PCR (Figure 5.2). Due to long-term culture limitations involving C or CF group with a high detachment rate, compared with CAF group, the experiment occurred until day 7. In the CF group, only the gels remaining on the frame were collected for analysis on day 7 (Figure 5.2A).

The expression of adipogenic marker genes including CCAAT/enhancer-binding protein β (*CEBPB*), CCAAT/enhancer-binding protein α (*CEBPA*), and peroxisome proliferator-activated receptor gamma (*PPARG*), and osteogenic marker genes including Runt-related transcription factor 2 (*RUNX2*), secreted phosphoprotein 1 (*SPP1*), and bone γ-carboxyglutamate protein (*BGLAP*) were compared between C, CF and CAF groups [48-50].

The CF and CAF groups showed significant differences ($p < 0.005$) in both adipogenic and osteogenic differentiation when compared with the C group (Figure 5.2B and C). There was no significant difference in the expression of adipogenic and osteogenic marker genes between CF and CAF groups. The C group showed a decreased expression in all marker genes except *PPARG*. The difference in relative fold induction between CF and C was higher than the difference between CF and CAF. Although the CF group can recapitulate the interaction between pure collagen and cells, they did not physically support the hydrogel long enough compared with the CAF group, as shown in Figure 5.2A. Therefore, it is necessary

to reproduce the stable culture conditions using the synergistic combination of alginate and PDA-coated frame.

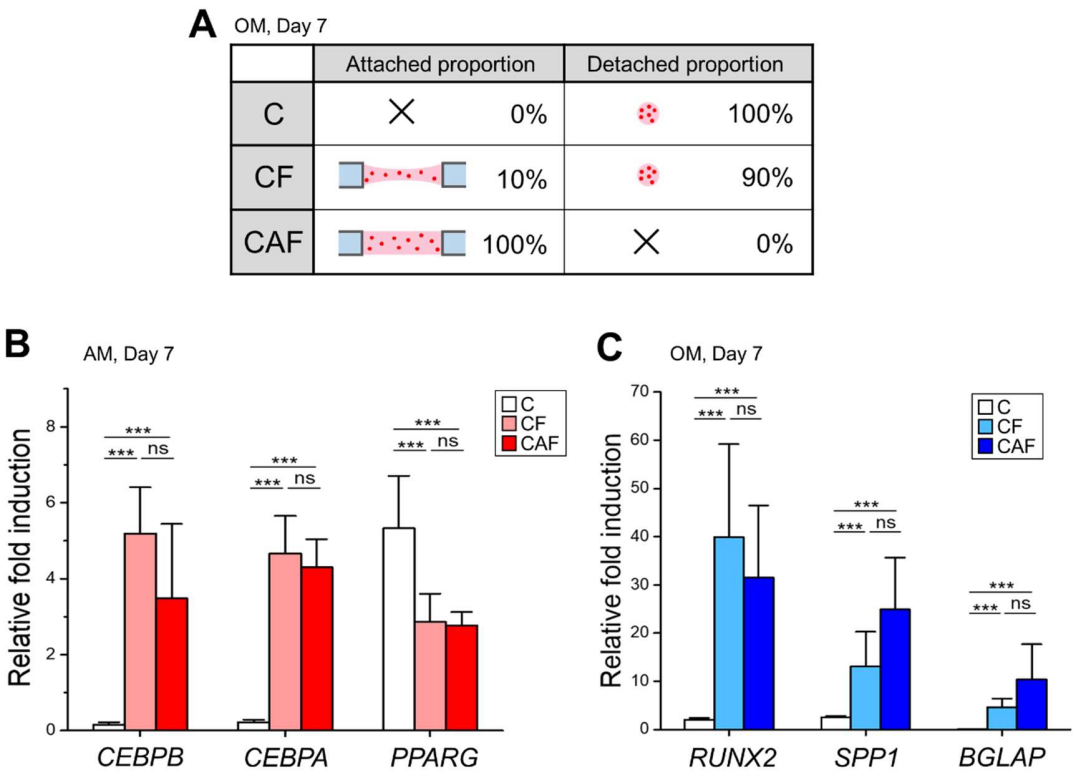

Figure 5.2 Cell lineage determination of ADSCs between adipogenesis and osteogenesis affected by collagen contraction.

ADSCs were embedded in hydrogel and cultured in OM and AM. Stem cell differentiation was analyzed by qRT-PCR. All data was normalized by each gene's relative fold induction of undifferentiated ADSCs.

(A) The attachment efficiency of hydrogel to the frame. Only 10% of CF hydrogel remained on the frame on day 7. Only CF hydrogel attached to the frame was collected to extract mRNA and represented graphically in B & C (n = 30).

(B) Adipogenic marker gene expression of cells cultured in AM. No statistically significant differences were observed between CF and CAF groups (n = 4).

(C) Osteogenic marker gene expression in cells cultured in OM. No statistically significant differences were observed between CF and CAF groups (n = 4).

5.3 Uncontrolled adipogenic tendency in C group regardless of differentiation induction medium

In addition to gene expression profile, the expression of RUNX2 and PPARγ proteins was investigated by immunostaining to determine whether the contraction of collagen hydrogel induced differentiation into mature osteoblasts or adipocytes. RUNX2 is a master regulator of osteogenesis, and its expression increases until the middle of bone differentiation period and undergoes intranuclear localization due to the nuclear matrix-targeting signal [51]. PPARγ is a master regulator of adipogenesis, and its expression increases steadily under progressive differentiation [49, 50].

RUNX2 protein in all groups showed intranuclear localization on day 7 regardless of the type of culture medium. The fluorescence intensity in the nuclear area of the CAF-OM group was relatively strong and showed clear contrast with cytosol compared with other groups (Figure 5.3.1A). To quantify the RUNX2 protein level in fluorescent images under different conditions, the ratio of RUNX2 mean intensities in nuclear/cytosol was calculated (Figure 5.3.1B). Only the CAF-OM group showed a significantly high value without significant differences between the remaining groups.

The fluorescence of PPARγ was intense in C group even in the OM whereas this protein was hardly expressed in CAF-OM (Figure 5.3.1C). When comparing the mean fluorescence intensity (MFI) of PPARγ among the groups, the MFI of the C group was significantly higher than that of the CAF group regardless of the type of culture medium (Figure 5.3.1D). The C-OM group showed lower RUNX2 intranuclear localization and higher PPARγ expression than the CAF-AM group.

LD (lipid droplet) deposition was observed in cells cultured for 14 days in the hydrogel suggesting differentiation into mature adipocytes. Hydrogels were stained by BODIPY and Oil red O to visualize lipid droplets (Figure 5.3.2A). Confocal microscopy revealed lipid droplet formation in C-AM, C-OM, and CAF-AM groups. Analysis of lipid deposition stained by Oil red O indicated LD formation overall in group C even in the OM. These data provide clear evidence demonstrating the role of uncontrolled gel contraction in inducing unintended cell fates. In CAF, however, few cells per unit area carry LDs. The overall lipid deposition inside the hydrogel was confirmed again at low magnification (Figure 5.3.2B). When the whole specimen was optically observed by Oil red O staining, LDs were formed throughout the hydrogel of group C. The Oil red O-stained LDs were quantified, and the number of LDs decreased as contraction was prevented by the window frame and alginate outer shell (Figure 5.3.2C). Quantification of LD results was consistent with PPARγ MFI data.

To explain the rationale for this high adipogenic tendency in C group, adipogenic marker gene expression profiles were analyzed in cells cultured both in AM and OM on days 3 and 7 (Figure 5.3.2D). Especially, the expression levels of *CEBPA* and *PPARG*, which are known to be expressed in late adipogenesis, were significantly high in C-OM group on days 3 and 7 [49]. It seems that this unintended high expression of adipogenic marker genes induces mature adipogenesis in ADSCs even in OM culture. The results established that the physical strain induced by shrinkage of the hydrogel plays a predominant role in cell lineage beyond the chemical differentiation induction by medium.

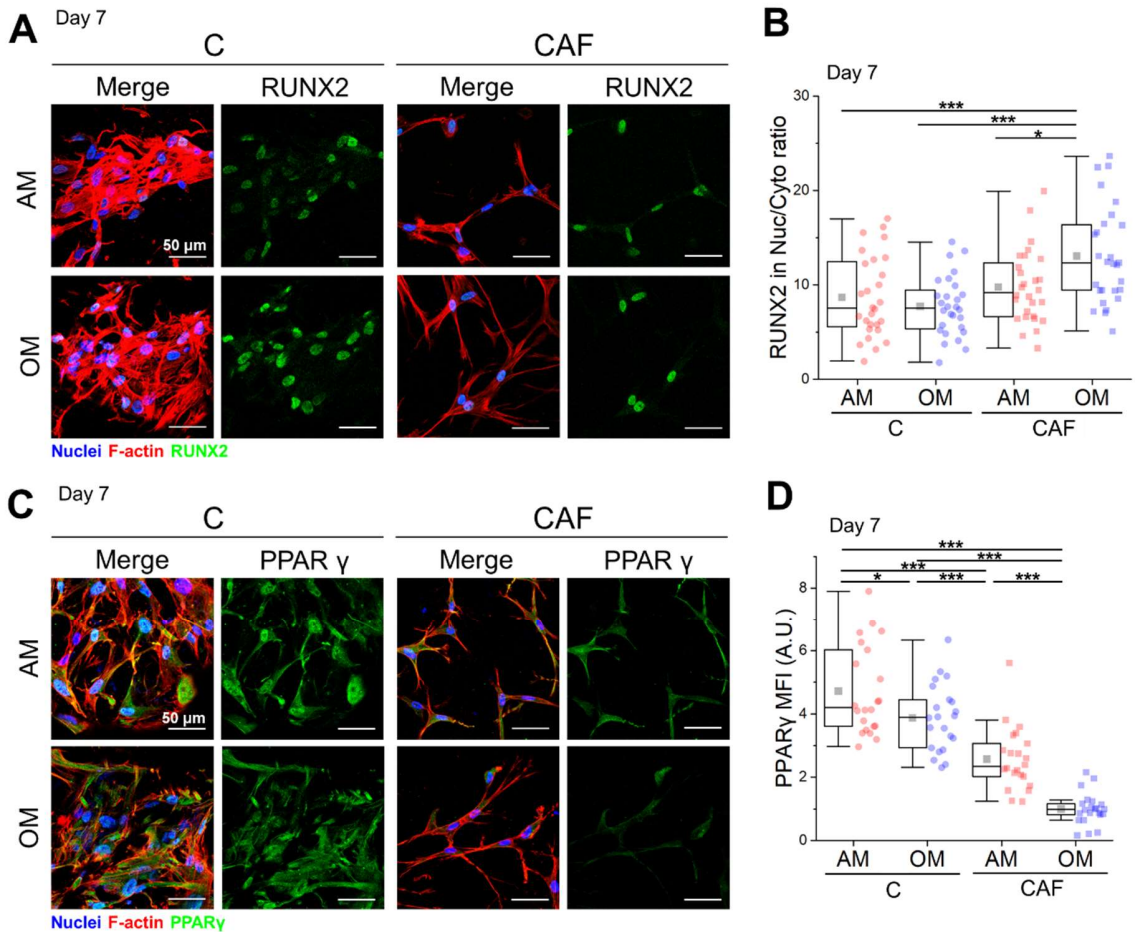

Figure 5.3.1 Expression and localization of RUNX2 and PPARγ in ADSCs

(A) Immunofluorescence images of RUNX2 in ADSCs of C and CAF groups cultured in AM or OM. RUNX2 proteins were localized in the nuclear area.

(B) Quantification of intranuclear localization of RUNX2 protein depending on the gel composition and the type of media on day 7 (n = 28).

(C) Immunofluorescence images of PPARγ in ADSCs of C and CAF groups cultured in AM or OM.

(D) Quantification of mean fluorescence intensity (MFI) of PPARγ protein depending on the gel composition and the type of media on day 7. MFI was measured in the nuclear area. All values were normalized with the mean value of CAF-OM (n = 22).

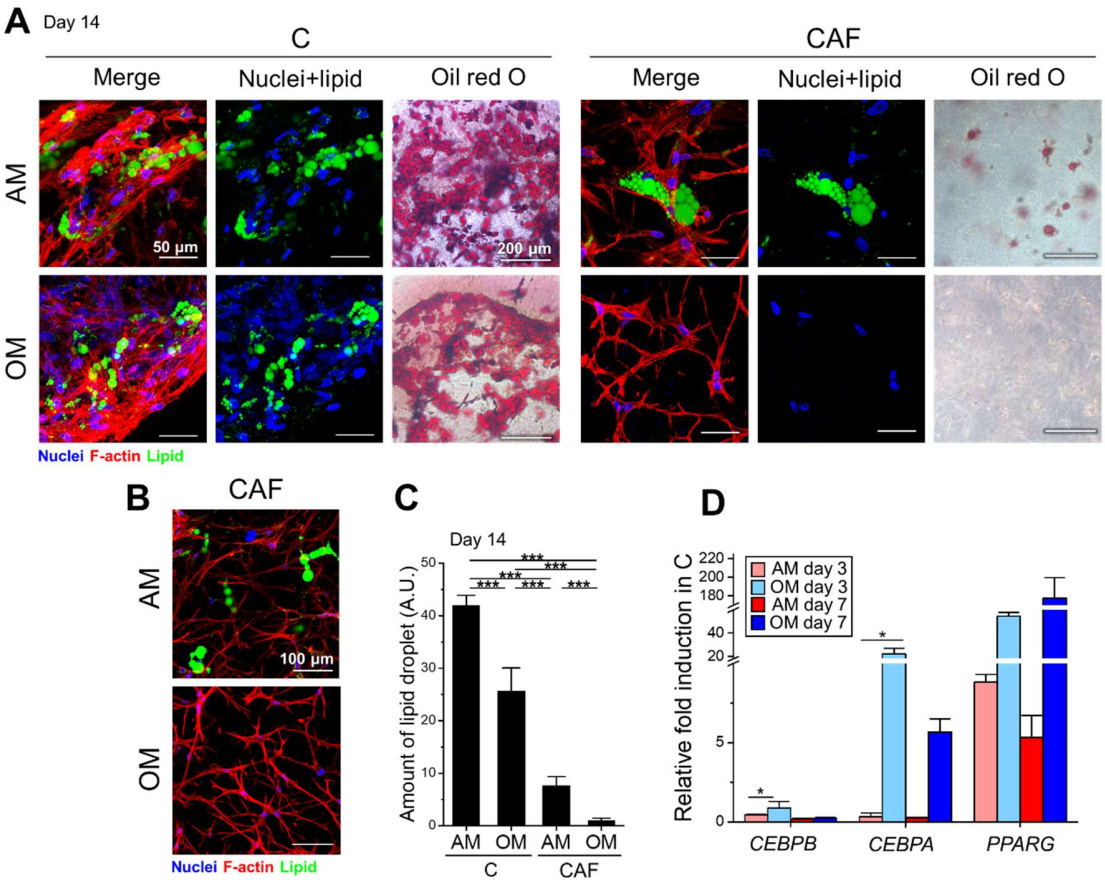

Figure 5.3.2 Comparison of adipogenesis of ADSCs depending on contraction

(A, B) Comparison of the LD deposition of ADSCs in C and CAF groups. **(A)** LDs were stained by BODIPY (green) in fluorescence image and Oil red O (pinky red) in bright field images. **(B)** Low magnification images of LD deposition in CAF group on day 14.

(C) Quantification of Oil red O-stained LD. All values were normalized with the mean value of CAF-OM group. The *p* values between all groups were < 0.005 (n = 3).

(D) The qRT-PCR results of C group's adipogenic marker genes on days 3 and 7. All values were normalized with the gene expression profile of non-differentiated ADSCs. Unless noted otherwise in graph, *p* value < 0.005 (n = 4).

5.4 Difference of YAP intranuclear localization between C and CAF groups

The cell differentiation induced by interaction with physical factors in the external environment is called mechanotransduction. The key regulator proteins of mechanotransduction include the Yes-associated protein (YAP)/transcriptional coactivator with PDZ-binding motif (TAZ). In general, cell shape, rigidity of ECM, and cell-ECM interaction promote osteogenesis and suppress adipogenesis. In this environment, YAP/TAZ enters the nucleus in stem cells and regulates downstream pathways to promote osteogenesis. In the opposite situation, YAP/TAZ is localized in the cytosol, and adipogenesis is induced [27, 29, 52] .

I hypothesized that changes in the ADSC differentiation are determined by collagen contraction based on the YAP/TAZ regulatory environment. The cells were cultured in a hydrogel for 1 day and observed, because the YAP localization due to the physical stimulus occurs within a few hours [53]. As mentioned above, the C group contracted significantly within a day and the cell density per unit gel volume was higher than in the CAF group. To exclude the effect of cell density, a low cell concentration group was included in the experiments to meet the similar cell-cell distance compared to that of CAF group on day 1. The cell concentrations in all groups except C-low group (125 cells/μL) were 500 cells/μL in the gel.

In the Z-stack images at day 1, the cell distributions in the C-Low group and CAF group were almost similar (Figure 5.4.1A). Hydrogel contraction in the C-Low group was relatively delayed than in C-High, but not inhibited. The hydrogel size in the C group was almost the same since 48 h (Figure 5.4.1B and C)

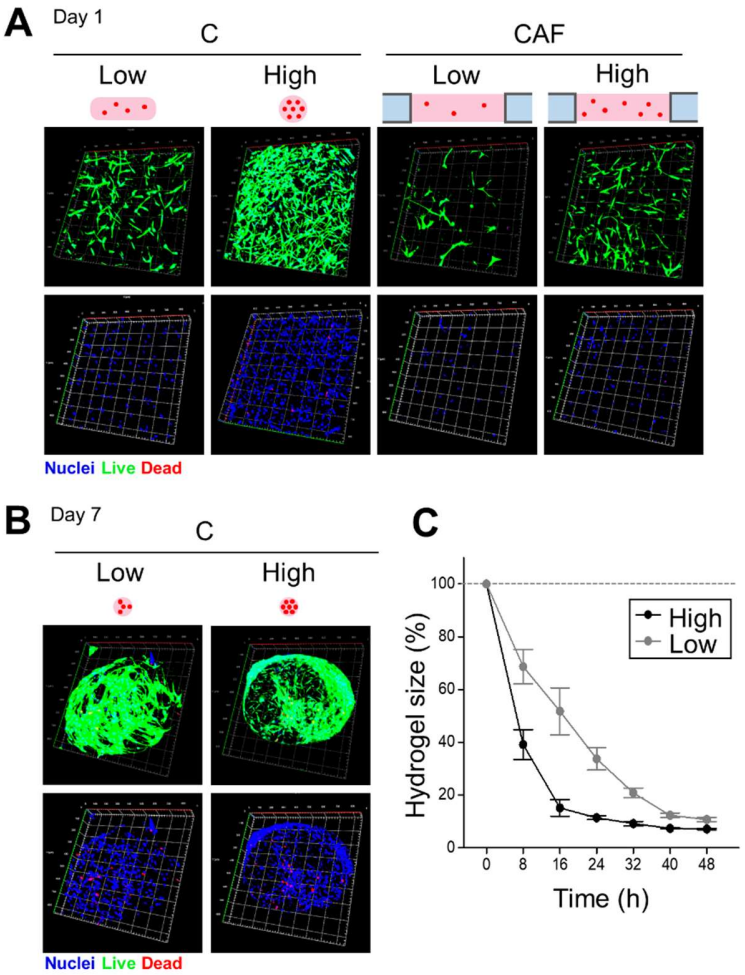

Figure 5.4.1 Effect of cell concentration on the cell distribution and hydrogel contraction

(A) Cell distribution in the hydrogel according to the cell concentration and the presence/absence frame.

(B,C) Changes in size of C group with different cell densities over time. The initial gel contraction of C-Low group was slow, but the final size of hydrogel reached the same level of C-High group after 48 h.

Monitoring of the hydrogel centers at 24 h and 48 h with a confocal microscope revealed the formation of a dense region of cell aggregates and a sparse region of cell network with a specific gap in both C-High and C-Low (Figure 5.4.2A). In the dense region of C-High group, most of the YAPs were localized in the cytosol on day 1 (Figure 5.4.2B). Cells adhered to each other to form a large mass in a dense group, which may contribute to high cell-cell interaction. The YAP localization was observed temporally in the C and CAF groups (Figure 5.4.2C). In C-High, cells spread completely at 16 h, and there was no noticeable change in YAP localization with time within each hydrogel group. However, the conspicuous nuclear localization of YAP was observed in CAF group at 24 h and lasted up to 48 h, which is indicated by white arrows.

To independently compare the effects of contraction on YAP localization between dense and sparse regions, a quantitative analysis of the YAP localization in two regions of C, CF and CAF groups was performed and compared separately. The YAP intranuclear localization increased as the contraction was prevented (Figure 5.4.3A). The CF group showed higher intranuclear localization tendency than the C-Low and C-High groups. Cells embedded in CF hydrogels were dispersed without forming cell aggregate-like dense regions in the C group (data not shown). As investigated earlier in CF group, the vertical contraction tends to occur in the center than at the fixed edge of the gel. To compare the effect of this heterologous structure, the outer portion within 500 μm from the frame was defined as the CF-edge, and the inner was defined as the CF-center. The intranuclear localization was higher at the edge than at the gel center. However, the YAP intranuclear localization ratio of CF was significantly lower than in the CAF group. The result that the localization of YAP was higher in the group that prevented contraction was consistent with the low levels of adipogenesis.

Based on results in Figure 5.4.2C, YAP localization in scattered cells over time was compared (Figure 5.4.3B). The localization ratio in C groups at the sparse region was higher than in the dense region regardless of cell concentration. The ratio of YAP localization at 24 h and 48 h in CAF was significantly higher than in C-High groups but there were no significant temporal variation in all groups.

The difference in YAP localization between C-dense and CAF can be explained by the differences in cell-cell interaction. However, the difference of YAP localization between scattered cells in C-sparse, CF, and CAF groups was associated with cell strain and cell contractile force. The cell contractile force and the ECM resisting tension interact and reinforce each other [54, 55]. However, in the freely contracting hydrogel, the cells become close as the cells pull the collagen fibers and the ECM resisting tension does not increase with cell pulling. The cell contractile force does not increase accordingly, and eventually cells get closer to form a cell aggregate.

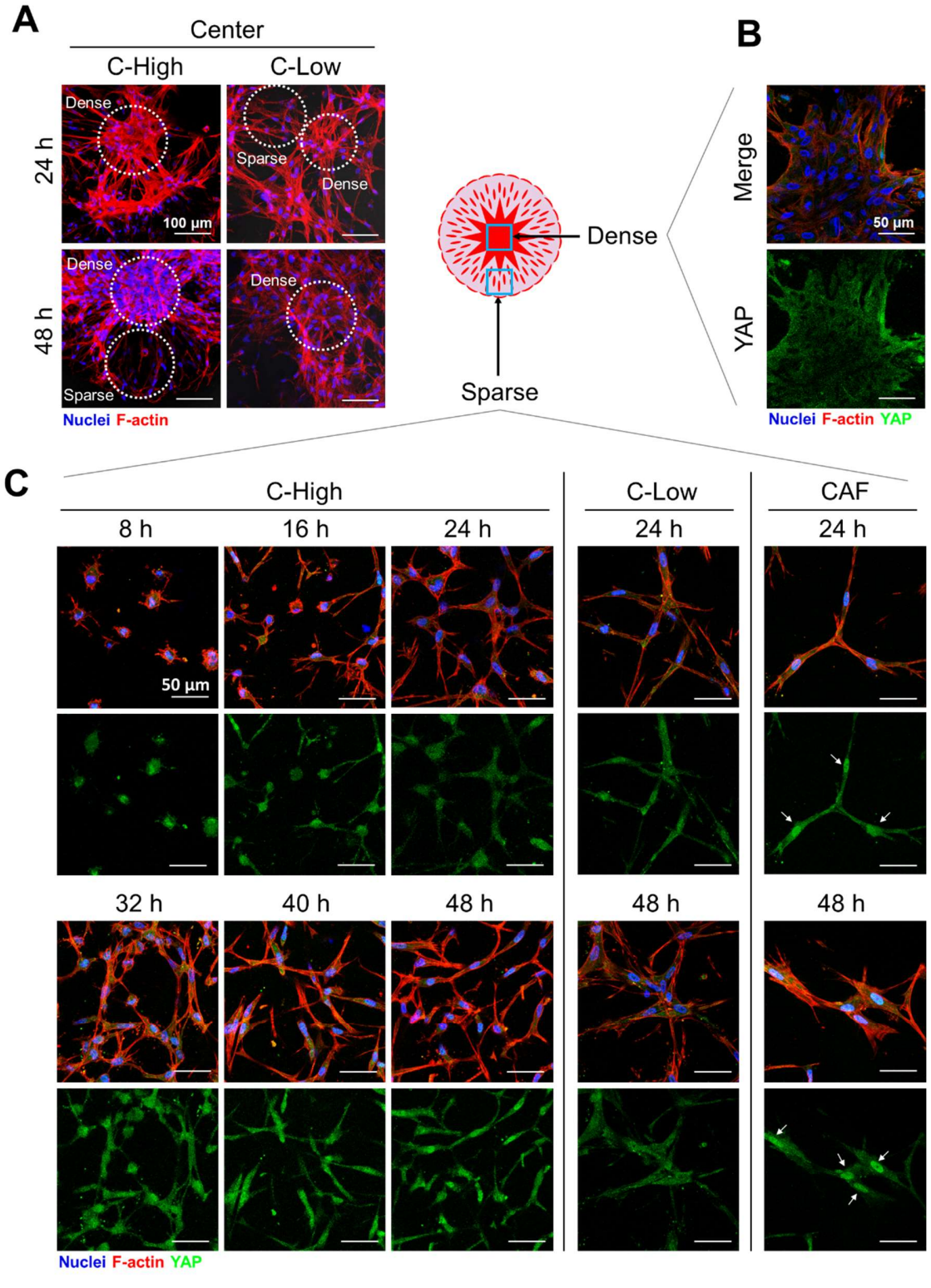
A
Center
C-High
C-Low
24 h
48 h
Dense
Sparse
100 μm
Nuclei F-actin
B
Merge
YAP
50 μm
Nuclei F-actin YAP
C
C-High
C-Low
CAF
8 h
16 h
24 h
32 h
40 h
48 h
50 μm
Nuclei F-actin YAP

Figure 5.4.2 YAP localization and cell distribution depending on the region, time, and cell density

(A) Heterogeneous cell distribution in C group regardless of cell density. Cellular aggregates were observed at the center indicated as 'dense' region, and single cell populations were observed at the edge of hydrogel indicated as 'sparse' region.
(B) YAP localization of dense region in C-High group mainly distributed in cytosol on day 1.
(C) Changes in cellular YAP distribution with single cell population over time. Cells were observed in the sparse region of C-High and C-Low groups. White arrows indicate YAP nuclear localization in cells observed in CAF group (24 h and 48 h).

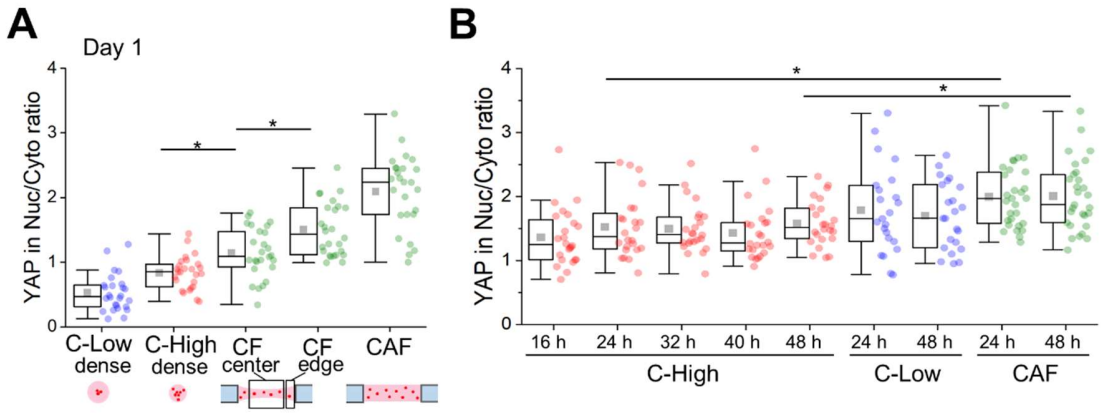

Figure 5.4.3 Intranuclear YAP localization ratio in ADSCs depending on the degree of contraction and time

(A) Intranuclear localization ratio of YAP under different gel conditions on day 1. The ratio was measured at the dense region in C group. In the CF group, cells located within 2 mm diameter were classified as CF-center and those at the sparse region located in the outer area were classified as CF-edge. Compared with the other groups, the CAF groups showed the highest YAP nuclear localization ratio. Unless noted otherwise in the graph, p value < 0.005 (n = 26).

(B) Time-dependent intranuclear localization ratio of YAP in single cells in the sparse region. Images based on Figure 5.4.2E were analyzed. The p values of groups were analyzed between 24 h and 48 h (n = 24 in C-High, n = 23 in C-Low, and n = 29 in CAF).

5.5 YAP intranuclear localization hindered by the inhibition of cell contraction

To demonstrate the effect of the cell contractile force, cell contraction inhibitors were used and the cellular YAP localization in C-sparse and CAF was compared. It is known that the contractile force of the cell cannot be transferred to the nucleus when cells are treated with a cell contraction inhibitor, Y27632 (ROCKi; Rho-associated coiled-coil containing protein kinase inhibitor) and blebbistatin (Bleb; myosin II ATPase inhibitor) [32, 33, 55, 56]. The Day 0+ group was treated with inhibitors since the cells were embedded in hydrogel, and the Day 1+ group was cultured in OM for 1 day, followed by treatment with the inhibitor for 3 h (Figure 5.5.1A). Unlike Day 0+ group, the hydrogel contraction and cell spread progressed normally and only the process of cell strain transfer to the nuclear membrane was blocked in the Day 1+ group (Figure 5.5.1B).

Bleb blocked the collagen contraction more effectively than ROCKi and prevented cell spread, especially in the C group (Figure 5.5.1C, Figure 5.5.2A and B). In the C group, the localization of YAP into the nucleus was generally decreased following inhibitor treatment compared with the C-normal group, but the YAP intranuclear localization ratio was exceptionally high in the C Bleb day 0+ group (Figure 5.5.2C). It is interesting to note that this result was obtained when mechanotransduction factors contributing to YAP localization, such as cell spread and cell-ECM strain, were blocked. Following the overall decrease of ratio with inhibitor treatment, the major factors affecting YAP localization of cells in the C-sparse and CAF groups were cell contractile forces to hydrogel strain. In comparison, among CAF groups, the YAP localization ratio was reduced by treating ROCKi and Bleb. In the

CAF ROCKi Day 1+ group, the decline in ratio was relatively small compared with other inhibitor groups, probably because ROCKi could not completely inhibit the cellular contractile force as much as Bleb (Figure 5.5.2A).

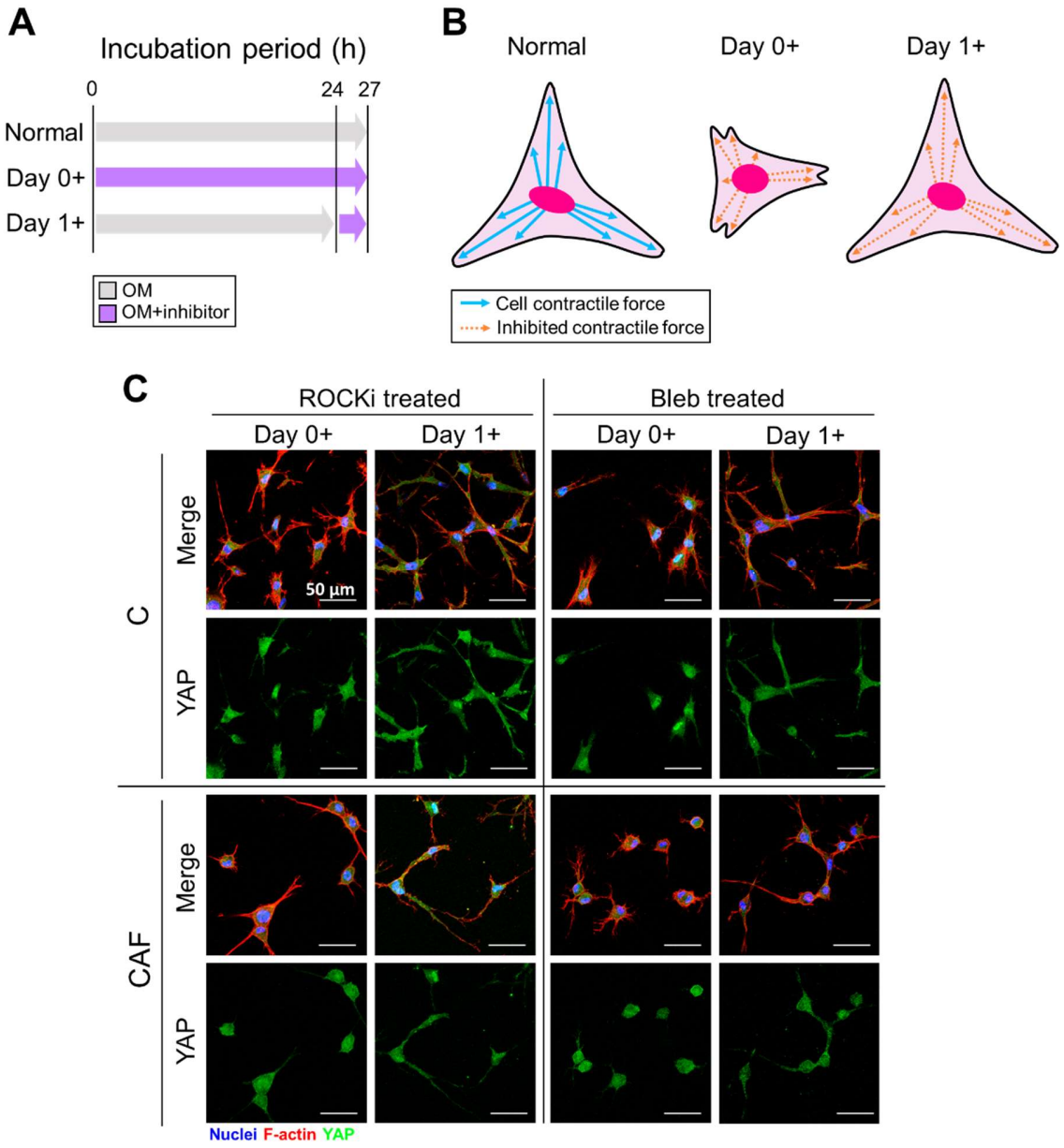
A
Incubation period (h)
0
24
27
Normal
Day 0+
Day 1+
OM
OM+inhibitor
B
Normal
Day 0+
Day 1+
Cell contractile force
Inhibited contractile force
C
ROCKi treated
Bleb treated
Day 0+
Day 1+
Day 0+
Day 1+
C
CAF
Merge
YAP
Merge
YAP
50 μm
Nuclei F-actin YAP

Figure 5.5.1 Effect of cell contraction inhibitor on cell morphology

In C group, only sparse region was analyzed. The cell contractile force in ADSCs was prevented with two inhibitors (10 μM ROCKi and 20 μM Bleb).

(A) Group design used in cell contractile inhibitor experiment. Normal indicates cells cultured without inhibitor. The Day 0+ group indicates the addition of inhibitors to the media immediately after embedding cells in the gel and the Day 1+ group represents cell treatment with inhibitors for 3 h after 24 h incubation of cells in the gel. All groups were analyzed at 27 h.
(B) Schematic of the changes in cell morphology and contractile force by inhibitors depending on the group. In Day 0+ group, cell spread, hydrogel contraction, and cell contractile force transfer are expected to be inhibited, while only cell contractile force transferred to the nucleus is expected to be inhibited in Day 1+ group.
(D) Immunofluorescence images of YAP localization affected by cell contraction inhibitors. In both Day 0+ and Day 1+ groups, inhibitors prevented the cell contractile force transfer and YAP nuclear localization was also prevented in both C and CAF groups.

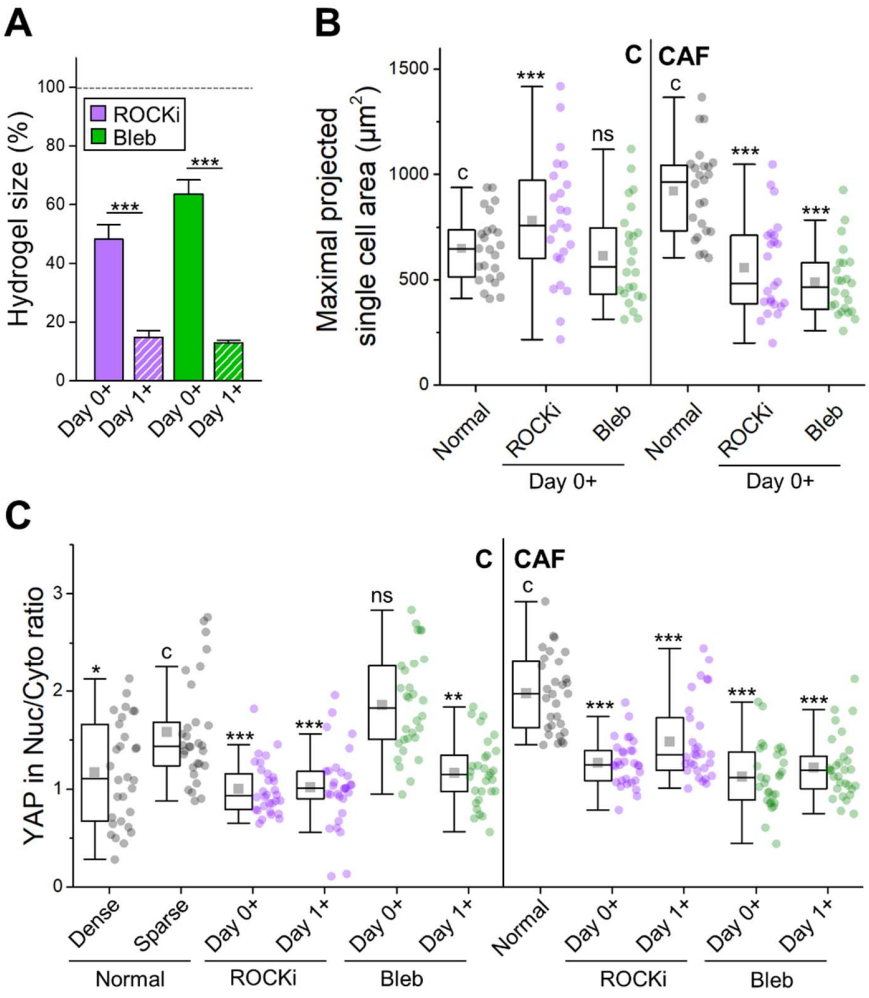

Figure 5.5.2 Effect of inhibiting cell contractile force on cell behavior

(A) Effect of cell contraction inhibitors on hydrogel contraction. The final hydrogel size was compared with the original hydrogel size (100%).

(B) Effect of cell contraction inhibitor on cell spread in the hydrogel. Cell spread in CAF group was hindered when cells were treated with inhibitors. The *p* values were calculated between control (c) and each group. (n = 24)

(C) Intranuclear localization ratio of YAP in cells according to cell contraction inhibitor. YAP localization ratio decreased following inhibitor treatment. The *p* values were calculated between control (c) and each group. (n = 30)

5.6. Conclusions

The shift in the balance of differentiation from adipogenesis to osteogenesis in mesenchymal stem cells was observed under the environment where gel contraction was prevented and confirmed that this phenomenon is closely associated with the mechanotransduction based on YAP localization. In contracting collagen hydrogel, the nuclear localization tendency of YAP was depressed compared to CAF, even when cell-cell contact was excluded. It was confirmed whether activation of YAP in CAF was induced by stronger cell contractile force through cell contraction inhibitor treatment. The development of this contraction inhibition platform made it possible to investigate the influence of regulation of cellular microenvironments.

Chapter 6.

Inducing efficient adipogenesis

of human adipose tissue-derived mesenchymal stem cells

by delayed collagen hydrogel contraction

Chapter 6. Inducing efficient adipogenesis of human adipose tissue-derived mesenchymal stem cells by delayed collagen hydrogel contraction

6.1 Introduction

To understand the metabolic syndrome, the need for research on obesity and adipose tissue is increasing. Obesity causes chronic inflammation, insulin resistance, ectopic fat storage, and lipotoxicity. These metabolic problems are not caused by volume expansion of the adipose tissue itself, but because there is no longer enough capacity to store excess nutrients.

Adipose tissue can increase in size in one of two ways under overnutrition: Hypertrophy (increasing the size of existing adipocytes) or hyperplasia (forming new adipocytes through differentiation of precursors) (Figure 6.1A). Although studies have focused on hypertrophy based on the observation that the total number of adipocytes is conserved throughout life, it has recently been shown that new adipocytes can emerge from long-term hypertrophic conditions, contributing to adipose tissue expansion [57, 58]. In addition, the need to focus on adipogenesis as a method to deal with metabolic diseases is suggested from the viewpoint that the generation of new adipocytes can alleviate metabolic abnormalities. Also, interest in adipogenesis is increasing from the viewpoint of alleviating metabolic syndrome through the generation of new adipocytes in obese condition [59, 60].

Previous *in vitro* adipocyte studies have been mainly conducted in two-dimensional (2D) culture platform using mouse preadipocyte cell lines including 3T3-L1, OP9, *etc.* Although this approach induces homogeneous and highly reproducible differentiation into mature

adipocyte and has advantages of simplicity, this approach has limitations in that differences between mice and humans exist and it could not reproduce many events that observed *in vivo*.

Aim of this chapter was to mimic the adipogenesis environment of ADSCs in 3D using collagen type I hydrogel. Although the specific mechanism of collagen type I has not been elucidated, it plays an essential role in the early stage of adipogenesis [61, 62]. Previous studies have focused on maintaining the adipocyte phenotype in collagen using human preadipocyte cell lines or primary adipocytes. However, studying adipogenesis of human MSC in collagen hydrogel is still challenging.

In this study, I showed that the adipogenesis of human ADSCs can be promoted by delaying collagen contraction using a window frame. Collagen type I hydrogel tends to contract within a few days by interaction with fibroblast-like cells including ADSCs. Through this phenomenon, cell morphology was changed into round shape and cell-cell interaction increased. ADSCs differentiated into mature adipocytes by delaying contraction using a window frame, compared to naturally contracted hydrogel and spheroid (Figure 6.1B). I suggest this human adipogenesis and mature adipocyte *in vitro* model as platform to study adipose tissue physiology.

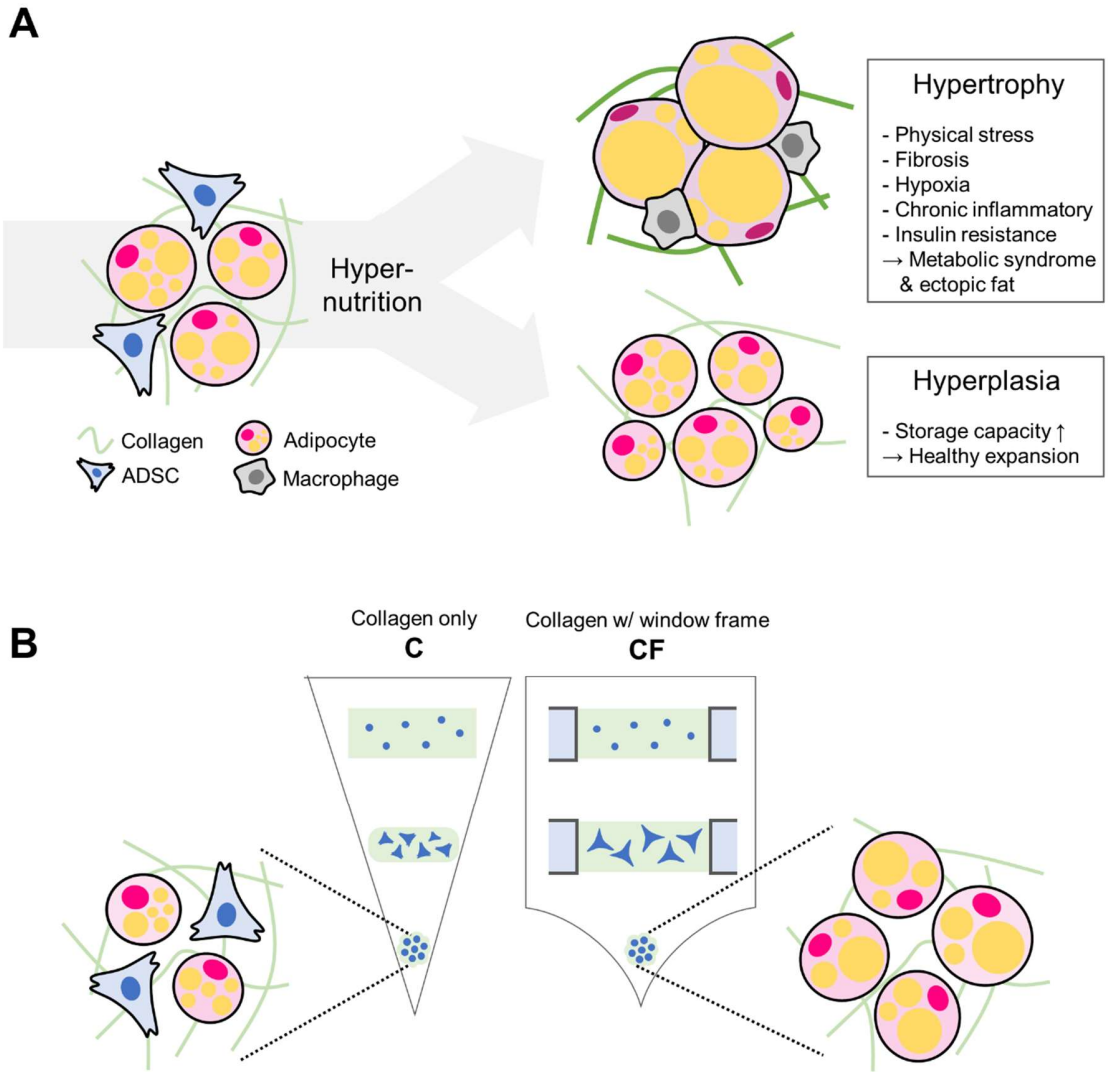

Figure 6.1 Schematic illustration of adipose tissue expansion and experimental design

(A) Two ways of adipose tissue expansion in hyper-nutrition. Adipose tissue can increase its volume by storing fat in the existing adipocyte (hypertrophy) and emergence of new adipocytes through adipogenesis (hyperplasia).

(B) Schematic image of the study. The group C, in which culturing ADSCs on collagen hydrogel, contracted continuously for a period of 14 days. In the CF group, in which the contraction was delayed using a window frame, hydrogels were detached spontaneously within a few days and undergoes rapid contraction.

6.2 Effect of window frame on collagen only hydrogel compared with spheroid

Requirements for adipogenesis discovered in 2D studies are the round shape of cell morphology and the environment in which cell-cell contact overcomes cell-ECM interaction [27, 63]. Cells cultured in collagen hydrogels naturally reach this environment. The spheroid model is a system for making and culturing spherical aggregates using only cells, and a widely used model in 3D differentiation experiments including the embryonic body [64, 65]. ADSCs cultured in collagen hydrogel was compared with spheroid model.

It was confirmed over time how much the hydrogel contracted by ADSCs. (Figure 6.2.1A) The contraction pattern of the hydrogel was significantly different depending on the presence or absence of a frame. C group showed a convergence curve for continuous contraction. CF group maintained the initial size of hydrogel until day 4 and was spontaneously detached from the frame and contracted rapidly. The final sizes of C and CF hydrogels on day 14 were similar.

Adipogenic marker gene expression levels were confirmed on days 1, 4, and 7 after induction of adipogenic differentiation. (Figure 6.2.1B and C) *CEBPB* is early adipogenic marker gene and *PPARG* is master regulator gene of adipogenesis [66, 67]. Both the C and CF groups, the expression level of the marker gene increased with time, whereas the expression level of sph group gradually decreased. In addition, the expression levels of the CF group were significantly higher than that of spheroids and C on the day 4 and 7.

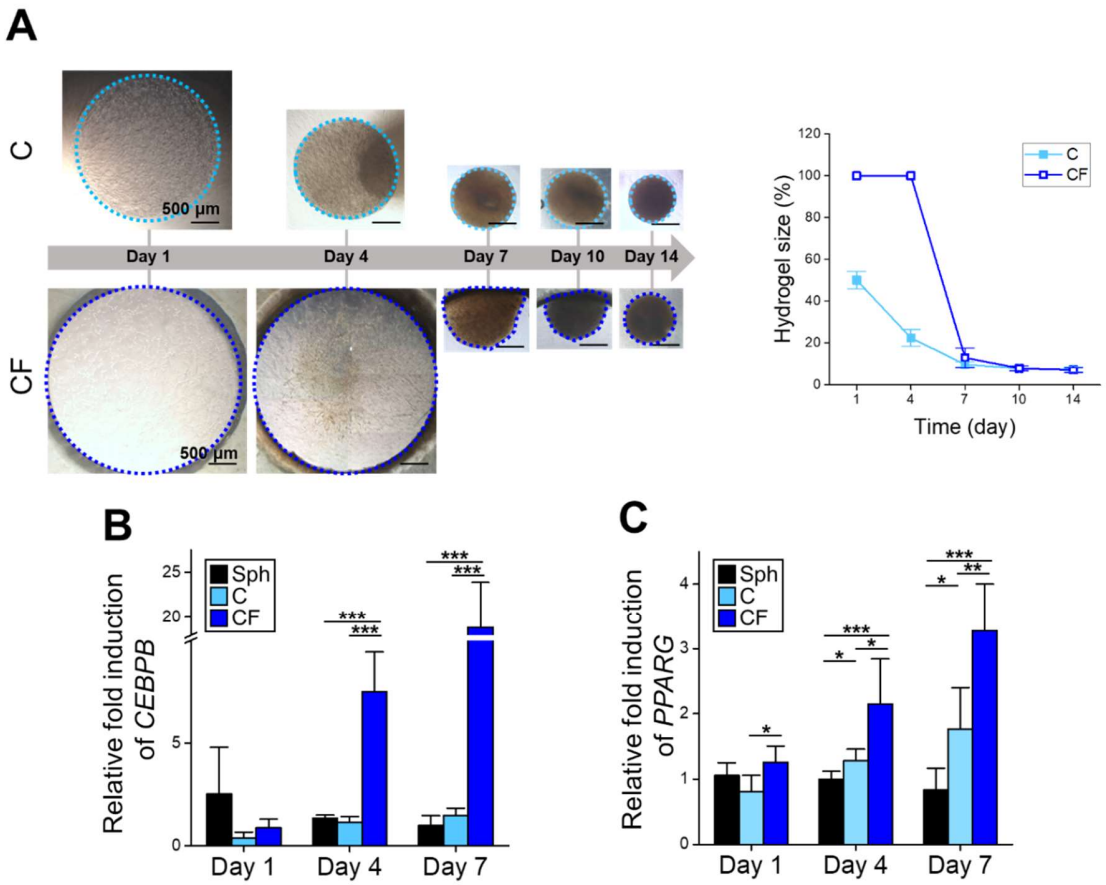

Figure 6.2.1 Effect of window frame on the collagen hydrogel contraction and adipogenic marker gene expression level

(A) Hydrogel contraction process according to the time. The C group contracted continuously through 7 days and converged. The CF group maintained their size until the day 4, then separated from the frame and drastically contracted. (n=10)

(B, C) Relative mRNA level of adipogenic marker gene of ADSCs cultured in 3D. All values were normalized with each gene's expression level of undifferentiated state of ADSCs. (n=3)

To evaluate the maturation of adipocytes, Response of ADSCs to fatty acid stimulus was analyzed. After 14 days of induction of adipogenesis, OA media was treated to induce fatty acid accumulation in adipocytes and lipolysis was induced by isoproterenol, a β-adrenergic agonist [68]. Groups were indicated as CTL (day 14), OA (day 21), and OA+ISO (day 22) according to the observation time point. (Figure 6.2.2A)

LDs stained with BODIPY dye were observed before and after fatty acid stimulation. Only a few cells in Sph formed LDs at day 14 (Figure 6.2.2B). Similarly, only a small number of LDs were observed in C, and no change in size or number of LDs was observed in the CTL, OA, and OA+ISO groups for both Sph and C (Figure 6.2.2C). In CF, almost all cells formed LDs, and it was observed that the size and quantity of LDs increased by fatty acid stimulus. These results were also confirmed with the bright field images through Oil red O staining, which stains the lipid to red color.

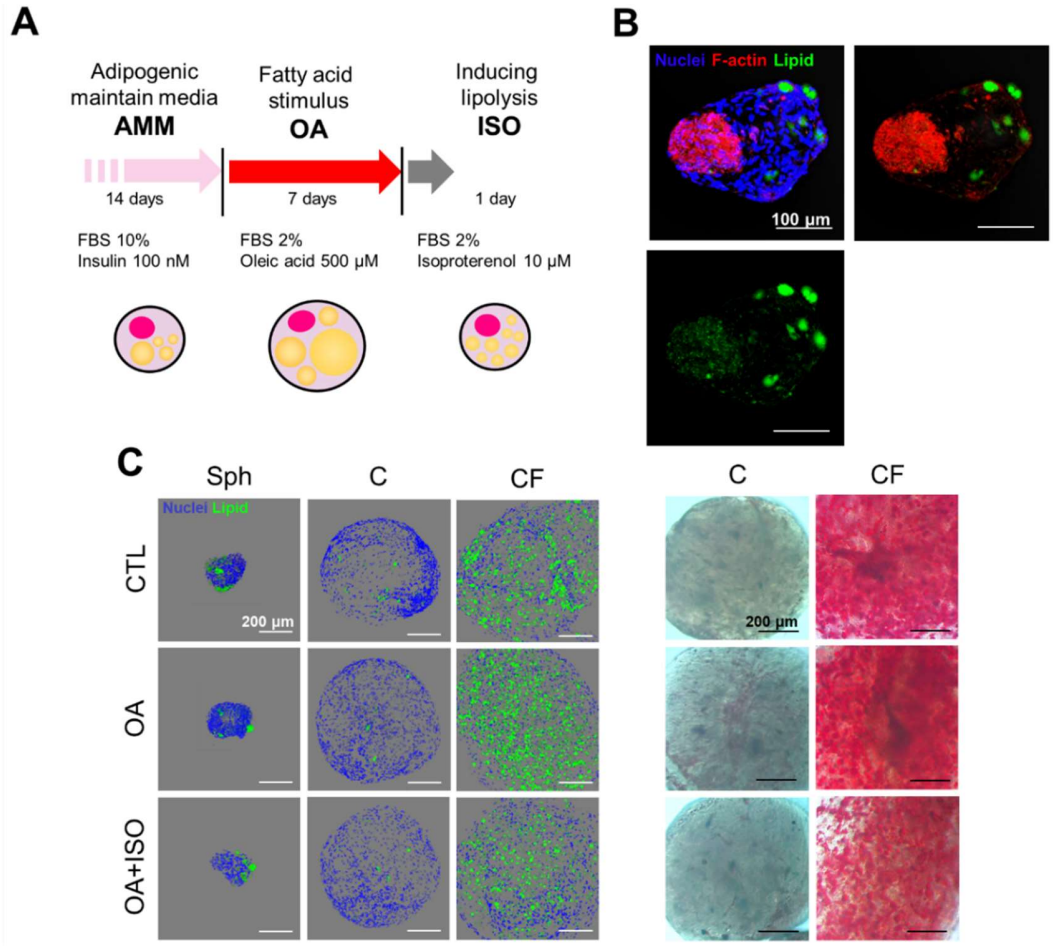

Figure 6.2.2 Response of ADSCs cultured in spheroid, C, and CF to the fatty acid stimulus.

(A) Schematic image of fatty acid stimulus experiment. Maturation of adipocyte was induced for 14 days and cells were treated with oleic acid (OA) for 7 days to induce fatty acid storage. And cells were treated with isoproterenol (ISO) to induce lipolysis.

(B) LD formation of ADSCs cultured in Sph at day 14. Only a few cells had LDs and showed a heterogeneous distribution.

(C) Effect of fatty acid stimulus on LD deposition of spheroid and collagen hydrogel. CTL group indicates mature adipocyte at day 14. Samples were stained with BODIPY (left) and Oil red O (right).

6.3 Effect of window frame on collagen-Matrigel IPN hydrogel

To identify whether this adipogenesis promoting effect is induced by the effect of the frame, collagen type I with Matrigel IPN hydrogel was fabricated. Collagen type I make cells to spread and feel strong tension due to long fiber structure. On the other hand, the main components of Matrigel are laminin and collagen type IV, which are relatively short in length and have a structure that is easy to modify by cells [2, 14]. Because laminin and collagen type IV are abundant in ECM of mature adipose tissue, Matrigel has been widely used in researches to mimic the actual microenvironment of adipose tissue [69-71].

ADSCs were cultured in GM and AM in a hydrogel mixed with collagen type I and Matrigel for a day (Figure 6.3.1A). When ADSCs were cultured with GM, the cells showed a spreading tripod shape regardless of the hydrogel composition. However, ADSCs cultured with AM in MF showed a round shape. When the adipogenic cocktail (contained in AM) is treated, the cells receive signals that changes cell morphology to a round shape in 2D culture platform [63]. It seems that this phenomenon occurred in Matrigel only hydrogel, which is relatively easy to physically modify.

When observing the contraction pattern according to the presence or absence of a window frame, the CM and CMF groups contracted slowly and compared to the collagen only hydrogels (Figure 6.3.1B). the CMF group maintained its shape and size by the frame until the day 4, and then spontaneously detached before the day 7 like in CF group.

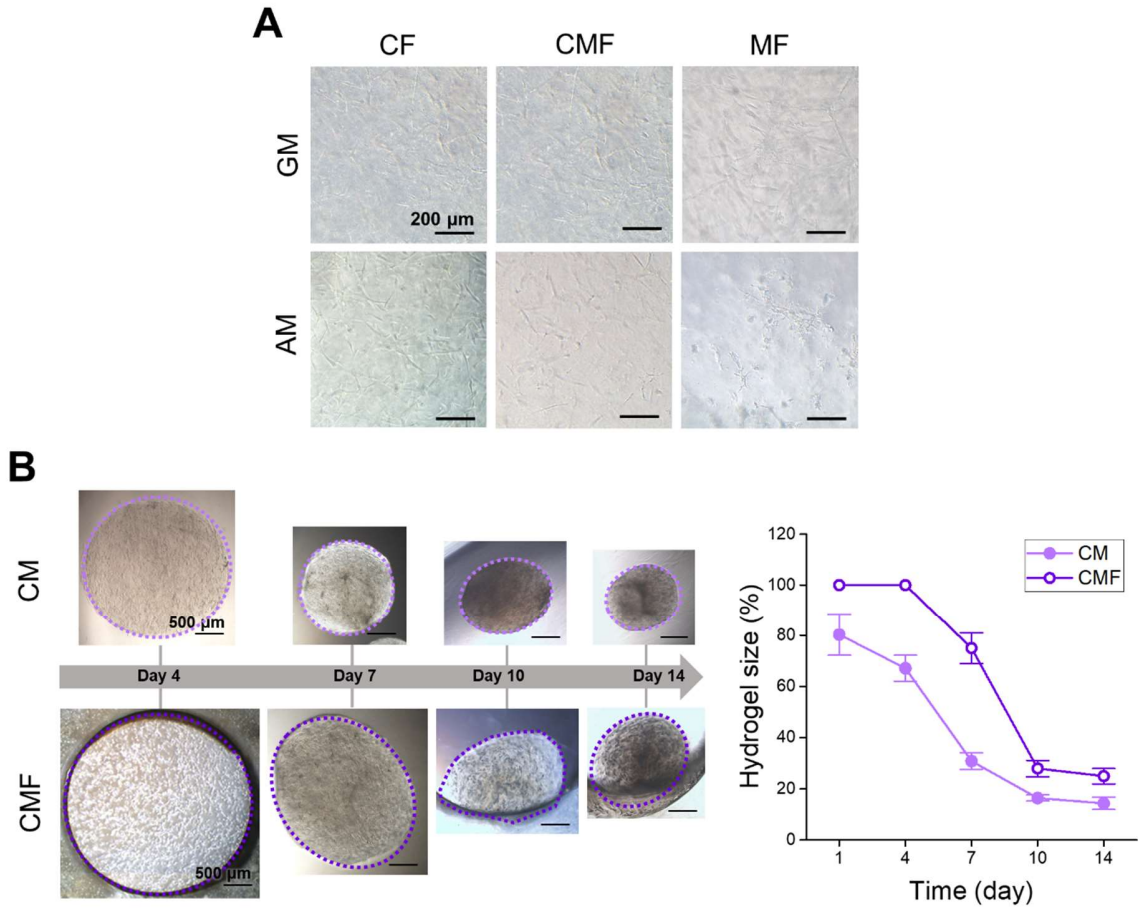

Figure 6.3.1 Effect of window frame on Collagen type I and Matrigel IPN hydrogel.

(A) Morphology of ADSCs depending on hydrogel composition and media at day 1. ADSCs cultured in other groups spread and showed a tripod shape, whereas ADSCs cultured in MF and AM showed relatively round shape.

(B) Hydrogel contraction process according to the time. The degree and speed of contraction were relieved compared to collagen-only hydrogel. The CF group maintained their size until the day 4, then separated from the frame before day 7. (n=10)

Responses to fatty acid stimuli were observed with hydrogel including Matrigel as was done with only collagen hydrogel. (Figure 6.3.2) Images of MF group were not compared because hydrogels were torn from the center due to weak physical properties of Matrigel. Before and after fatty acid stimulus, relatively more LDs were formed in CMF compared to the CM and M groups. This result was also confirmed by Oil red O staining.

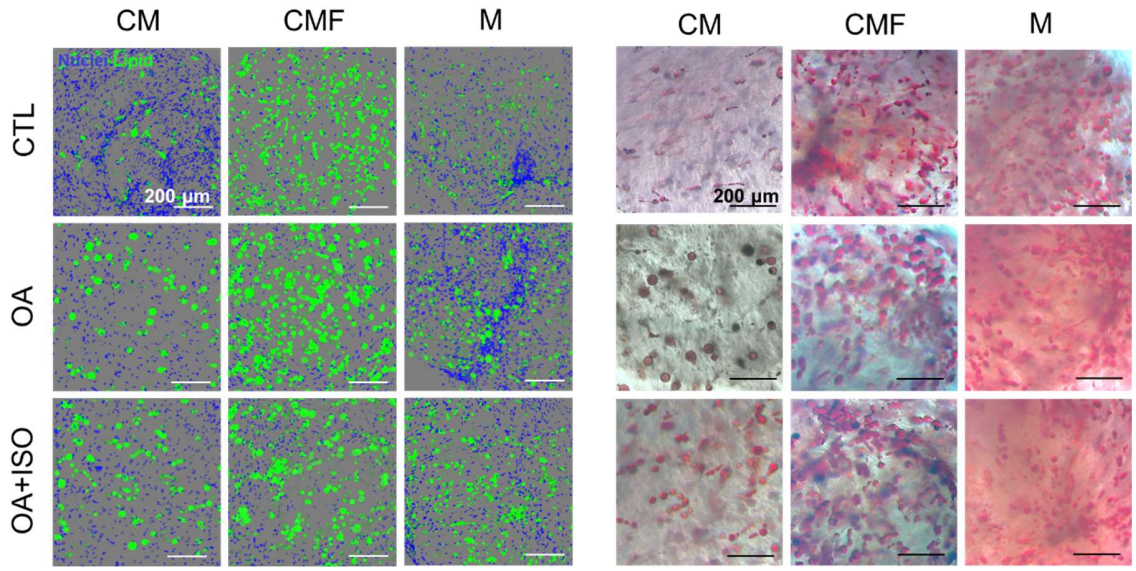

Figure 6.3.2 Response of ADSCs cultured in CM, CMF, and M to the fatty acid stimulus. Effect of fatty acid stimulus on LD deposition of collagen type I and Matrigel IPN hydrogel groups. Samples were stained with BODIPY (left) and Oil red O (right).

6.4 Increased lipid storage in the hydrogel fabricated within window frames regardless of composition

For quantitative analysis, the amount of lipid per cell and the LD size distribution were measured by image analysis. In accordance with the data presented in Figure 6.2.2 and 6.3.2, the amount of lipid/cell was higher in CF and CMF groups than sph, C, and CM groups. And Amount of lipid increased in OA condition and decreased again in OA+ISO condition. These results indicate that ADSCs induced adipogenesis using frames are sufficiently mature to actively respond to external fatty acid stimulus.

Adipocytes dynamically changes LD size and locularity according to the physiological condition. Role of LDs are repositories of energy, fatty acids and sterols. Adipocytes specialized for storage function can form large LDs, unlike ectopic fat formation due to the high concentration of free fatty acids. Also, adipocytes actively remodel LDs in response to external stimuli. To investigate that these changes occur on ADSCs, LD size distribution was analyzed (Figure 6.4). In all groups, the ratio of large droplet (>5000 μm^3) increased in OA condition and decreased again in OA+ISO condition. Both CF and CMF groups showed that the proportion of larger LDs was higher compared with C and CM each, suggesting that the presence of frames contributed to increasing both the total fat storage and LD size.

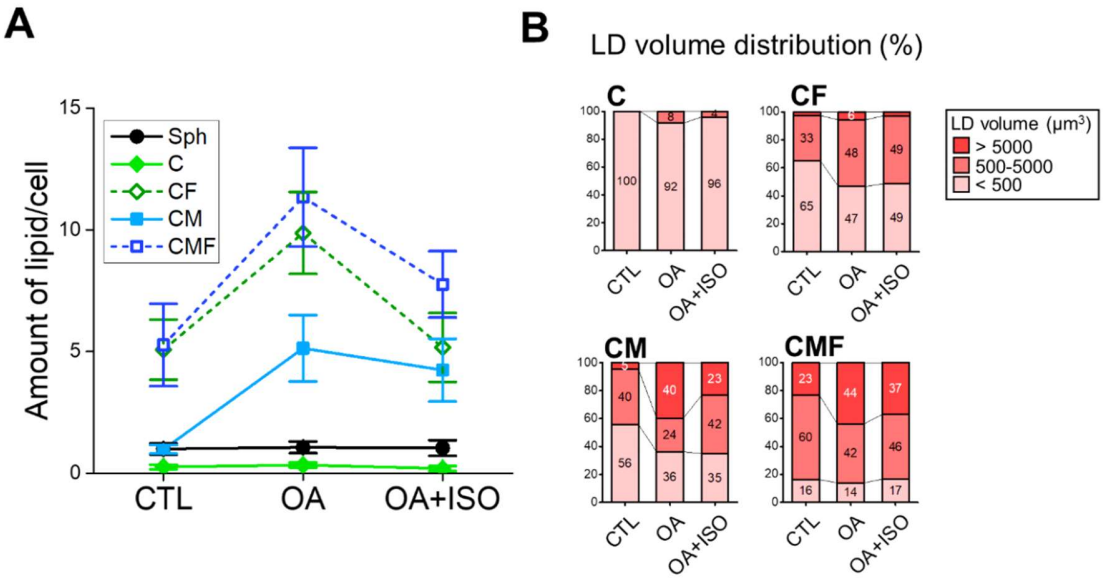

Figure 6.4 Quantification of lipid deposition and LD changed by fatty acid stimulus.

(A) Quantitative data of the area of lipid per cell number (nuclei) in images observed by confocal microscope. In CF and CMF, the amount of lipid increased by OA and decreased by ISO stimulus, and the amount was relatively high in compared to other 3D culture groups. (n=4)

(B) Distribution of LD size graph. When the composition of the hydrogel was the same, the proportion of larger LDs was higher in the hydrogel fabricated with frame (CF and CMF). The distributions of all groups were changed according to the fatty acid stimulus. (n>80)

6.5 Comparison between the conventional spheroid and the spheroid expanded in hydrogel

To confirm whether this adipogenesis-promoting effect is simply due to the difference in when the exposure timing to non-contracted collagen is, adipogenesis in the spheroid expansion group was compared (Figure 6.5A). After forming spheroids in AM for 3 days, spheroids were embedded in a hydrogel fabricated as same concentration and size with the previous experiments. After inducing adipogenesis up to 14 days, LD formation was confirmed by BODIPY staining. (Figure 6.5B) The ADSCs migrated from the spheroids and were evenly distributed throughout the hydrogel. And the number of LDs formed or the proportion of cells having LDs were lower than those of all the hydrogel groups identified above. It was confirmed that late exposure to hydrogel could not induce the same promoting adipogenesis effect.

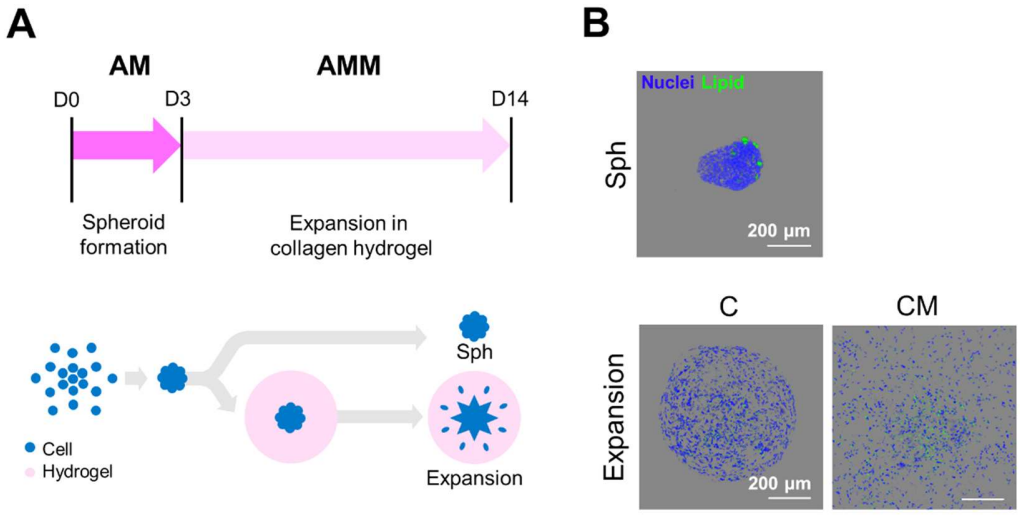

Figure 6.5 Ineffective late exposure of Sph to collagen on adipogenesis

(A) Schematic image of spheroid expansion in C and CM hydrogel. Sphs were embedded in the hydrogel having same size and concentration of C and CM group.

(B) Confocal images of nuclei and lipid at day 14. ADSCs in expansion groups migrated from the spheroids and were distributed throughout the hydrogel, and the observed LDs were not significantly different from those of the spheroids.

6.6 Conclusions

It was able to delay the natural contraction of the collagen-containing hydrogel by ADSCs using the window frame. The expression of the adipogenic marker genes of ADSCs was increased, and the proportion of cells having LDs increased when the frame was used. In addition, ADSCs induced adipogenesis had lipid buffering ability in response to stimuli that induce fatty acid accumulation and lipolysis. I suggest that this method as research tool to study physiological event occur during adipogenesis of human ADSCs. Further study is needed to identify specific mechanism of how window frame influences on adipogenesis.

Chapter 7.

In vitro model of inflammation in obese adipose tissue using human adipose tissue-derived mesenchymal stem cells

Chapter 7. *In vitro* model of inflammation in obese adipose tissue using human adipose tissue-derived mesenchymal stem cell

7.1 Introduction

One of the phenomena observed in adipose tissue *in vivo* but is not fully reproduced *in vitro* is an interaction with inflammation. In the obese state, adipocytes become hypertrophy and undergo hypoxia and necrosis due to excessive physical stress and a limited mass transfer, which causes the influx of immune cells and chronic inflammation. The pro-inflammatory cytokines secreted by adipocytes and macrophages induce insulin resistance and lipolysis (Figure 7.1A). These steps synergistically lead to metabolic syndrome. When this inflammatory situation was reproduced *in vitro*, and results showed that the differentiation of adipocytes and lipid deposition were inhibited.

However, contradictory results have been reported *in vivo* (Figure 7.1B). Repeated LPS injections into adipose tissue stimulate adipogenesis without affecting overall weight gain [72]. When local inflammation occurs in adipose tissue, an increase in new adipogenesis, an increase in lipid deposition, and a decrease in the amount of collagen in the tissue were observed [73]. On the other hand, when signals of pro-inflammatory cytokines were suppressed with RIDα/β, decreased weight gain, insulin resistance, and enhanced fibrosis were observed in HFD [74]. Unlike the previous perspectives that inflammation was a just side effect of obesity, it is suggested that inflammation is a process of remodeling adipose tissue and increase the capacity to store excess lipid. These phenomena were not reproduced

in 3D spheroid model composed only of cells [65]. It seems that these substantial differences between *in vitro* and *in vivo* results are due to lack of cell-ECM interaction *in vitro*.

I focused on reproducing the events occurred in morbid obese tissue with *in vitro* model proposed in this chapter. As mentioned above, a 3D culture model was fabricated in which ADSCs were uniformly differentiated into mature adipocytes through the control of the collagen hydrogel and contraction process. In addition, when excessive fatty acids and pro-inflammatory cytokines were treated to induce a situation similar to that of obese inflamed tissues, the overall lipid deposition increased. I propose that this human obese inflammation model *in vitro* could be used for the study of human obesity and metabolic syndrome.

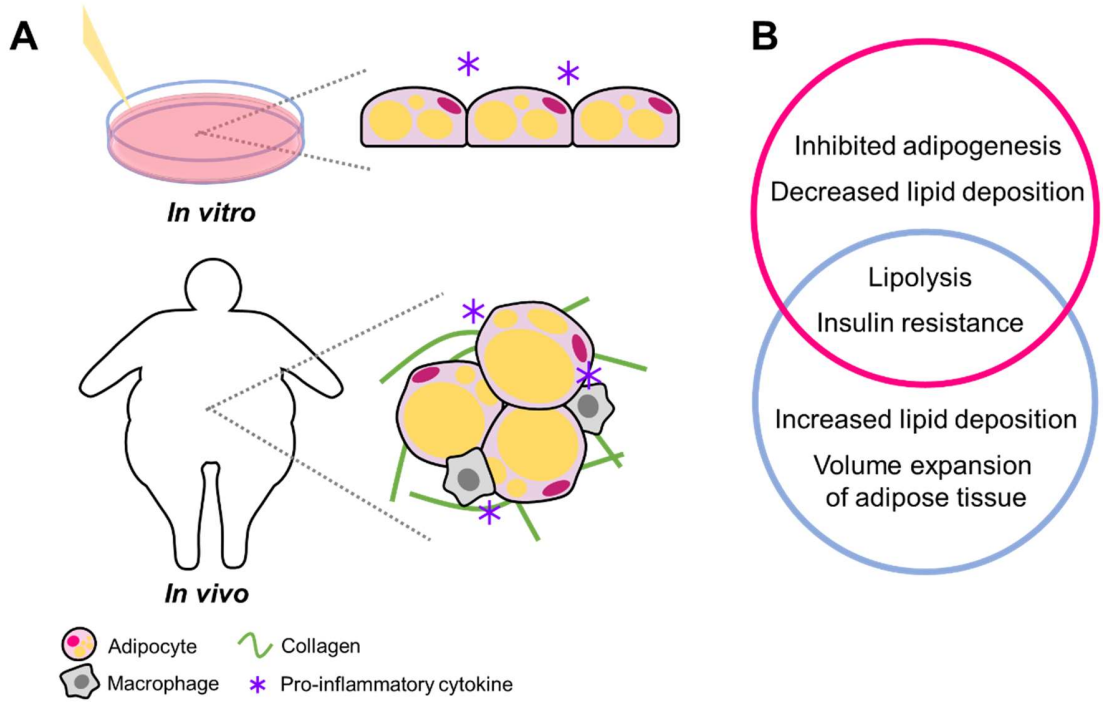

Figure 7.1 Comparison of effects of inflammation on adipocyte *in vitro* and *in vivo*

7.2 Experimental design

Previously, it was confirmed that using the window frame can induce differentiation of ADSCs into mature adipocytes in chapter 6. It was observed that ADSCs increased the volume of the LDs and amount of deposited lipid by responding to the fatty stimulus (OA medium). Here, pro-inflammatory cytokine stimulation (INF condition) was added and the response of ADSCs was investigated (Figure 7.2). There are numerous pro-inflammatory cytokines proved to be increased in pathological obesity, but among them, TNFα (tumor necrosis factor α), IL-1β (interleukin-1β), and IL-6 (interleukin-6) was considered as candidates. It was found that these cytokines increased their expression in both adipocytes and macrophages of hypertrophy adipose tissue, and could induce insulin resistance at the adipocyte level, inhibit adipogenesis, and induce lipolysis [75-78].

However, the effect of IL-6 on the development of insulin resistance is controversial, and it is secreted from various tissues except adipose and macrophages and has wide impact throughout the body, resulting in complex results. Also, conflicting conclusions were reported in animal experiments focusing on the action of IL-6 on adipose tissue, so it was excluded [79-81].

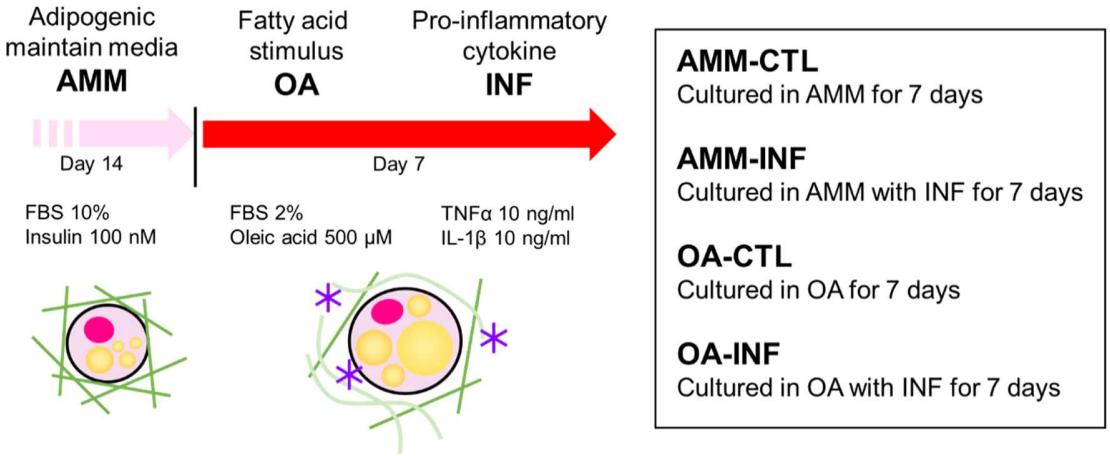

Figure 7.2 Schematic illustration of experimental design

7.3 Effect of excess lipid and pro-inflammatory cytokines on lipid deposition and proliferation of ADSCs in 2D culture

As a control group, the effect of inflammation was analyzed in ADSCs cultured in 2D. ADSCs were seeded in 96 wells at 20,000 each, and after 1 day they became confluent, and then adipogenesis was induced. On day 21, the lipid deposition inside the cells was observed by bright field microscope (Figure 7.3A). Bubble-like structure in cell referred to LDs stored within the cell. In OA-CTL, the LD size increased in response to excess fatty acid. However, both the sizes of the LDs and the area present were reduced in the INF conditions in AMM and OA. LD size distribution was also confirmed by image analysis (Figure 7.3B). As confirmed by the image, the sizes of LDs also decreased in the INF condition regardless of the type of medium.

To compare the amount of lipid stored by the cells in the total sample, the number of cells and the amount of total triglyceride in a sample were quantified (Figure 7.3C and 7.3D). Amount of dsDNA was measured by lysing the entire mass except for the medium inside the well. Compared to the number of cells seeded initially, the number of cells increased through cell growth in all groups. Among them, the number of cells increased more when cells were cultured in OA medium and in INF condition. This appears to be due to the effect of promoting cell proliferation of pro-inflammatory cytokines, especially TNFα [82, 83].

As observed in the bright field image above, fat stores stored a greater amount of lipids in OA media in response to a fatty acid stimulus, and lipid loss occurred in the INF condition. Both AMM and OA decreased the total amount of triglyceride statistically significantly in the INF condition. To determine the amount of stored lipid per cell number, the amount of

triglyceride per sample divided by the number of cells was compared. (Figure 7.3E) As with the results previously confirmed, the amount of fat decreased in the INF condition. Taken together, these results indicate that when ADSCs were treated with pro-inflammatory cytokines in 2d culture, the lipid stored in the cells was reduced overall, and the LD size was reduced, which is likely due to lipolysis.

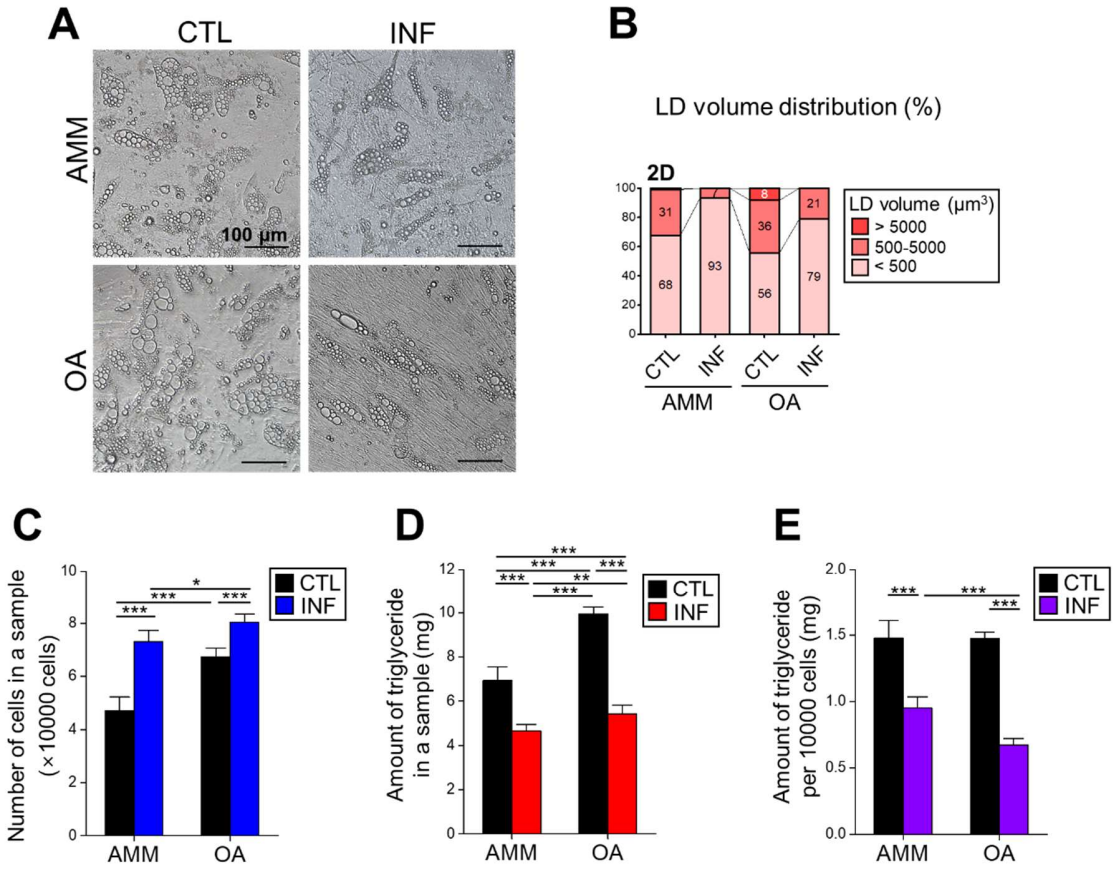

Figure 7.3 Loss of intracellular triglyceride by pro-inflammatory cytokines in 2D culture.

(A) Brightfield images of ADSCs observed at day 21. Compared to CTL, the proportion of cells having LDs was reduced in INF condition

(B) Distribution of LDs' volume in ADSCs associated with pro-inflammatory cytokine. Proportion of small size LDs increased in INF condition. (n>90)

(C) Number of cells in the sample analyzed by dsDNA quantification. The number of cells Initially seeded per well was 20000. Cells proliferated more in INF condition. (n=3)

(D) Quantification of triglyceride in a sample. Total amount of triglyceride increased when cultured in OA medium, while it decreased with INF condition. (n=3)

(E) Amount of triglyceride deposited by unit number of cells. (n=3)

7.4 Effect of excess lipid and pro-inflammatory cytokines on lipid deposition and proliferation of ADSCs in 3D culture

ADSCs were induced adipogenesis in collagen hydrogels prepared by the method presented in Chapter 6. It was expected that the CF group which was sufficiently differentiated into mature adipocytes, would reproduce the *in vivo* situation well. Additionally, C group was compared to observe cell behaviors in which had a small proportion of lipid-stored cells due to insufficient differentiation. As for ADSCs stimulated with OA and INF until day 21, there were still lots of cells not having LDs in group C, similar to ADSCs cultured for day 14 in chapter 6 (Figure 7.4.1A). On the other hand, in the CF group, LDs were evenly formed in all conditions. When the size of the LDs in the CF group was analyzed, overall larger LDs were formed than in 2D culture condition, and the ratio of medium size (500-5000 μm^3) LDs in the INF condition increased regardless of the type of medium. (Figure 7.4.1B) To analyze this change in detail, the distribution of all data was showed with Boxplot (Figure 7.4.1C). In the INF condition, the LD size distribution ratio was not adjusted simply because the number of medium-sized LDs (500~5000 μm^3) increased, but as the size of large LDs (over 5000 μm^3) became smaller.

The amount of cell and deposited lipid deposition in the overall hydrogel were measured in the same way as in 2D culture data. Cell proliferation rate was higher in INF condition, similar to ADSCs cultured in 2D (Figure 7.4.2A). On the other hand, unlike in 2D, the total amount of triglyceride increased statistically significantly in INF condition compared to CTL except for C-AMM (Figure 7.4.2B). When compared as the amount of triglyceride per unit cell number, the CF showed a decrease of triglyceride amount in the INF condition (Figure

7.4.2C). Considering the result of LD size distribution, when pro-inflammatory cytokines were treated in the CF group, it seems that the excess lipids were newly stored in the proliferated cells and cells with small LDs, and more lipids could be deposited. This tendency was observed more obviously in the environment where excess fatty acid was present by the OA medium.

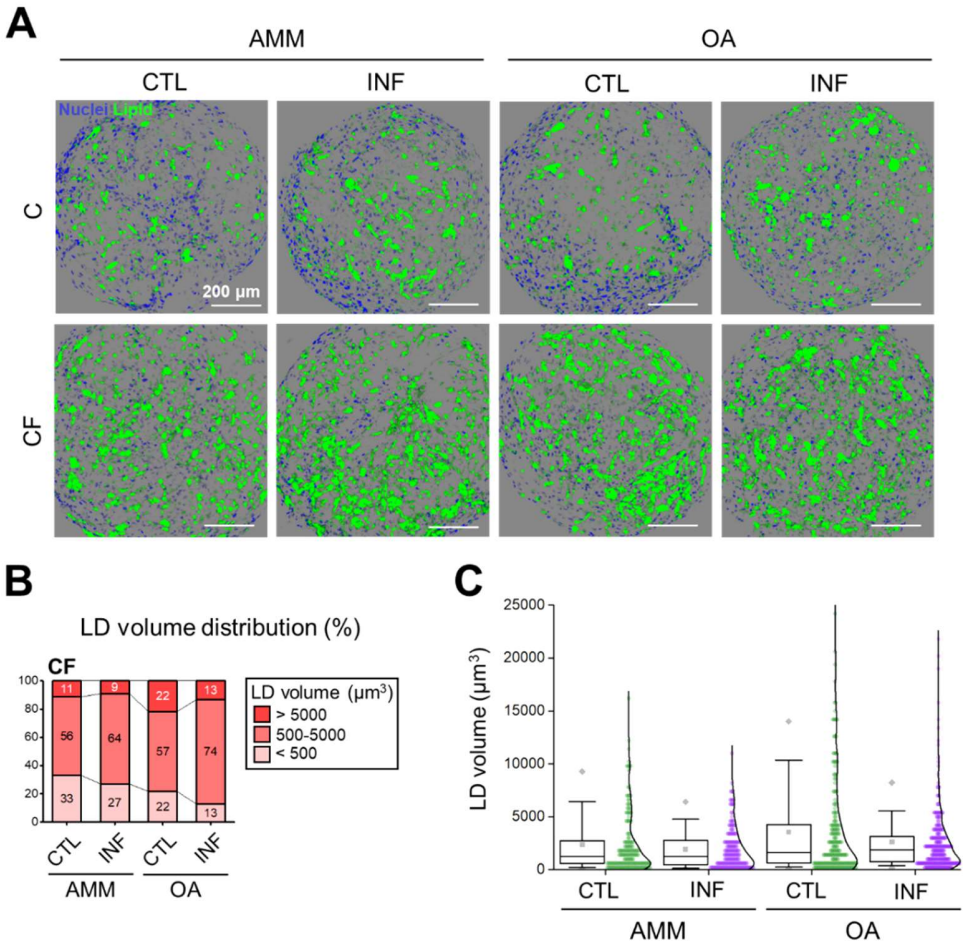

Figure 7.4.1 LD formation and size distribution in ADSCs cultured in 3D.

(A) LD formation in ADSCs cultured in 3D at day 21. Green fluorescence indicates LDs stained by BODIPY.

(B) LD size distribution at day 21 in CF group. In the INF condition, the proportion of LDs with a volume in the range of 500~5000 µm^3 increased. (n>150)

(C) Box plot of LD size distribution in CF. All data points were showed next to box plot with kernel smooth curves. Whiskers indicate 10% and 90% of distribution. Grey ◆ marks indicate 5% and 95%. Grey ■ marks in the boxes indicate mean values.

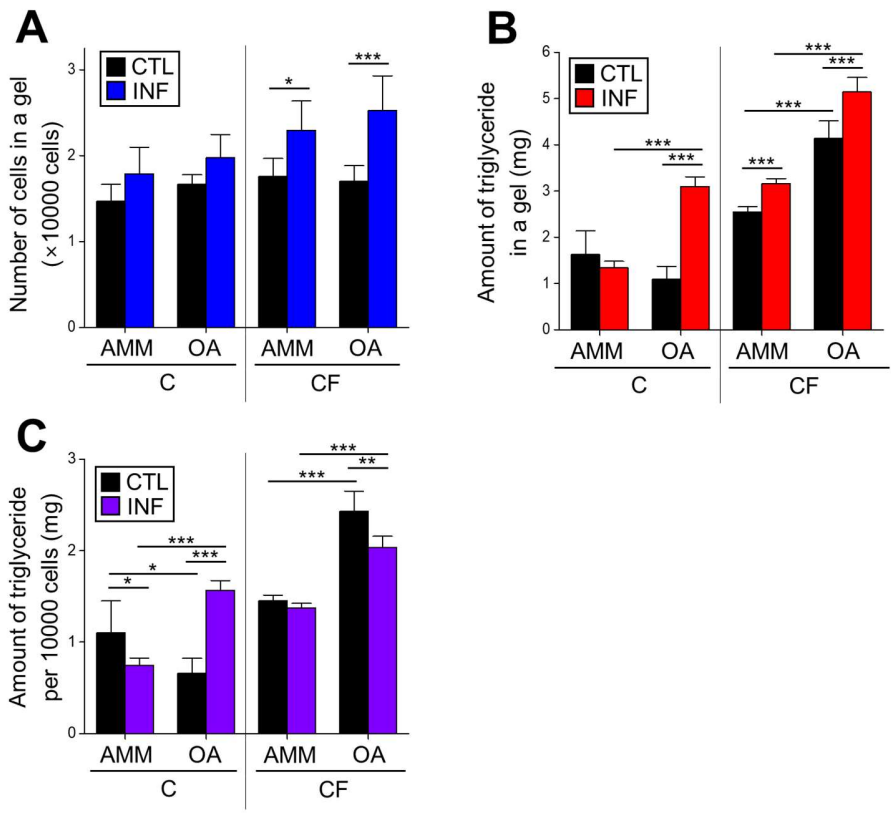

Figure 7.4.2 Proliferation and lipid deposition associated with the treatment of pro-inflammatory cytokines.

All *p* values were calculated respectively within the C group and within the CF group in each graph.

(A) Number of cells in the sample analyzed by dsDNA quantification. The number of cells Initially seeded per well was 10000. Proliferation rate was higher in INF condition. In CF, the increase in cell number was larger in INF condition than in C. (n=3)

(B) Quantification of triglyceride in a sample. In CF, both OA and INF condition increased the total amount of triglyceride. (n=3)

(C) Amount of triglyceride deposited by unit number of cells. (n=3)

7.5 Upregulation of pluripotency, proliferation, and lipid deposition-related gene by pro-inflammatory cytokines

Quantitative qRT-PCR was performed to confirm these cell behaviors at the transcriptional level. Expression of both pluripotency and proliferation markers *SOX2* (SRY-box transcription factor 2) and *MYC* (MYC proto-oncogene) and cell proliferation marker *CDK1* (cyclin dependent kinase 1) was analyzed (Figure 7.5A). When compared with the expression of not differentiated ADSCs (relative fold induction=1), the expression levels of *SOX2* and *MYC* were similar or higher in all groups, and *CDK1* was also OA-INF was higher than 1. And in all groups, relative fold induction was higher than that of CTL in INF condition.

The expression of genes related to lipid deposition, *CD36*, a membrane protein that mediates fatty acid import into cytosol, and *GLUT4* (insulin-responsive glucose transporter 4), a glucose transport protein were analyzed (Figure 7.5B). The expression levels of these genes were statistically higher in the INF condition, regardless of medium. This result was consistent with the result that the number of cells and the amount of lipid deposition in the CF confirmed earlier increased in the INF condition. However, it is contrary to the results of previous studies that TNFα suppressed the expression of *GLUT4* in 3T3-L1 cells cultured in 2D [84, 85]. It seems that sequential adipogenesis of ADSCs in 3D model contributed to these different behaviors.

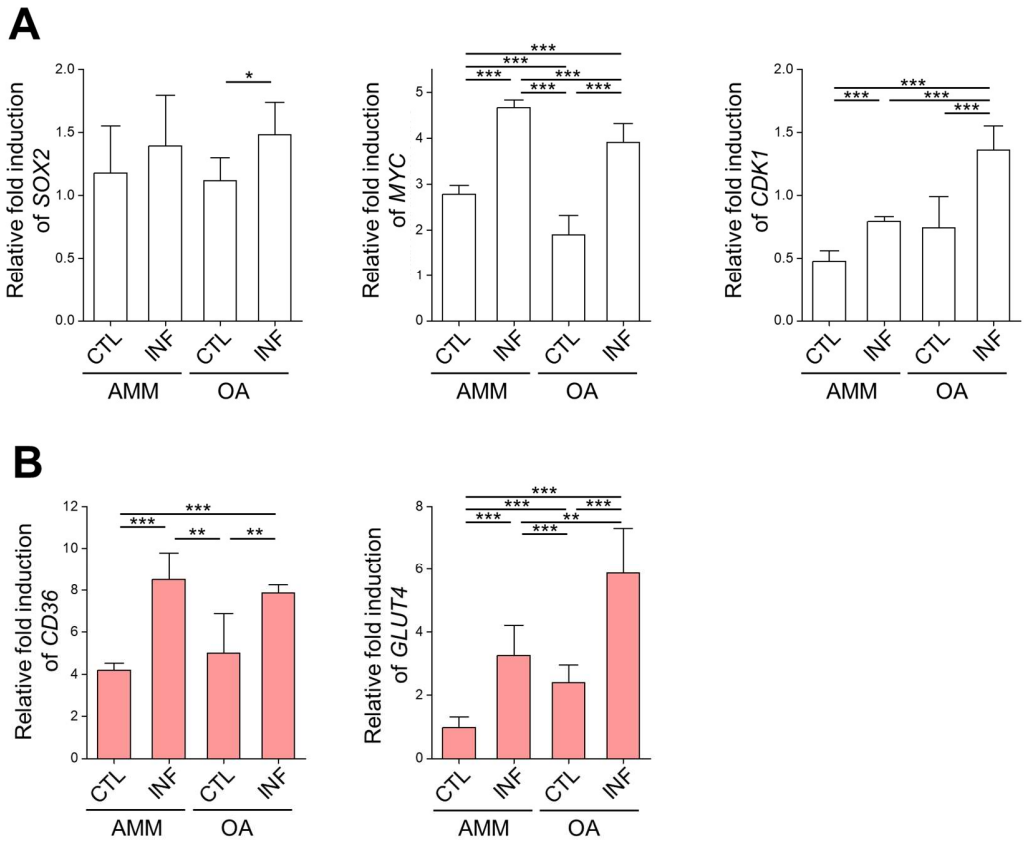

Figure 7.5 Relative fold induction of pluripotency, proliferation, and lipid deposition-related genes in CF group.

All values were normalized with expression level of each gene in not differentiated ADSCs.

(A) Expression levels of pluripotency and cell proliferation-related genes. (n=3)

(B) Expression levels of lipid deposition-related genes. (n=3)

7.6 Conclusions

Conflicting results on inflammatory response *in vitro* have confused researchers, although results have been reported that inflammation enables the expansion of adipose tissue and restoration of lipid buffering ability. Using a human ADSCs 3D model, I found clue that might explain what happens *in vivo*. Cell proliferation and lipid deposition were promoted when there was cell-ECM interaction by collagen and an inflammatory response occurred. As lipids were distributed to proliferated cells, the amount of lipid stored in single cells decreased. Nevertheless, the adipose tissue expansion observed *in vivo* was reproduced with the overall triglyceride storage increased. It is expected that this model can be used to study obesity and metabolic syndrome in humans.

Chapter 8.

Overall discussion and further suggestions

Chapter 8. Overall discussion and further suggestions

It cannot be said without mentioning the effect of collagen on the reproduction of in vivo microenvironment *in vitro* [2, 86]. Especially, the interaction between cells and collagen is important for cells present in connective tissue, a tissue rich in collagen. The cell contractile force and transmission of force to the collagen is natural phenomenon of fibroblast itself [5, 87]. In this thesis, I developed a method to control this contraction by applying an external support to the collagen hydrogel culturing ADSCs. Active controlling the contraction process enabled control of the differentiation of ADSCs.

In the chapter 4, a method to prevent contraction using a window frame and an alginate outer shell was proposed. When these two methods were synergistically applied, the shrinkage could be completely prevented in all directions, and the crosslinked alginate outer shell was formed at the outside of hydrogel as intended through the sequential gelation step. The internal physical properties were also similar to those of pure collagen. However, since there is no *in vitro* gold standard that completely blocks contraction using pure collagen, the effects of alginate present in the outer shell and non-crosslinked fibers in the inner shell could not be fully confirmed.

In the chapter 5, the effect of collagen hydrogel shrinkage on adipogenesis and osteogenesis of ADSCs was investigated. In the case of inhibiting the contraction (CAF group), differentiation could proceed in the desired direction by the induction medium, but in the case of freely contracting collagen hydrogel (C group), only adipogenesis proceeded regardless of the induction medium. From a mechanotransduction point of view, exposure to

more adhesive ligand and to a stiffer environment contribute to an osteogenesis-friendly environment [27, 88]. When the distribution of cells and YAP localization [52, 89] inside the shrinking collagen gel were analyzed, the cells not only form cell-cell contact (dense region) in the process of pulling each other, but also single cells (sparse region) showed low YAP intranuclear tendency. Inferred from these results, it seems that preventing the contraction maintains the contractile force of the cell and the cell-ECM contact at a high level, and forms an environment in which osteogenesis can proceed. Also, a phenomenon that cells exerting a pulling force on the ECM to the neighboring cells increases the stiffness of the local ECM would contribute to osteogenesis tendency in CAF group [90, 91]. Although these observations were made at the single cell level, to further clarify the causal relationship, it is necessary to follow-up the contractile process using tracking force microscope (TFM) [92].

In the chapter 6, when contraction of collagen was incompletely blocked using only the window frame, adipogenesis could be induced in higher efficiency than in the freely contracted collagen gel. When only window frames are used except for alginate, the gel naturally separated from the frame within a few days and delayed contraction occurred. A higher percentage of ADSCs were converted into adipocytes compared to collagen that had contracted from the beginning, and cells were differentiated into mature adipocytes with lipid buffering ability.

This is meaningful in that it induced differentiation with high efficiency under microenvironment similar to the *in vivo* adipogenesis composed of collagen type I using ADSCs. Although the effect of the window frame on the induction of adipogenesis was not confirmed here, it is inferred that the growth of cell volume or the formation of G-actin may have had an effect [63, 93]. Compared to the rapidly contracting hydrogel, the cells could

sufficiently grow the cell volume during the stimulation of adipogenic induction, thus storing more lipid. It has also been reported that G-actin, which is produced by the deconstruction of F-actin in the cytoplasm, enables the action of PPARγ as a transcription factor and induces adipogenesis. The process of contracting after spreading sufficiently at the early stage might have increased the total amount of G-actin.

In the chapter 7, an *in vitro* inflamed adipose tissue model was constructed. This model reproduced the phenomenon of increasing lipid deposition while lipolysis was induced in the inflammatory environment, which had not been reproduced *in vitro*, The differences from existing studies using a preadipocyte cell line such as 3T3-L1 are, first, cell-ECM interaction is provided. The degradation of collagen by MMP14 (matrix metalloproteinase) has been reported as playing an important role in adipocyte differentiation and lipid deposition [62, 94]. In 2D culture, there is no restriction on the volumetric growth of cells, so the factors of physical stress applied in morbid obesity and the process of ECM remodeling in response to this environment are excluded in 2D. In addition, the construction of a 3D model using ADSCs may also be the cause of eliciting a response to inflammation. It seems that few of ADSCS remained in a fibroblast or preadipocyte state without undergoing differentiation, and then actively proliferated by inflammatory stimulus and differentiated to a state capable of storing new lipid. Alternatively, proliferation and differentiation could be promoted due to dedifferentiation as cells received greater stress through collagen contraction and excess fatty acid [95]. It is necessary to verify whether this process is reproduced in the preadipocyte cell line in collagen hydrogel.

In this thesis, it was confirmed the effect of collagen contraction over time on the differentiation of mesenchymal stem cells. Furthermore, by controlling the contraction

process, it was possible to construct a complex physical environment by adding variable that had not been controlled in previous studies performed *in vitro*. It seems that the approaches and physical discoveries proposed in this study could help understanding the stem cells and the stem cell niche.

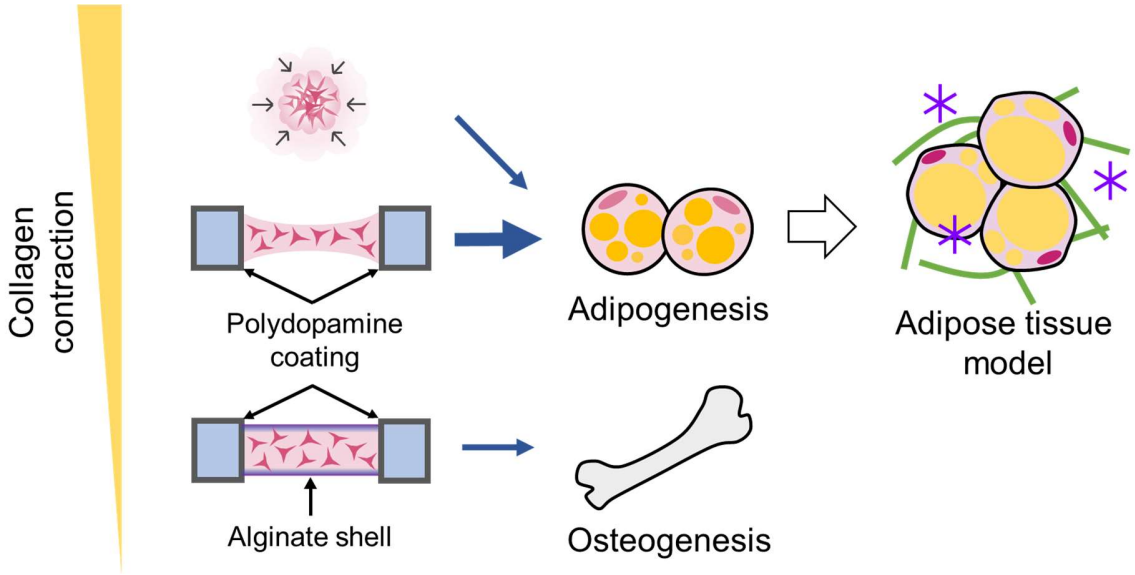

Figure 8.1 Schematic image of overview in thesis

Appendix

Application of osteoblast cell line-derived extracellular matrix as osteoinductive biomaterial

Appendix - Application of osteoblast cell line-derived extracellular matrix as osteoinductive biomaterial

A.1 Introduction

Extracellular matrix (ECM) is a complex microenvironment surrounding cells. It consists of secreted proteins, polysaccharides, growth factors and cytokine. It has been shown that the ECM has different composition depending on the type of organs and tissues [96]. ECM plays a critical role in various cellular behaviors such as adhesion, proliferation, migration, and differentiation [97]. In addition, ECM has been evaluated as a functional biomaterial that can provide naturally occurring microenvironment to cells. Therefore, numerous studies have attempted to find a way to utilize ECM in tissue engineering and regenerative medicine [97-102].

One of commercialized ECM biomaterials is a demineralized bone matrix (DBM), for which cellular components and minerals are removed from the actual bone while only bone ECM is left. The DBM contains various important components of the actual bone, including collagen type I and bone-specific protein. Thus, it has very effective osteoconductivity and osteoinductivity. Long-term clinical studies have demonstrated that DBM can promote bone regeneration and fuse well with original bone tissue *in vivo* when it is implanted [103, 104].

Although the demand for real bone-derived DBM is increasing for patients with bone defects, the supply of bone tissue is limited. In addition, DBM shows different clinical performance depending on tissue donor's age and health state [105, 106]. Moreover, biomaterials including DBM derived from decellularized organs can be costly and time-

consuming because sufficient inspection and sterilization process are required so that it will not carry deadly infectious diseases such as Creutzfeldt-Jakob disease, SARS, and AIDS [107, 108]. These disadvantages of DBM have led to the development of inorganic materials such as mineralized xenografts, hydroxyapatite, and polymers that can be produced with uniform quality in factories to replace DBM. However, their therapeutic effects are not sufficient enough to be used as substitutes for DBM [109].

To solve this problem, I aimed to develop ECM that could be obtained from cell line, cultured *in vitro*. Such ECM has some advantages compared to organ-derived ECM or chemically synthesized inorganic materials. First, ECM derived from a cell line can be obtained in a uniform and controlled condition. Second, the process of removing cells and sterilizing is much easier and faster than that for the actual bone. Actual bone contains not only some other neighboring tissues such as fat and blood vessels, but also high content of minerals. Thus, a decellularization of actual bone for clinical usage should proceed in strong and toxic conditions. Furthermore, for this process, reagents are treated for a quite long time ranging from several hours (h) to days [110-114]. On the contrary, the ECM produced by a cell line is obtained in the form of a thin sheet without unnecessary tissue. It is also expected to reduce the loss of important functional components due to mild treatment for decellularization.

Most studies about cell-derived ECM have focused on stem cell-derived ECM. It has been demonstrated that stem cells secrete their cell-lineage specific ECM when induced differentiation [115-122]. MC3T3-E1 cell line was used in this study: preosteoblast cell line obtained from mouse calvaria. This cell line can rapidly proliferate, differentiate into osteoblast and secrete a large amount of collagen-based ECM [123, 124].

Although MC3T3-E1 has a limitation of heterologous cell line, decellularized ECM can be considered in clinical use. Because, if most cellular components are removed from ECM graft, even heterologous ECM implants show low immune response [104, 125]. I investigated MC3T3-E1 in this study because it is a widely used osteoblast model cell line and secrets ECM abundantly [123, 124, 126, 127]. Compared to stem cells as an ECM source, MC3T3-E1 has the advantages of low cost of culture, less quality distribution by passage dependency, much faster and easier induction of differentiation into the bone, and high ECM yield.

A recent study has suggested the feasibility of using decellularized ECM (dECM) secreted by MC3T3-E1 for bone regeneration [128, 129]. However, effects of pure ECM on bone regeneration were unclear because MC3T3-E1 cells were cultured on a hybrid bio-composite consisting of collagen gel and dECM in the experiment. In addition, the assessment of dECM was performed only in *in vitro* studies.

In this study, the bone-specific efficacy of osteoblast-derived ECM was investigated. I suggested a simple decellularization process for MC3T3-E1 to obtain pure dECM and evaluated whether this dECM could be used as a biomaterial for bone regeneration *in vivo*. First, the decellularization process for MC3T3-E1 was optimized. Second, the osteoinductivity of the partially digested decellularized ECM (ddECM) was then evaluated using human bone marrow-derived mesenchymal stem cells (hMSCs) *in vitro*. This ddECM was compared with collagen type I to confirm the specific contribution to osteogenesis in ddECM-embedded polyethylene glycol (PEG) scaffold. I found that MC3T3-E1 cell line-derived ECM itself has the effect of promoting bone regeneration and differentiation, and demonstrated its feasibility as a bone graft.

A.2 Evaluation of decellularization and dECM digestion

To assess the feasibility of using MC3T3-E1 cell line-derived ECM for bone regeneration *in vitro and in vivo*, a stepwise procedure was performed and validated as shown in Figure A.2.1 First, ECM was produced and decellularized with various methods to optimize the process for MC3T3-E1-derived ECM. hMSCs were cultured with ddECM in 3D *in vitro* to investigate the osteoinductive effect of ddECM. At last, ddECM-hybrid scaffold was implanted into a mouse calvaria defect model to determine its bone regeneration effect *in vitro*.

A simple process that can be implemented in a laboratory to obtain pure ECM was designed and optimized. First, I compared decellularization efficacy of freeze and thaw, TE treatment, SDS treatment, and Triton X-100 treatment with various cycle numbers, time, and concentrations (Table A.2 and Figure A.2.2A). These methods were commonly used in decellularization [130-132]. Immediately after applying single step decellularization procedures, eruption of cells was observed after DAPI staining and compared to the control. Blurring of nuclear edge indicates demolition of both cellular membrane and intracellular structure.

Results revealed that the freeze and thaw cycle method was almost ineffective because stained nuclei maintained their own forms. On the contrary, cells were completely eliminated after TE treatment for 4, 8, or 16 min and after treatment with 0.1% SDS. These experimental conditions were not adopted in subsequent studies because ECM

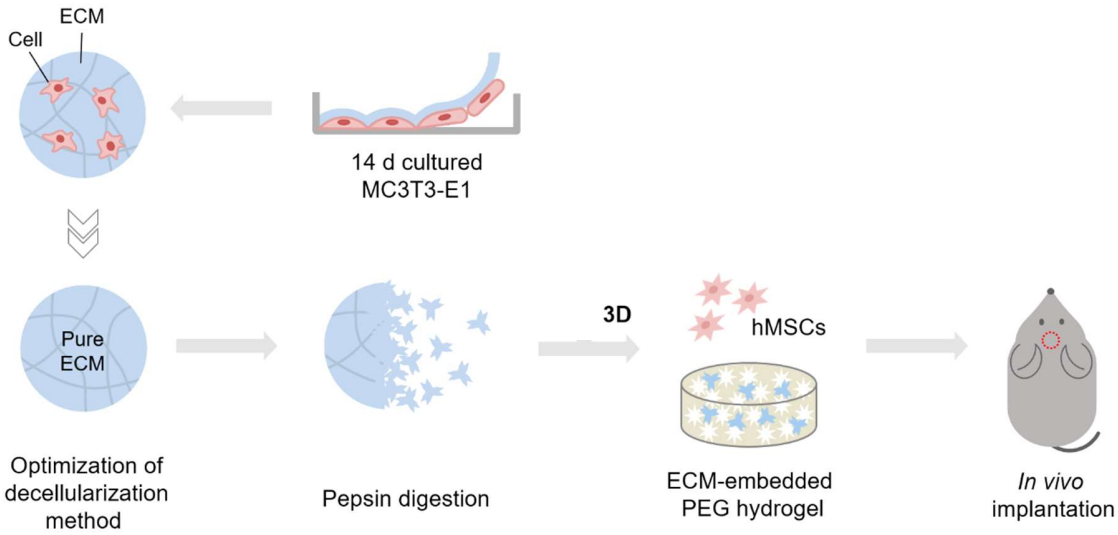

Figure A.2.1 Schematic overview of the study.

sheets completely lost their own structure. It was too liquefied to reconstruct a matrix (data not shown). Regarding Triton X-100 treatment, cells treated with 0.01% Triton X-100 for 5 min appeared to be less stained, suggesting that this condition was insufficient for cell permeabilization. Based on results of comparison, 0.1% Triton X-100 for 10 min, 1% Triton X-100 for 5 min, 1% Triton X-100 for 10 min, 0.05% SDS for 5 min, and 0.05% SDS for 10 min were chosen among experimental groups for subsequent optimization of decellularization.

To remove cells effectively and synergistically, combined pretreatment was attempted to add TE pretreatment process prior to methods selected above. Trypsin is a proteolytic enzyme that could cut specific amino acid sequence of the ECM. Nevertheless, TE was added to detach cells as much as possible to increase decelullarization efficiency and prevent proteases in cells from flowing out and damaging the ECM in second step. DAPI and H&E staining were followed to confirm that cells were fully removed at all steps. After removing cells with two different combined steps (TE+TritonX-100 or TE+SDS), DAPI staining revealed that degrees of cell removal in all groups were similar (Figure A.2.2B, top). However, H&E staining confirmed that the remaining blue fluorescence in DAPI staining result was not from nuclei themselves (Figure A.2.2B, bottom). It appeared that exploded genomic DNA debris congealed on the ECM. This was because staining of effluent genomic DNA debris clogged within the ECM after disrupting cellular and nuclear membranes.

After additional washing with DDW for 1 hr, dsDNA amount in dECM sheets was measured by picogreen assay. Compared to the control, about 90% of dsDNA was removed in all groups, showing no significant difference between experimental groups (Figure A.2.2C). The amount of DNA debris is considered to be negligible for downstream

applications to cell culture and tissue engineering compared to that in previous study [132]. As shown in Figure A.2.2, the mildest method was 0.25% TE for 1 min followed by 0.1% Triton X-100 for 10 min. Thus, it was selected as the final optimized decellularization method. Triton X-100 is preferred over SDS for treatment is because even a small amount of residual SDS can be toxic to cells [133].

	Concentration	Time	Detail
Freeze and thaw cycle	DDW	1~6 cycles	Freezing for 30 min at -80 °C and thawing for 30 min at 37 °C. ECM sheets were vortexed 30 sec and DDW was exchanged between cycles.
Trypsin-EDTA	0.25% Trypsin-EDTA	1, 2, 4, 8, 16 min	ECM sheets were vortexed 30 sec in DDW after the step. Left trypsin was inactivated by 20 mM $CaCl_2$ in DDW solution.
Triton X-100	0.01% in PBS	5, 10 min	ECM sheets were vortexed 30 sec in DDW after the step
	0.1% in PBS	5, 10 min	
	1% in PBS	5, 10 min	
SDS	0.01% in PBS	5, 10 min	ECM sheets were vortexed 30 sec in DDW after the step
	0.05% in PBS	5, 10 min	
	0.1% in PBS	5, 10 min	

Table A.2 Detail processes of single-step decellularization method

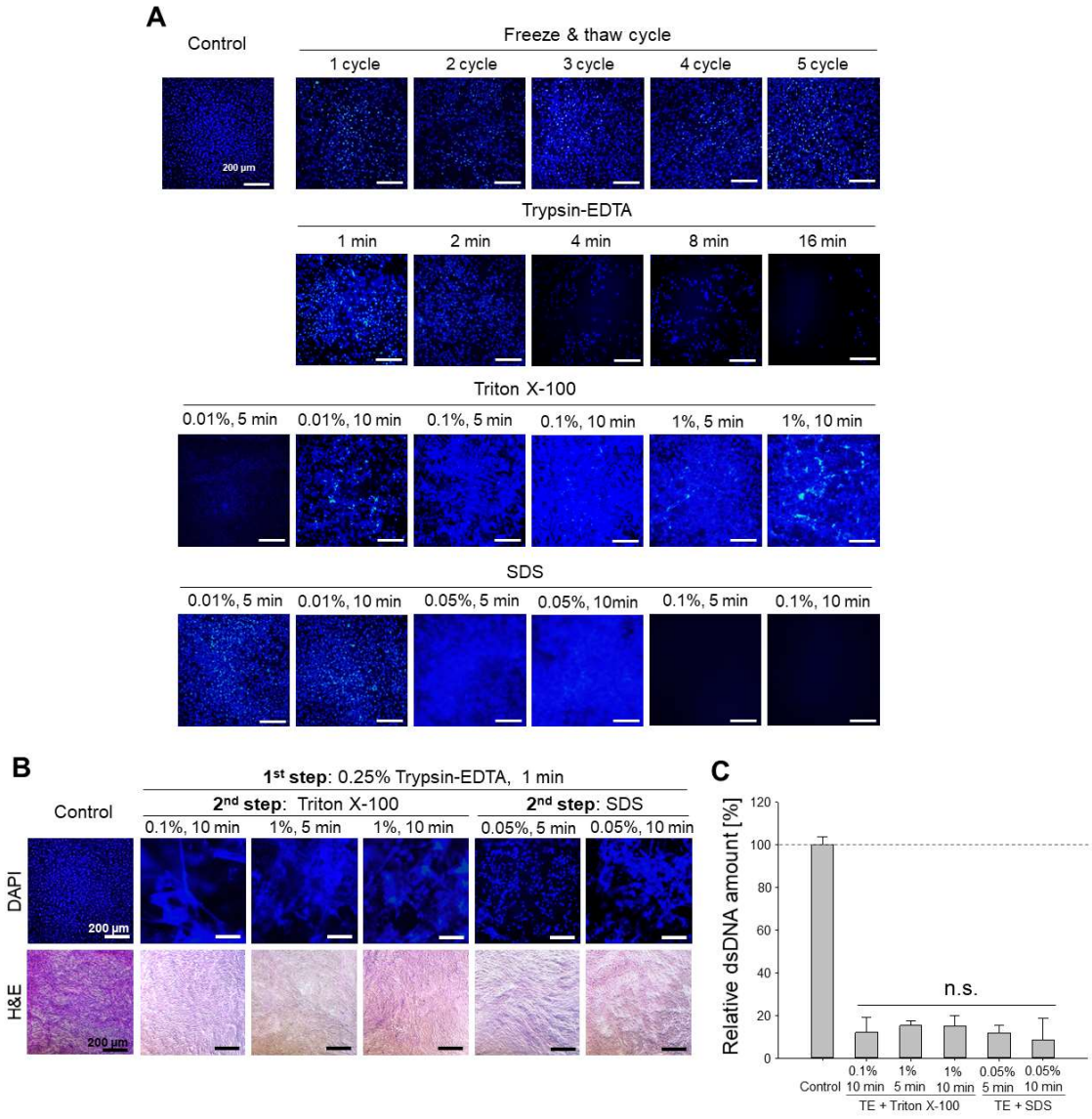
A
Control
Freeze & thaw cycle
1 cycle
2 cycle
3 cycle
4 cycle
5 cycle
200 μm
Trypsin-EDTA
1 min
2 min
4 min
8 min
16 min
Triton X-100
0.01%, 5 min
0.01%, 10 min
0.1%, 5 min
0.1%, 10 min
1%, 5 min
1%, 10 min
SDS
0.01%, 5 min
0.01%, 10 min
0.05%, 5 min
0.05%, 10min
0.1%, 5 min
0.1%, 10 min
B
1st step: 0.25% Trypsin-EDTA, 1 min
Control
2nd step: Triton X-100
2nd step: SDS
0.1%, 10 min
1%, 5 min
1%, 10 min
0.05%, 5 min
0.05%, 10 min
DAPI
H&E
200 μm
200 μm
C
Relative dsDNA amount [%]
120
100
80
60
40
20
0
n.s.
Control
0.1% 10 min
1% 5 min
1% 10 min
0.05% 5 min
0.05% 10 min
TE + Triton X-100
TE + SDS

Figure A.2.2 Comparison of decellularization efficiency between decellularization methods.

(A) Evaluation of single step decellularization methods. DAPI staining shows outline of nuclei. Destructive efficiency of each method was confirmed by investigating the blurring of the nuclear edges.

(B) Evaluation of 2-steps decellularization methods. Amount of residual cells after 2-step decllularization were quantitatively analyzed by DAPI and H&E staining. All of the samples were exposed to the 0.25% TE for 1 minute first and chemically decellularized SDS or Triton X-100. Samples were washed twice with DDW before staining. Nuclei of the control group were stained in purple color, but the other groups were stained with bright pink, indicating collagen.

(C) quantification of dsDNA debris after 2-steps decellularization. ECM sheets were washed for 1 hour before measured by picogreen assay (n=5).

A.3. Osteoinductivity of dECM in 3D culture

*d*ECM-hybrid scaffold was prepared by cryogel method with a modified procedure [134]. Concentrations of polyethylene glycol diacrylate (PEGDA; M.W. 3400; Alfa Aesar, 46497), ammonium persulfate (APS; Sigma, A3678), and N,N,N,N-tetramethyl-ethylenediamine (TEMED; Sigma, T9281) in all groups were the same (at 9.5% (w/v), 0.5% (w/v), and 0.25% (w/v), respectively). Only the concentration of dECM was linearly changed. For example, in the 0.12% ECM group, the concentration of dECM in the scaffold was 0.12% (w/v). All reactants were dissolved in PBS at 4 ℃. The reagents were mixed, and immediately added to the mold to maintain the scaffold homogeneous structure, and the scaffold mixture was polymerized overnight at -20 ℃. Schematic procedure of fabrication and morphology of scaffold is described in Figure A.3.1.

To clarify the osteoinductivity of the ddECM in scaffolds, expression levels of osteogenic marker proteins OPN and OCN on day 14 were investigated by immunocytochemistry (Figure A.3.2A and B). OPN and OCN are well-known osteogenic marker proteins. OPN plays an important role in the mineralization of osteoblast [135]. OCN is upregulated at late stage of bone differentiation and maturation [136]. Results showed that both marker proteins were expressed in all samples. However, the higher the ECM concentration was, the higher the OPN expression level was. OCN showed markedly higher expression levels in the group containing ddECM than that in the group of scaffold without ECM. there was no discernable difference of OCN expression level among 0.24% and 0.48% ECM group.

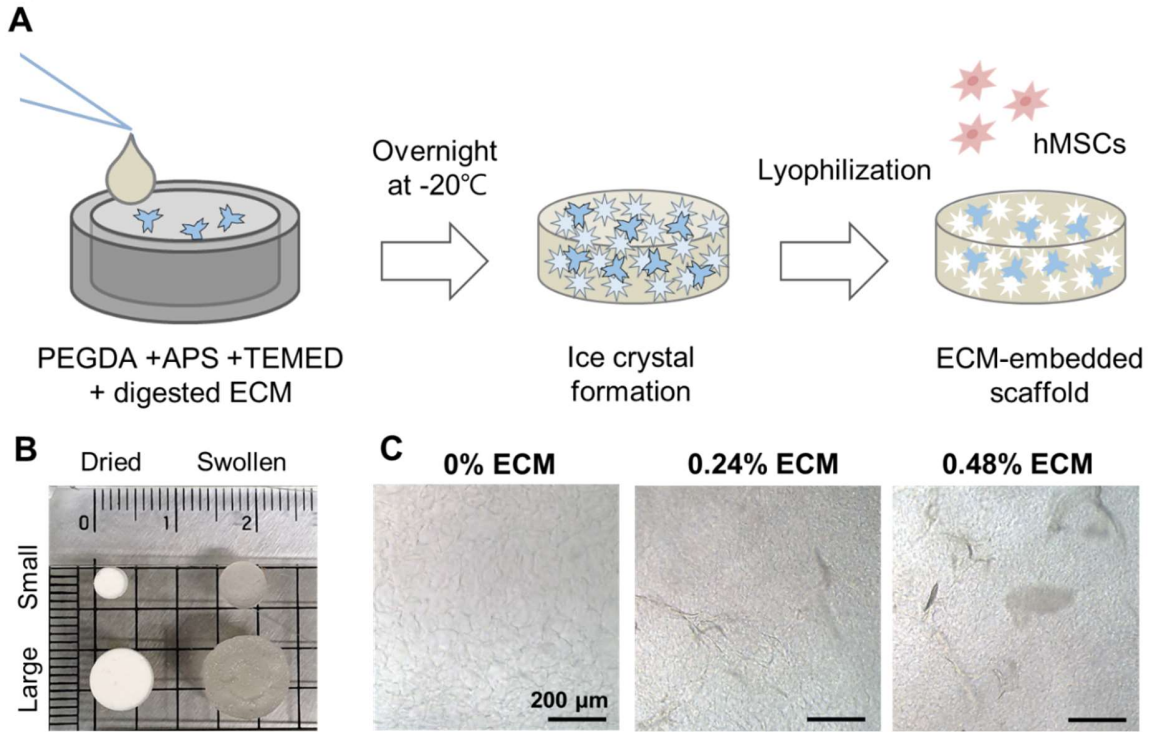

Figure A.3.1 Preparation of ECM-embedded scaffold

(A) Scheme of scaffold preparation. Scaffold was produced with a cryogel method. Ice crystal was formed between polymer and lyophilized to construct porous structure.

(**B)** Images of manufactured scaffolds.

(**C)** Phase contrast microscopic images of the scaffolds. Scaffolds were observed in wet condition without cells. Translucent fibers observed in 0.24% and 0.48% ECM group were ECM fragments.

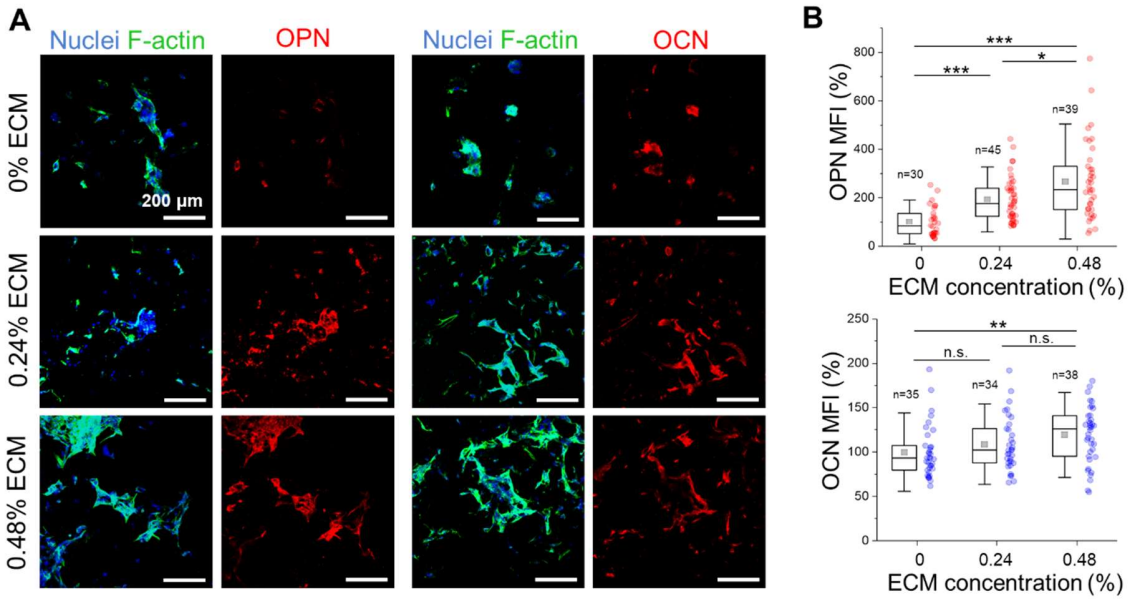

Figure A.3.2 Osteogenesis of hMSCS cultured on 3D scaffolds.

(A) Immunostaining of osteogenic marker proteins expressed by hMSCs cultured on the scaffolds with different ECM conconcentrations. Cells were cultured in the osteogenic medium for 14 days and observed by confocal microscopy.

(B) Mean fluorescence intensity (MFI) of OPN and OCN expressions in hMSCs. Gray squares at the center indicates mean value. All values were normalized with 0% ECM group.

A.4 Bone regeneration *in vivo*

To verify the biological effect of ddECM-embedded scaffolds on bone regeneration *in vivo*, the regenerated bone was observed in 4 mm-sized bone defect in mouse calvaria. This size of defect was not naturally healed. After 8 weeks of ddECM scaffold implantation, new bone formation was observed. In micro-CT images, white areas in black circle indicated regenerated bone (Figure A.4A, top). In representative images, 0.24% and 0.48% ECM groups showed considerable bone regeneration than the control group (0% ECM). These micro-CT images were three-dimensionally reconstructed to quantify the volume of newly regenerated bones (Figure A.4A, bottom). The percentage of regenerated bone volume to total defect volume (BV/TV) was estimated for all groups. As ddECM content increased, the volume of newly formed bones also increased. The level of bone regeneration increased to 2 folds in 0.24% ECM and 4 folds in 0.48% ECM, higher than that in the control. The difference between experimental groups was statistically significant ($p < 0.005$). Histological analysis was performed by H&E staining and Masson's trichrome staining to observe the regenerated bone tissue (Figure A.4B and C). Normal bone at both ends which looked thick could be obviously distinguished from the bone that originally had a defect in the middle. In groups with ECM content of 0% and 0.24%, only a thin layer of collagen was formed (pink in Figure A.4B and blue in Figure A.4C). However, in the group with ECM content of 0.48%, a new collagen block with a thickness similar to intact bone was formed at bone defects. This indicated that the promoted osteoid production in the 0.48% ECM scaffold group seemed to accelerate mineralization.

These results indicated that ddECM could promote osteogenesis and mineralization of hMSCs both *in vitro* and *in vivo*. It means that growth factors and osteoinductive proteins are intact and conserved in the ddECM. They will maintain their function activities even after decellularization and digestion processes optimized by us. Research on which components included in the ECM contribute to osteogenesis is still in its early stage, although it has been revealed that small integrin-binding ligand and N-linked glycoproteins (SIBLING) play an important role, which occupy a large part of ECM's non-collagenous proteins. These proteins are essential for mineralization in bone. They are involved in the formation of hydroxyapatite crystals through matrix vesicles in bone. They are also involved in the spread of minerals into osteoids.[137, 138] Experimentally significant differences in the degree of mineralization supported this hypothesis.

This study was meaningful in that it focused on evaluating the functionality of osteoblast cell line-derived ECM itself. To ensure the feasibility of ddECM for clinical applications as a replacement for conventional materials, comparative studies with DBM obtained from actual bones is necessary. Furthermore, for the synergistic effects on bone regeneration, an approach to fusion with a stiff material like titatnium to promote osteogenesis has been suggested**.**

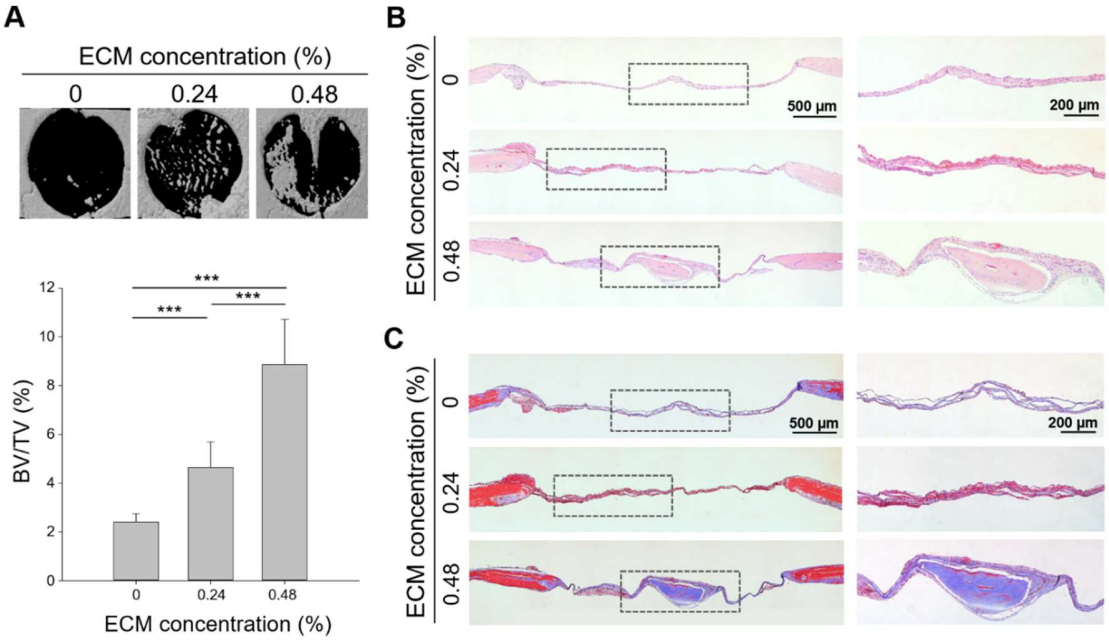

Figure A.4 *In vivo* bone regeneration in mouse calvarial defect model.

Scaffolds with different ECM concentrations were implanted on the calvarial defect of mouse after 3-hour-incubation with 5×104 cells of hMSCs seeded. Cranial samples were harvested after 8 weeks and then analyzed.

(**A)** micro-CT results of the calvaria. Regenerated bone in defect was measured by micro-CT. Black circle indicates artificially generated 4 mm size defect and white area indicate regenerated bone (top). The ratio of the regenerated bone volume to total defect volume (BV/TV) was analyzed from three-dimensional reconstructed images (bottom, n=4).

(**B,C)** Histological images of cranial segments stained by H&E (B) and Masson's trichrome (C), respectively. Bright pink color in (B) and blue color in (C) indicates collagen.

A.5 Conclusions

In summary, I developed an easy and simple decellularization method that could be used in a laboratory scale to obtain pure ECM derived from osteoblast cell line compared to general native tissue decellularization methods described in previous works. MC3T3-E1 cell-derived ECM could efficiently promote osteogenesis of hMSCs both *in vitro* and *in vivo*. Even after decellularization and digestion, significant osteogenic factors in the ECM were intactly preserved with their functions. Cell line-derived ECM-hybrid scaffold was manufactured with appropriate ratio of components, resulting in suitable-constructed structure and pore size for bone regeneration. ECM embedded on the PEG scaffold enhanced cell adhesion and osteogenesis of hMSCs. In animal experiments, the addition of ddECM markedly promoted bone regeneration. Results confirmed that a mineralized mature bone was formed. In conclusion, MC3T3-E1 cell-derived ECM can provide microphysiological bone-specific microenvironment for stem cells. Therefore, osteoblast cell line-derived ECM could be suggested as a new source of ECM used in tissue engineering and regenerative medicine, which can be used as an alternative to natural ECM obtained from actual tissue.

Biblography

[1] S.H. Kim, J. Turnbull, S. Guimond, Extracellular matrix and cell signalling: the dynamic cooperation of integrin, proteoglycan and growth factor receptor, J Endocrinol 209(2) (2011) 139-51.

[2] V.W. Tang, Collagen, stiffness, and adhesion: the evolutionary basis of vertebrate mechanobiology, Mol Biol Cell 31(17) (2020) 1823-1834.

[3] M. Maher, M. Castilho, Z. Yue, V. Glattauer, T.C. Hughes, J.A.M. Ramshaw, G.G. Wallace, Shaping collagen for engineering hard tissues: Towards a printomics approach, Acta Biomaterialia 131 (2021) 41-61.

[4] E. Bell, B. Ivarsson, C. Merrill, Production of a tissue-like structure by contraction of collagen lattices by human fibroblasts of different proliferative potential in vitro, Proc Natl Acad Sci U S A 76(3) (1979) 1274-8.

[5] B. Hinz, C.A. McCulloch, N.M. Coelho, Mechanical regulation of myofibroblast phenoconversion and collagen contraction, Exp Cell Res 379(1) (2019) 119-128.

[6] C.M. Madl, S.C. Heilshorn, Engineering Hydrogel Microenvironments to Recapitulate the Stem Cell Niche, Annu Rev Biomed Eng 20 (2018) 21-47.

[7] D. Noël, D. Caton, S. Roche, C. Bony, S. Lehmann, L. Casteilla, C. Jorgensen, B. Cousin, Cell specific differences between human adipose-derived and mesenchymal–stromal cells despite similar differentiation potentials, Experimental Cell Research 314(7) (2008) 1575-1584.

[8] S.E. Haynesworth, J. Goshima, V.M. Goldberg, A.I. Caplan, Characterization of cells with osteogenic potential from human marrow, Bone 13(1) (1992) 81-88.

[9] P.A. Zuk, M. Zhu, H. Mizuno, J. Huang, J.W. Futrell, A.J. Katz, P. Benhaim, H.P. Lorenz, M.H. Hedrick, Multilineage Cells from Human Adipose Tissue: Implications for Cell-Based Therapies, Tissue Engineering 7(2) (2001) 211-228.

[10] Y. Zhu, T. Liu, K. Song, X. Fan, X. Ma, Z. Cui, Adipose-derived stem cell: A better stem cell than BMSC, Cell Research 18(1) (2008) S165-S165.

[11] J.K. Kular, S. Basu, R.I. Sharma, The extracellular matrix: Structure, composition, age-related differences, tools for analysis and applications for tissue engineering, J Tissue Eng 5 (2014) 2041731414557112.

[12] R.O. Hynes, A. Naba, Overview of the matrisome--an inventory of extracellular matrix constituents and functions, Cold Spring Harb Perspect Biol 4(1) (2012) a004903.

[13] N. Alam, H.L. Goel, M.J. Zarif, J.E. Butterfield, H.M. Perkins, B.G. Sansoucy, T.K. Sawyer, L.R. Languino, The integrin—growth factor receptor duet, Journal of Cellular Physiology 213(3) (2007) 649-653.

[14] J.K. Mouw, G. Ou, V.M. Weaver, Extracellular matrix assembly: a multiscale deconstruction, Nat Rev Mol Cell Biol 15(12) (2014) 771-85.

[15] P. Balasubramanian, M.P. Prabhakaran, M. Sireesha, S. Ramakrishna, Collagen in Human Tissues: Structure, Function, and Biomedical Implications from a Tissue Engineering Perspective, Polymer Composites – Polyolefin Fractionation – Polymeric Peptidomimetics – Collagens2012, pp. 173-206.

[16] G.T. Grant, E.R. Morris, D.A. Rees, P.J.C. Smith, D. Thom, Biological interactions between polysaccharides and divalent cations: The egg-box model, FEBS Letters 32(1) (1973) 195-198.

[17] K.Y. Lee, D.J. Mooney, Alginate: properties and biomedical applications, Prog Polym Sci 37(1) (2012) 106-126.

[18] A.Y. Hsiao, T. Okitsu, H. Teramae, S. Takeuchi, 3D Tissue Formation of Unilocular Adipocytes in Hydrogel Microfibers, Adv Healthc Mater 5(5) (2016) 548-56.

[19] C.K. Kuo, P.X. Ma, Ionically crosslinked alginate hydrogels as scaffolds for tissue engineering: Part 1. Structure, gelation rate and mechanical properties, Biomaterials 22(6) (2001) 511-521.

[20] S.R. Moxon, N.J. Corbett, K. Fisher, G. Potjewyd, M. Domingos, N.M. Hooper, Blended alginate/collagen hydrogels promote neurogenesis and neuronal maturation, Mater Sci Eng C Mater Biol Appl 104 (2019) 109904.

[21] E.A. Growney Kalaf, R. Flores, J.G. Bledsoe, S.A. Sell, Characterization of slow-gelling alginate hydrogels for intervertebral disc tissue-engineering applications, Mater Sci Eng C Mater Biol Appl 63 (2016) 198-210.

[22] H. Lee, M. Dellatore Shara, M. Miller William, B. Messersmith Phillip, Mussel-Inspired Surface Chemistry for Multifunctional Coatings, Science 318(5849) (2007) 426-430.

[23] T. Ahmad, H. Byun, H.J. Shin, J. Lee, S.K. Madhurakkat Perikamana, E.M. Kim, Y.M. Shin, H. Shin, Polydopamine-assisted one-step modification of nanofiber surfaces with adenosine to tune the osteogenic differentiation of mesenchymal stem cells and the maturation of osteoclasts, Biomaterials Science 8(10) (2020) 2825-2839.

[24] R.S. Ambekar, B. Kandasubramanian, A polydopamine-based platform for anti-cancer drug delivery, Biomaterials Science 7(5) (2019) 1776-1793.

[25] Z. Deng, W. Wang, X. Xu, Y. Nie, Y. Liu, O.E.C. Gould, N. Ma, A. Lendlein, Biofunction of Polydopamine Coating in Stem Cell Culture, ACS Applied Materials & Interfaces 13(9) (2021) 10748-10759.

[26] P. Romani, L. Valcarcel-Jimenez, C. Frezza, S. Dupont, Crosstalk between mechanotransduction and metabolism, Nat Rev Mol Cell Biol 22(1) (2021) 22-38.

[27] R. McBeath, D.M. Pirone, C.M. Nelson, K. Bhadriraju, C.S. Chen, Cell shape, cytoskeletal tension, and RhoA regulate stem cell lineage commitment, Dev Cell 6(4) (2004) 483-95.

[28] A.S. Mao, J.W. Shin, D.J. Mooney, Effects of substrate stiffness and cell-cell contact on mesenchymal stem cell differentiation, Biomaterials 98 (2016) 184-91.

[29] H.P. Lee, R. Stowers, O. Chaudhuri, Volume expansion and TRPV4 activation regulate stem cell fate in three-dimensional microenvironments, Nat Commun 10(1) (2019) 529.

[30] A. Elosegui-Artola, I. Andreu, A.E.M. Beedle, A. Lezamiz, M. Uroz, A.J. Kosmalska, R. Oria, J.Z. Kechagia, P. Rico-Lastres, A.L. Le Roux, C.M. Shanahan, X. Trepat, D. Navajas, S. Garcia-Manyes, P. Roca-Cusachs, Force Triggers YAP Nuclear Entry by Regulating Transport across Nuclear Pores, Cell 171(6) (2017) 1397-1410 e14.

[31] Z. Li, K.M. Bratlie, Fibroblasts treated with macrophage conditioned medium results in phenotypic shifts and changes in collagen organization, Materials Science and Engineering: C 122 (2021) 111915.

[32] S. Rhee, H. Jiang, C.H. Ho, F. Grinnell, Microtubule function in fibroblast spreading is modulated according to the tension state of cell-matrix interactions, Proc Natl Acad Sci U S A 104(13) (2007) 5425-30.

[33] W.R. Legant, A. Pathak, M.T. Yang, V.S. Deshpande, R.M. McMeeking, C.S. Chen, Microfabricated tissue gauges to measure and manipulate forces from 3D microtissues, Proc Natl Acad Sci U S A 106(25) (2009) 10097-102.

[34] A. Mehlem, C.E. Hagberg, L. Muhl, U. Eriksson, A. Falkevall, Imaging of neutral lipids by oil red O for analyzing the metabolic status in health and disease, Nat Protoc 8(6) (2013) 1149-54.

[35] P.U. Muñoz-González, P. Rooney, I.L. Mohd Isa, A. Pandit, J. Delgado, M. Flores-Moreno, L.E. Castellano, B. Mendoza-Novelo, Development and characterization of an immunomodulatory and injectable system composed of collagen modified with trifunctional oligourethanes and silica, Biomaterials Science 7(11) (2019) 4547-4557.

[36] D.V. Bax, N. Davidenko, S.W. Hamaia, R.W. Farndale, S.M. Best, R.E. Cameron, Impact of UV- and carbodiimide-based crosslinking on the integrin-binding properties of collagen-based materials, Acta Biomaterialia 100 (2019) 280-291.

[37] Y.J. Hwang, J. Larsen, T.B. Krasieva, J.G. Lyubovitsky, Effect of genipin crosslinking on the optical spectral properties and structures of collagen hydrogels, ACS Appl Mater Interfaces 3(7) (2011) 2579-84.

[38] K. Yang, J. Sun, Z. Guo, J. Yang, D. Wei, Y. Tan, L. Guo, H. Luo, H. Fan, X. Zhang, Methacrylamide-modified collagen hydrogel with improved anti-actin-mediated matrix contraction behavior, J Mater Chem B 6(45) (2018) 7543-7555.

[39] R.H. Koh, Y. Jin, B.J. Kang, N.S. Hwang, Chondrogenically primed tonsil-derived mesenchymal stem cells encapsulated in riboflavin-induced photocrosslinking collagen-hyaluronic acid hydrogel for meniscus tissue repairs, Acta Biomater 53 (2017) 318-328.

[40] W. Kong, Y. Gao, Q. Liu, L. Dong, L. Guo, H. Fan, Y. Fan, X. Zhang, The effects of chemical crosslinking manners on the physical properties and biocompatibility of collagen type I/hyaluronic acid composite hydrogels, Int J Biol Macromol 160 (2020) 1201-1211.

[41] R.M. Desai, S.T. Koshy, S.A. Hilderbrand, D.J. Mooney, N.S. Joshi, Versatile click alginate hydrogels crosslinked via tetrazine-norbornene chemistry, Biomaterials 50 (2015) 30-7.

[42] C. Liu, B. Chiang, D. Lewin Mejia, K.E. Luker, G.D. Luker, A. Lee, Mammary fibroblasts remodel fibrillar collagen microstructure in a biomimetic nanocomposite hydrogel, Acta Biomaterialia 83 (2019) 221-232.

[43] M. Asmani, S. Velumani, Y. Li, N. Wawrzyniak, I. Hsia, Z. Chen, B. Hinz, R. Zhao, Fibrotic microtissue array to predict anti-fibrosis drug efficacy, Nature Communications 9(1) (2018) 2066.

[44] M.A. Lancaster, J.A. Knoblich, Generation of cerebral organoids from human pluripotent stem cells, Nat Protoc 9(10) (2014) 2329-40.

[45] D.A. Cisneros, C. Hung, C.M. Franz, D.J. Muller, Observing growth steps of collagen self-assembly by time-lapse high-resolution atomic force microscopy, Journal of Structural Biology 154(3) (2006) 232-245.

[46] R. Gottardi, U. Hansen, R. Raiteri, M. Loparic, M. Duggelin, D. Mathys, N.F. Friederich, P. Bruckner, M. Stolz, Supramolecular Organization of Collagen Fibrils in

Healthy and Osteoarthritic Human Knee and Hip Joint Cartilage, PLoS One 11(10) (2016) e0163552.

[47] M. Zahid, N. Saqib, J. Nadia, S. Asma, A. Adnan, Adsorption studies of phosphate ions on alginate-calcium carbonate composite beads, African Journal of Environmental Science and Technology 9(3) (2015) 274-281.

[48] M. Kawai, C.J. Rosen, PPARgamma: a circadian transcription factor in adipogenesis and osteogenesis, Nat Rev Endocrinol 6(11) (2010) 629-36.

[49] S. Muruganandan, A.A. Roman, C.J. Sinal, Adipocyte differentiation of bone marrow-derived mesenchymal stem cells: cross talk with the osteoblastogenic program, Cell Mol Life Sci 66(2) (2009) 236-53.

[50] L.A. Stechschulte, B. Lecka-Czernik, Reciprocal regulation of PPARgamma and RUNX2 activities in marrow mesenchymal stem cells: Fine balance between p38 MAPK and Protein Phosphatase 5, Curr Mol Biol Rep 3(2) (2017) 107-113.

[51] H. Lee, S.H.L. Kim, H. Yoon, J. Ryu, H.H. Park, N.S. Hwang, T.H. Park, Intracellular Delivery of Recombinant RUNX2 Facilitated by Cell-Penetrating Protein for the Osteogenic Differentiation of hMSCs, ACS Biomaterials Science & Engineering 6(9) (2020) 5202-5214.

[52] T.P. Driscoll, B.D. Cosgrove, S.J. Heo, Z.E. Shurden, R.L. Mauck, Cytoskeletal to Nuclear Strain Transfer Regulates YAP Signaling in Mesenchymal Stem Cells, Biophys J 108(12) (2015) 2783-93.

[53] A.R. Killaars, J.C. Grim, C.J. Walker, E.A. Hushka, T.E. Brown, K.S. Anseth, Extended Exposure to Stiff Microenvironments Leads to Persistent Chromatin Remodeling in Human Mesenchymal Stem Cells, Adv Sci (Weinh) 6(3) (2019) 1801483.

[54] K.H. Vining, D.J. Mooney, Mechanical forces direct stem cell behaviour in development and regeneration, Nat Rev Mol Cell Biol 18(12) (2017) 728-742.

[55] L. Feld, L. Kellerman, A. Mukherjee, A. Livne, E. Bouchbinder, H. Wolfenson, Cellular contractile forces are nonmechanosensitive, Sci Adv 6(17) (2020) eaaz6997.

[56] N. Komatsu, M. Kajiya, S. Motoike, M. Takewaki, S. Horikoshi, T. Iwata, K. Ouhara, K. Takeda, S. Matsuda, T. Fujita, H. Kurihara, Type I collagen deposition via osteoinduction ameliorates YAP/TAZ activity in 3D floating culture clumps of mesenchymal stem cell/extracellular matrix complexes, Stem Cell Research & Therapy 9(1) (2018) 342.

[57] Q.A. Wang, C. Tao, R.K. Gupta, P.E. Scherer, Tracking adipogenesis during white adipose tissue development, expansion and regeneration, Nat Med 19(10) (2013) 1338-44.

[58] L. Vishvanath, K.A. MacPherson, C. Hepler, Q.A. Wang, M. Shao, S.B. Spurgin, M.Y. Wang, C.M. Kusminski, T.S. Morley, R.K. Gupta, Pdgfrβ+ Mural Preadipocytes Contribute to Adipocyte Hyperplasia Induced by High-Fat-Diet Feeding and Prolonged Cold Exposure in Adult Mice, Cell Metab 23(2) (2016) 350-9.

[59] C.M. Kusminski, W.L. Holland, K. Sun, J. Park, S.B. Spurgin, Y. Lin, G.R. Askew, J.A. Simcox, D.A. McClain, C. Li, P.E. Scherer, MitoNEET-driven alterations in adipocyte mitochondrial activity reveal a crucial adaptive process that preserves insulin sensitivity in obesity, Nature Medicine 18(10) (2012) 1539-1549.

[60] A.L. Ghaben, P.E. Scherer, Adipogenesis and metabolic health, Nat Rev Mol Cell Biol 20(4) (2019) 242-258.

[61] A. Ibrahimi, F. Bonino, S. Bardon, G. Ailhaud, C. Dani, Essential role of collagens for terminal differentiation of preadipocytes, Biochemical and Biophysical Research Communications 187(3) (1992) 1314-1322.

[62] T.H. Chun, K.B. Hotary, F. Sabeh, A.R. Saltiel, E.D. Allen, S.J. Weiss, A pericellular collagenase directs the 3-dimensional development of white adipose tissue, Cell 125(3) (2006) 577-91.

[63] H. Nobusue, N. Onishi, T. Shimizu, E. Sugihara, Y. Oki, Y. Sumikawa, T. Chiyoda, K. Akashi, H. Saya, K. Kano, Regulation of MKL1 via actin cytoskeleton dynamics drives adipocyte differentiation, Nat Commun 5 (2014) 3368.

[64] M. Zanoni, F. Piccinini, C. Arienti, A. Zamagni, S. Santi, R. Polico, A. Bevilacqua, A. Tesei, 3D tumor spheroid models for in vitro therapeutic screening: a systematic approach to enhance the biological relevance of data obtained, Scientific Reports 6(1) (2016) 19103.

[65] P.A. Turner, Y. Tang, S.J. Weiss, A.V. Janorkar, Three-dimensional spheroid cell model of in vitro adipocyte inflammation, Tissue Eng Part A 21(11-12) (2015) 1837-47.

[66] F. Louis, Y. Sowa, S. Kitano, M. Matsusaki, High-throughput drug screening models of mature adipose tissues which replicate the physiology of patients' Body Mass Index (BMI), Bioactive Materials (2021).

[67] N. Contessi Negrini, M. Bonnetier, G. Giatsidis, D.P. Orgill, S. Fare, B. Marelli, Tissue-mimicking gelatin scaffolds by alginate sacrificial templates for adipose tissue engineering, Acta Biomater 87 (2019) 61-75.

[68] J.I. Kim, During Adipocyte Remodeling, Lipid Droplet Configurations Regulate Insulin Sensitivity through F-Actin and G-Actin Reorganization, (2019).

[69] J.L. Kelly, M.W. Findlay, K.R. Knight, A. Penington, E.W. Thompson, A. Messina, W.A. Morrison, Contact with existing adipose tissue is inductive for adipogenesis in matrigel, Tissue Eng 12(7) (2006) 2041-7.

[70] A. Ioannidou, S. Alatar, R. Schipper, F. Baganha, M. Ahlander, A. Hornell, R.M. Fisher, C.E. Hagberg, Hypertrophied human adipocyte spheroids as in vitro model of weight gain and adipose tissue dysfunction, J Physiol (2021).

[71] K.C. O'Connor, H. Song, N. Rosenzweig, D.A. Jansen, Extracellular matrix substrata alter adipocyte yield and lipogenesis in primary cultures of stromal-vascular cells from human adipose, Biotechnology Letters 25(23) (2003) 1967-1972.

[72] D. Sadler, C.A. Mattacks, C.M. Pond, Changes in adipocytes and dendritic cells in lymph node containing adipose depots during and after many weeks of mild inflammation, J Anat 207(6) (2005) 769-81.

[73] I. Wernstedt Asterholm, C. Tao, T.S. Morley, Q.A. Wang, F. Delgado-Lopez, Z.V. Wang, P.E. Scherer, Adipocyte inflammation is essential for healthy adipose tissue expansion and remodeling, Cell Metab 20(1) (2014) 103-18.

[74] Q. Zhu, Y.A. An, M. Kim, Z. Zhang, S. Zhao, Y. Zhu, I.W. Asterholm, C.M. Kusminski, P.E. Scherer, Suppressing adipocyte inflammation promotes insulin resistance in mice, Mol Metab 39 (2020) 101010.

[75] G.S. Hotamisligil, P. Arner, J.F. Caro, R.L. Atkinson, B.M. Spiegelman, Increased adipose tissue expression of tumor necrosis factor-alpha in human obesity and insulin resistance, The Journal of clinical investigation 95(5) (1995) 2409-2415.

[76] S. Gasic, B. Tian, A. Green, Tumor necrosis factor alpha stimulates lipolysis in adipocytes by decreasing Gi protein concentrations, J Biol Chem 274(10) (1999) 6770-5.

[77] B. Gustafson, U. Smith, Cytokines promote Wnt signaling and inflammation and impair the normal differentiation and lipid accumulation in 3T3-L1 preadipocytes, J Biol Chem 281(14) (2006) 9507-16.

[78] C. Lagathu, L. Yvan-Charvet, J.P. Bastard, M. Maachi, A. Quignard-Boulangé, J. Capeau, M. Caron, Long-term treatment with interleukin-1β induces insulin resistance in murine and human adipocytes, Diabetologia 49(9) (2006) 2162-2173.

[79] G.B. Di Gregorio, L. Hensley, T. Lu, G. Ranganathan, P.A. Kern, Lipid and carbohydrate metabolism in mice with a targeted mutation in the IL-6 gene: absence of development of age-related obesity, American Journal of Physiology-Endocrinology And Metabolism 287(1) (2004) E182-E187.

[80] B.K. Pedersen, M.A. Febbraio, Muscles, exercise and obesity: skeletal muscle as a secretory organ, Nature Reviews Endocrinology 8(8) (2012) 457-465.

[81] R.W. Grant, J.M. Stephens, Fat in flames: influence of cytokines and pattern recognition receptors on adipocyte lipolysis, American Journal of Physiology-Endocrinology and Metabolism 309(3) (2015) E205-E213.

[82] X. Bai, J. Xi, Y. Bi, X. Zhao, W. Bing, X. Meng, Y. Liu, Z. Zhu, G. Song, TNF-α promotes survival and migration of MSCs under oxidative stress via NF-κB pathway to attenuate intimal hyperplasia in vein grafts, J Cell Mol Med 21(9) (2017) 2077-2091.

[83] M. Shioda, T. Muneta, K. Tsuji, M. Mizuno, K. Komori, H. Koga, I. Sekiya, TNFα promotes proliferation of human synovial MSCs while maintaining chondrogenic potential, PLOS ONE 12(5) (2017) e0177771.

[84] J.M. Stephens, J. Lee, P.F. Pilch, Tumor necrosis factor-alpha-induced insulin resistance in 3T3-L1 adipocytes is accompanied by a loss of insulin receptor substrate-1 and GLUT4 expression without a loss of insulin receptor-mediated signal transduction, J Biol Chem 272(2) (1997) 971-6.

[85] J.M. Stephens, P.H. Pekala, Transcriptional repression of the GLUT4 and C/EBP genes in 3T3-L1 adipocytes by tumor necrosis factor-alpha, Journal of Biological Chemistry 266(32) (1991) 21839-21845.

[86] K. Lin, D. Zhang, M.H. Macedo, W. Cui, B. Sarmento, G. Shen, Advanced Collagen-Based Biomaterials for Regenerative Biomedicine, Advanced Functional Materials 29(3) (2019) 1804943.

[87] Y.K. Zhu, T. Umino, X.D. Liu, H.J. Wang, D.J. Romberger, J.R. Spurzem, S.I. Rennard, Contraction of fibroblast-containing collagen gels: initial collagen concentration regulates the degree of contraction and cell survival, In Vitro Cell Dev Biol Anim 37(1) (2001) 10-6.

[88] A.E. Miller, P. Hu, T.H. Barker, Feeling Things Out: Bidirectional Signaling of the Cell-ECM Interface, Implications in the Mechanobiology of Cell Spreading, Migration, Proliferation, and Differentiation, Adv Healthc Mater 9(8) (2020) e1901445.

[89] B.C. Low, C.Q. Pan, G.V. Shivashankar, A. Bershadsky, M. Sudol, M. Sheetz, YAP/TAZ as mechanosensors and mechanotransducers in regulating organ size and tumor growth, FEBS Lett 588(16) (2014) 2663-70.

[90] F. Yang, A. Carmona, K. Stojkova, E.I. Garcia Huitron, A. Goddi, A. Bhushan, R.N. Cohen, E.M. Brey, A 3D human adipose tissue model within a microfluidic device, Lab Chip 21(2) (2021) 435-446.

[91] Y.L. Han, P. Ronceray, G. Xu, A. Malandrino, R.D. Kamm, M. Lenz, C.P. Broedersz, M. Guo, Cell contraction induces long-ranged stress stiffening in the extracellular matrix, Proc Natl Acad Sci U S A 115(16) (2018) 4075-4080.

[92] W.J. Polacheck, C.S. Chen, Measuring cell-generated forces: a guide to the available tools, Nature methods 13(5) (2016) 415-423.

[93] S. Le Lay, N. Briand, I. Dugail, Adipocyte size fluctuation, mechano-active lipid droplets and caveolae, Adipocyte 4(2) (2014) 158-160.

[94] X. Li, Y. Zhao, C. Chen, L. Yang, H.H. Lee, Z. Wang, N. Zhang, M.G. Kolonin, Z. An, X. Ge, P.E. Scherer, K. Sun, Critical Role of Matrix Metalloproteinase 14 in Adipose Tissue Remodeling during Obesity, Mol Cell Biol 40(8) (2020).

[95] Y. Li, A.S. Mao, B.R. Seo, X. Zhao, S.K. Gupta, M. Chen, Y.L. Han, T.Y. Shih, D.J. Mooney, M. Guo, Compression-induced dedifferentiation of adipocytes promotes tumor progression, Sci Adv 6(4) (2020) eaax5611.

[96] Q. Xing, Z. Qian, W. Jia, A. Ghosh, M. Tahtinen, F. Zhao, Natural Extracellular Matrix for Cellular and Tissue Biomanufacturing, ACS Biomaterials Science & Engineering 3(8) (2017) 1462-1476.

[97] D.M. Faulk, S.A. Johnson, L. Zhang, S.F. Badylak, Role of the extracellular matrix in whole organ engineering, J Cell Physiol 229(8) (2014) 984-9.

[98] S.F. Badylak, The extracellular matrix as a scaffold for tissue reconstruction, Seminars in Cell & Developmental Biology 13(5) (2002) 377-383.

[99] L.T. Saldin, M.C. Cramer, S.S. Velankar, L.J. White, S.F. Badylak, Extracellular matrix hydrogels from decellularized tissues: Structure and function, Acta Biomater 49 (2017) 1-15.

[100] C. Williams, K. Sullivan, L.D. Black, 3rd, Partially Digested Adult Cardiac Extracellular Matrix Promotes Cardiomyocyte Proliferation In Vitro, Adv Healthc Mater 4(10) (2015) 1545-54.

[101] S. Rathan, L. Dejob, R. Schipani, B. Haffner, M.E. Mobius, D.J. Kelly, Fiber Reinforced Cartilage ECM Functionalized Bioinks for Functional Cartilage Tissue Engineering, Adv Healthc Mater 8(7) (2019) e1801501.

[102] L. Gaffney, E.A. Wrona, D.O. Freytes, Potential Synergistic Effects of Stem Cells and Extracellular Matrix Scaffolds, ACS Biomaterials Science & Engineering 4(4) (2018) 1208-1222.

[103] E. Gruskin, B.A. Doll, F.W. Futrell, J.P. Schmitz, J.O. Hollinger, Demineralized bone matrix in bone repair: history and use, Adv Drug Deliv Rev 64(12) (2012) 1063-77.

[104] B. Peterson, P.G. Whang, R. Iglesias, J.C. Wang, J.R. Lieberman, Osteoinductivity of commercially available demineralized bone matrix. Preparations in a spine fusion model, J Bone Joint Surg Am 86-A(10) (2004) 2243-50.

[105] B. Groessner-Schreiber, M. Krukowski, C. Lyons, P. Osdoby, Osteoclast recruitment in response to human bone matrix is age related, Mechanisms of Ageing and Development 62(2) (1992) 143-154.

[106] Z. Schwartz, A. Somers, J.T. Mellonig, D.L. Carnes, Jr., D.D. Dean, D.L. Cochran, B.D. Boyan, Ability of commercial demineralized freeze-dried bone allograft to induce new bone formation is dependent on donor age but not gender, Journal of periodontology 69(4) (1998) 470-8.

[107] E. Munting, J.F. Wilmart, A. Wijne, P. Hennebert, C. Delloye, Effect of sterilization on osteoinduction. Comparison of five methods in demineralized rat bone, Acta orthopaedica Scandinavica 59(1) (1988) 34-8.

[108] J.L. Russell, J.E. Block, Clinical utility of demineralized bone matrix for osseous defects, arthrodesis, and reconstruction: impact of processing techniques and study methodology, Orthopedics 22(5) (1999) 524-31; quiz 532-3.

[109] E. Nyberg, A. Rindone, A. Dorafshar, W.L. Grayson, Comparison of 3D-Printed Poly-varepsilon-Caprolactone Scaffolds Functionalized with Tricalcium Phosphate, Hydroxyapatite, Bio-Oss, or Decellularized Bone Matrix, Tissue Eng Part A 23(11-12) (2017) 503-514.

[110] M.J. Sawkins, W. Bowen, P. Dhadda, H. Markides, L.E. Sidney, A.J. Taylor, F.R. Rose, S.F. Badylak, K.M. Shakesheff, L.J. White, Hydrogels derived from demineralized and decellularized bone extracellular matrix, Acta Biomaterialia 9(8) (2013) 7865-73.

[111] B.P. Hung, B.A. Naved, E.L. Nyberg, M. Dias, C.A. Holmes, J.H. Elisseeff, A.H. Dorafshar, W.L. Grayson, Three-Dimensional Printing of Bone Extracellular Matrix for Craniofacial Regeneration, ACS Biomaterials Science & Engineering (2016).

[112] X. Yao, L.-J. Ning, S.-K. He, J. Cui, R.-N. Hu, Y. Zhang, Y.-J. Zhang, J.-C. Luo, W. Ding, T.-W. Qin, Stem Cell Extracellular Matrix-Modified Decellularized Tendon Slices Facilitate the Migration of Bone Marrow Mesenchymal Stem Cells, ACS Biomaterials Science & Engineering 5(9) (2019) 4485-4495.

[113] H. Lee, W. Han, H. Kim, D.-H. Ha, J. Jang, B.S. Kim, D.-W. Cho, Development of Liver Decellularized Extracellular Matrix Bioink for Three-Dimensional Cell Printing-Based Liver Tissue Engineering, Biomacromolecules 18(4) (2017) 1229-1237.

[114] Y. Seo, S. Jeong, J.J. Chung, S.H. Kim, N. Choi, Y. Jung, Development of an Anisotropically Organized Brain dECM Hydrogel-Based 3D Neuronal Culture Platform for

Recapitulating the Brain Microenvironment in Vivo, ACS Biomaterials Science & Engineering 6(1) (2020) 610-620.

[115] N. Datta, Q.P. Pham, U. Sharma, V.I. Sikavitsas, J.A. Jansen, A.G. Mikos, In vitro generated extracellular matrix and fluid shear stress synergistically enhance 3D osteoblastic differentiation, Proc Natl Acad Sci U S A 103(8) (2006) 2488-93.

[116] C. Sears, E. Mondragon, Z.I. Richards, N. Sears, D. Chimene, E.P. McNeill, C.A. Gregory, A.K. Gaharwar, R. Kaunas, Conditioning of 3D Printed Nanoengineered Ionic-Covalent Entanglement Scaffolds with iP-hMSCs Derived Matrix, Adv Healthc Mater (2020) e1901580.

[117] W. Zhang, Y. Zhu, J. Li, Q. Guo, J. Peng, S. Liu, J. Yang, Y. Wang, Cell-Derived Extracellular Matrix: Basic Characteristics and Current Applications in Orthopedic Tissue Engineering, Tissue Eng Part B Rev 22(3) (2016) 193-207.

[118] S. Sart, T. Ma, Y. Li, Extracellular matrices decellularized from embryonic stem cells maintained their structure and signaling specificity, Tissue Eng Part A 20(1-2) (2014) 54-66.

[119] J.N. Harvestine, N.L. Vollmer, S.S. Ho, C.A. Zikry, M.A. Lee, J.K. Leach, Extracellular Matrix-Coated Composite Scaffolds Promote Mesenchymal Stem Cell Persistence and Osteogenesis, Biomacromolecules 17(11) (2016) 3524-3531.

[120] A.D. Dikina, H.V. Almeida, M. Cao, D.J. Kelly, E. Alsberg, Scaffolds Derived from ECM Produced by Chondrogenically Induced Human MSC Condensates Support Human MSC Chondrogenesis, ACS Biomaterials Science & Engineering 3(7) (2017) 1426-1436.

[121] H.V. Almeida, A.D. Dikina, K.J. Mulhall, F.J. O'Brien, E. Alsberg, D.J. Kelly, Porous Scaffolds Derived from Devitalized Tissue Engineered Cartilaginous Matrix Support

Chondrogenesis of Adult Stem Cells, ACS Biomaterials Science & Engineering 3(6) (2017) 1075-1082.

[122] Y. Chen, K. Lee, Y. Chen, Y. Yang, N. Kawazoe, G. Chen, Preparation of Stepwise Adipogenesis-Mimicking ECM-Deposited PLGA–Collagen Hybrid Meshes and Their Influence on Adipogenic Differentiation of hMSCs, ACS Biomaterials Science & Engineering 5(11) (2019) 6099-6108.

[123] D. Wang, K. Christensen, K. Chawla, G. Xiao, P.H. Krebsbach, R.T. Franceschi, Isolation and characterization of MC3T3-E1 preosteoblast subclone with Distinct In Vitro and In Vivo Differentiation/Mineralization Potential, J Bone Miner Res 14(6) (1999) 893-903.

[124] R.T. Franceschi, B.S. Iyer, Y. Cui, Effects of ascorbic acid on collagen matrix formation and osteoblast differentiation in murine MC3T3-E1 cells, J Bone Miner Res 9(6) (1994) 843-54.

[125] E. García-Gareta, Y. Abduldaiem, P. Sawadkar, C. Kyriakidis, F. Lali, K.V. Greco, Decellularised scaffolds: just a framework? Current knowledge and future directions, Journal of Tissue Engineering 11 (2020) 2041731420942903.

[126] W.N. Addison, V. Nelea, F. Chicatun, Y.C. Chien, N. Tran-Khanh, M.D. Buschmann, S.N. Nazhat, M.T. Kaartinen, H. Vali, M.M. Tecklenburg, R.T. Franceschi, M.D. McKee, Extracellular matrix mineralization in murine MC3T3-E1 osteoblast cultures: An ultrastructural, compositional and comparative analysis with mouse bone, Bone 71 (2015) 244-256.

[127] R.K. Kankala, X.M. Xu, C.G. Liu, A.Z. Chen, S.B. Wang, 3D-Printing of Microfibrous Porous Scaffolds Based on Hybrid Approaches for Bone Tissue Engineering, Polymers 10(7) (2018).

[128] H. Lee, G.H. Yang, M. Kim, J. Lee, J. Huh, G. Kim, Fabrication of micro/nanoporous collagen/dECM/silk-fibroin biocomposite scaffolds using a low temperature 3D printing process for bone tissue regeneration, Mater Sci Eng C Mater Biol Appl 84 (2018) 140-147.

[129] H.J. Lee, Y.B. Kim, S.H. Ahn, J.S. Lee, C.H. Jang, H. Yoon, W. Chun, G.H. Kim, A New Approach for Fabricating Collagen/ECM-Based Bioinks Using Preosteoblasts and Human Adipose Stem Cells, Adv Healthc Mater 4(9) (2015) 1359-68.

[130] M. Caralt, J.S. Uzarski, S. Iacob, K.P. Obergfell, N. Berg, B.M. Bijonowski, K.M. Kiefer, H.H. Ward, A. Wandinger-Ness, W.M. Miller, Z.J. Zhang, M.M. Abecassis, J.A. Wertheim, Optimization and critical evaluation of decellularization strategies to develop renal extracellular matrix scaffolds as biological templates for organ engineering and transplantation, Am J Transplant 15(1) (2015) 64-75.

[131] H. Lu, T. Hoshiba, N. Kawazoe, G. Chen, Comparison of decellularization techniques for preparation of extracellular matrix scaffolds derived from three-dimensional cell culture, J Biomed Mater Res A 100(9) (2012) 2507-16.

[132] Q. Xing, K. Yates, M. Tahtinen, E. Shearier, Z. Qian, F. Zhao, Decellularization of fibroblast cell sheets for natural extracellular matrix scaffold preparation, Tissue Eng Part C Methods 21(1) (2015) 77-87.

[133] L.J. White, A.J. Taylor, D.M. Faulk, T.J. Keane, L.T. Saldin, J.E. Reing, I.T. Swinehart, N.J. Turner, B.D. Ratner, S.F. Badylak, The impact of detergents on the tissue decellularization process: A ToF-SIMS study, Acta Biomaterialia 50 (2017) 207-219.

[134] Y. Hwang, N. Sangaj, S. Varghese, Interconnected macroporous poly(Ethylene Glycol) cryogels as a cell scaffold for cartilage tissue engineering, Tissue Engineering - Part A 16(10) (2010) 3033-3041.

[135] W. Huang, B. Carlsen, G. Rudkin, M. Berry, K. Ishida, D.T. Yamaguchi, T.A. Miller, Osteopontin is a negative regulator of proliferation and differentiation in MC3T3-E1 pre-osteoblastic cells, Bone 34(5) (2004) 799-808.

[136] N.E. Saygin, W.V. Giannobile, M.J. Somerman, Molecular and cell biology of cementum, Periodontology 2000 24 (2000) 73-98.

[137] W. Bouleftour, L. Juignet, G. Bouet, R.N. Granito, A. Vanden-Bossche, N. Laroche, J.E. Aubin, M.H. Lafage-Proust, L. Vico, L. Malaval, The role of the SIBLING, Bone Sialoprotein in skeletal biology - Contribution of mouse experimental genetics, Matrix Biol 52-54 (2016) 60-77.

[138] A.C. Allori, A.M. Sailon, S.M. Warren, Biological basis of bone formation, remodeling, and repair-part II: extracellular matrix, Tissue Eng Part B Rev 14(3) (2008) 275-83.

국 문 초 록

콜라겐 하이드로겔 수축의 조절을 통한 인간 중간엽 줄기세포의 분화 결정

김 슬 하

서울대학교 대학원

화학생물공학부

콜라겐은 포유류의 세포외기질에서 가장 풍부하게 존재하는 단백질로, 세포의 부착, 분화, 이동을 포함한 많은 세포 거동에 큰 영향을 미친다. 하지만 콜라겐을 하이드로겔 형태로 실험실에서 세포 배양하는 경우 심한 수축이 발생하기 때문에 이용에 어려움이 있다. 수축이 발생하는 경우 전체적인 하이드로겔의 부피가 줄어들면서, 세포의 분포와 물질전달 등 물리적 환경이 크게 변하게 된다. 이러한 통제할 수 없는 세포외기질의 물리적, 생리학적 요인들의 변화는 그 안에 존재하는 세포들의 통제되지 않은 세포 거동의 변화를 가져온다. 이러한 관점에서, 콜라겐 수축을 조절했을 때 지방 조직에서 유래한 인간 중간엽 줄기세포 (human adipose tissue-derived mesenchymal stem cells, ADSCs)의 분화에 어떤 영향을 미치는지 살펴보았다.

먼저, 콜라겐 하이드로겔의 수축을 막을 수 있는 플랫폼을 개발했다. 두 가지 접근법으로 콜라겐의 수축을 완전히 막을 수 있었는데, 폴리도파민으로 코팅된 디스크 모양의 프레임이 하이드로겔을 수평 방향으로 잡아주고, 알긴산으로 만들어진 외곽의 껍질이 수직 방향의 수축을 막아주었다. 하이드로겔 내부의 물성은 순수한 콜라겐으로 만들어진 하이드로겔과 유사했으며, 이 플랫폼에서 장기간의 세포 배양에서도 수축을 막을 수 있었다.

이렇게 수축을 막은 경우와 비교했을 때, 자유로운 수축을 방치한 콜라겐 하이드로겔에서는 화학적인 분화 유도 인자들을 처리했음에도 불구하고 인간 중간엽 줄기세포의 분화를 원하는 방향으로 유도할 수 없었으며, 오직 지방분화만이 유도되는 모습을 보였다. 세포가 콜라겐이 수축하는 환경을 어떻게 감지하는지를 메카노트랜스덕션 (mechanotransduction) 관점에서 확인하기 위해 Yes-associated protein (YAP)의 핵과 세포질 간 이동을 관찰했다. 수축을 막는 경우 세포는 더 강한 수축력을 콜라겐에 행사했으며, 이것이 분화 방향 결정에 영향을 미쳐 골분화를 유도할 수 있음을 보였다.

수축이 일어날 때 중간엽 줄기세포에서 지방분화가 촉진되는 것에 주목하여, 수축하는 속도를 조절하는 것이 지방분화에 미치는 영향을 분석했다. 폴리도파민 코팅된 프레임으로 수축을 지연시켰을 때, 자유롭게 수축한 하이드로겔에 비해 더 높은 비율의 세포들이 지방 방울을 세포질에 형성하면서 지방세포로의 분화가 일어났다. 이렇게 성숙한 지방세포로 분화한 중간엽 줄기세포들은 과잉 지방 자극과 지방 분해 유도 자극에 활발히 반응할 수 있었다. 이처럼, 콜라겐 수축의 시간적인 조절을 통해서 인간 중간엽 줄기세포의 빠르고 균일한 지방분화를 유도할 수 있었다.

더 나아가, 병적 비만 상태의 지방 조직에서 발생하는 염증 반응을 모사하는 시험관 모델을 개발했다. 비만으로 인한 만성적인 염증은 대사증후군으로 연결되는 인슐린 저항성 발생의 주된 원인이다. 하지만, 체내에서 염증으로 인해 지방조직에서 일어나는 현상은 지방 세포주를 이용한 시험관 2 차원 배양 환경에서는 잘 재현되지 않는다. 이러한 시험관과 체내에서의 격차가 세포-세포외기질 사이의 상호작용이 시험관에서 배제되었기 때문이라고 가정했다. 위와 같은 방법으로 지방분화를 유도한 인간 중간엽 줄기세포에 전염증인자 (pro-inflammatory cytokine)와 과량의 지방산을 공급했을 때, 세포분열이 촉진되면서 기존 세포에 밀집되어 있던 지방들이 주변 세포로 분산되는 현상을 확인했다. 이를 통해 지방 체내 조직에서 염증이 발생했을 때 지방 조직의 부피 성장이 일어나는 현상을 재현할 수 있었다.

이와 같이, 콜라겐의 수축을 막는 접근법을 개발하고 인간 중간엽 줄기세포에 어떤 변화를 가져오는지 확인했다. 또한, 콜라겐 수축을 조절하는 것만으로도 줄기세포의 분화를 조절할 수 있으며, 체내에서 일어나는 현상을 재현하는 것을 가능케 한다는 것을 보였다. 콜라겐의 수축을 조절할 수 있는 플랫폼을 통해 세포의 미세 환경을 바꿀 수 있었고, 이를 통해 세포와 세포외기질 간의 상호작용을 연구하는 데에 활용할 수 있을 것으로 기대된다.